Electromagnetic moments and transitions in nuclear density functional theory

Alejandro Restrepo-Giraldo

Master of Science by Research

University of York

School of Physics, Engineering and Technology

December 2025

Abstract

We investigate the electromagnetic moments and transition properties of atomic nuclei within the framework of nuclear density functional theory (DFT). We focus on presenting the role of pairing interaction, spontaneous symmetry breaking and symmetry restoration techniques in nuclear structure studies with particular emphasis on their influence over electromagnetic multipole moments and transition strengths. We present a self-complete theoretical framework covering the seniority and quasiparticle formalisms of pairing, given by the Bardeen-Cooper-Schreiffer (BCS) and Hartree–Fock–Bogoliubov (HFB) theories. Additionally, we cover the fundamentals of DFT in the context of the atomic nucleus and symmetry restoration techniques in the framework of the generator coordinate method (GCM). We also introduce the phenomenology of multipole moments, transitions and spin isomerism from theoretical and experimental perspectives.

We apply these topics to perform systematic self-consistent parameter-free calculations to describe odd-mass isotopic chains of yttrium and zirconium using the implementations in the code HFODD. We calculate spectroscopic electric quadrupole and magnetic dipole moments which are compared with available experimental data resulting in overall good quantitative agreement. We analyse the effects of pairing, deformation, blocking and time-odd components of the functionals. Additionally, we calculate the transition strength and multipole moments of the isomeric and ground states of ^{229}Th using advanced beyond mean-field techniques and compare with recent experimental data. Overall, this work implements and tests modern DFT approaches to reproduce electromagnetic observables demonstrating them to provide a robust framework to study the atomic nucleus across the nuclear chart.

Acknowledgements

I would like to thank my parents Diego and Mónica who have been my greatest supporters, thank you for always believing in me and inspiring me to face life with courage. Special thanks to my sisters Carolina and Nataly, and my brother Jerónimo for their cheerful support and remaining close despite the distance. To all my extended family, grandparents, aunts, uncles, cousins, brother-in-law and nephew, thank you for your caring support.

I want to express gratitude to my supervisor Jacek, for trusting me in joining his team and for his always caring supervision and advice. Huge thanks to my colleagues and collaborators Betania, Herlik and Xuwei for their constant guidance and kind help even before I joined you. Thanks to my external supervisors Lee and Aaron for devising and supporting this research project. To the rest of the academics and postdocs of the department, thank you for the many valuable interactions. To my friends and colleagues of the department Alex, Ali, Anthony, Asli, Beatriz, Betania, Charlie, Guy, John, Josh S., Josh W., Laura and Luke, thank you for so many good moments and unforgettable memories. Enormous thanks to COLFUTURO for funding my degree.

The University of York is a place where science is lived beyond the work environment. For me science is not just a set of knowledge, a method or a community, but a way of thinking and thus a lifestyle that encourages us to remain open to having our ideas challenged through dialogue grounded in the principles of freedom and equality. I am deeply grateful for the warm welcome I received and for all the lessons I have learned here.

Alejandro Restrepo-Giraldo,
York,
December 2025.

Author declaration

I declare that this thesis is a presentation of original work and I am the sole author. This work has not previously been presented for an award at this, or any other, University. All sources are acknowledged as References. Related publications are listed below.

Chapter 4 was based on ideas presented in the following preprint

> J. Dobaczewski, B. C. Backes, R. P. de Groote, **A. Restrepo-Giraldo**, X. Sun and H. Wibowo. Electromagnetic and exotic moments in nuclear DFT, arXiv:2511.04632, 2025.

Chapter 5 contains materials presented in the following preprint

> **A. Restrepo-Giraldo**, J. Dobaczewski, P. Becker, J. Bonnard, A. Pastore and X. Sun. Radiative decay of the ^{229}Th isomer determined within nuclear DFT, arXiv:2602.02429, 2026.

Other publications in preparation are

> **A. Restrepo-Giraldo**, J. Dobaczewski, *et. al.*. How to calculate your own nucleus in nuclear DFT: A primer in using the code HFODD, 2026.

> **A. Restrepo-Giraldo**, J. Dobaczewski, L. Morgan and A. Stott. Electromagnetic moments of odd-A yttrium and zirconium isotopes determined within nuclear DFT, 2026.

Contents

List of Tables

List of Figures

1 Introduction

The atomic nuclei are quantum many-body systems whose observables and properties emerge from the interplay of single-particle and collective motion via three out of four of the known fundamental interactions. This places the atomic nucleus as an interesting quantum mechanical system despite the fact that the exact analytical form of the nuclear interaction is still unknown, presenting a significant theoretical challenge. However, some aspects have been figured out, like the short range residual interaction between pairs of like particles, also called pairing [6, 7]. This component of the residual interaction favours the spatial overlap of like nucleons and plays a crucial role in its stability, physical dimensions and observables. Early descriptions incorporated pairing phenomenologically which was later formalized by the quasiparticle formalisms adapted from solid state physics.

An intrinsic complication for the study of the nucleus is its many-body character. This is a well-known problem from classical mechanics where the lack of enough conserved quantities makes many-body systems analytically irresolvable. Quantum mechanics inherits same complications of classical mechanics, where in addition we have to account for the in-indistinguishability of particles and spontaneous symmetry breaking of quantum systems. Because theoretical progress needs to produce practical results to test with experimental data, many-body theorists developed the density functional theory (DFT) initially for solid state physics but quickly applied to nuclear physics [8, 9, 7, 10]. It replaced the requirement to obtain full many-body wavefunctions by solving for the one-body local density of the system, reducing computational complexity and gaining feasibility for actual applications. Since then, DFT has thrived in the several areas of many-body quantum mechanics.

The atomic nucleus is also an exceptional case of emergent phenomena where discrete changes in nucleon numbers lead to distinctive structure and properties across the whole nuclear chart [11]. These emergent features give rise to a rich variety of observables including binding energies, deformations, collective excitations, decay modes and electromagnetic properties. In particular, the electromagnetic interactions represent important probes of the nucleus and because these are well controlled by current laboratory techniques, it is the interaction of choice for nuclear structure studies. Quantities such as electric quadrupole and octupole moments, as well as magnetic dipole moments encode detailed information about charge and current distributions inside the nucleus. The associated electromagnetic decays and isomerism reveal subtle aspects of the nuclear interaction which are essential to increase our understanding of the nucleus [12]. For our benefit, several measurements of static multipole moments and electromag-

netic decays have been compiled over the years in evaluated and accessible databases providing a reliable source of information to test theories and representing a general interest to the scientific community for applications.

The reliability of any theoretical description rests on its internal consistency and ability to reproduce and explain experimental data. Nuclear observables serve as benchmarks for models of the structure of matter, reflecting the consistency of the interactions and many-body methods. In this thesis we employ the theoretical frameworks of pairing, DFT and symmetry restoration techniques to perform realistic and consistent calculations of electromagnetic observables across specific open-shell deformed nuclei. We review the theoretical framework required to explain the methodologies and results obtained, organizing the contents as follows. In chapter 2 we introduce the pairing interaction in the nucleus from the models of seniority, Bardeen-Cooper-Schreiffer (BCS) [13, 14] and Hartree–Fock–Bogoliubov (HFB) theories [7]. We emphasize in the concept of quasiparticles, its usefulness to simplify many-body quantum mechanics and also the breaking of particle-number it introduces. In chapter 3 we present the foundations of DFT from its general theory applicable to any quantum system and the particular case of the atomic nucleus. Additionally, we introduce the beyond mean field methods essential to restore symmetries and mix multi-configuration wavefunctions. In chapter 4 we review the multipole moments and transitions showing its theory and experimental interplay to interpret several nuclear properties. Finally in chapter 5 we present systematic self-consistent parameter-free calculations of electromagnetic moments for odd-mass isotopic chains of yttrium and zirconium, and the isomeric transition strength of ^{229}Th using the implementations in the code HFODD [15]. We detail methodologies and compare with available experimental data. Additionally, a set of appendices have been included to complement the main text.

2

Descriptions of pairing in the nucleus

Since the beginning of experimental nuclear physics, distinctive features of even-even nuclei have been identified which indicate a strong contribution to the nuclear phenomenology and stability from the interactions of pairs. Consistent observations of ground state zero angular momentum of even-even nuclei, odd-even staggering of binding energies, single-particle separation energies and density of states indicate an additional interaction within the nucleus that is not contained *a priori* in the mean-field nuclear force. Such interaction must be attractive and favour large spatial overlaps between like nucleons, *i. e.*, between protons and between neutrons. This additional and non-negligible contribution to the residual interaction is called pairing.

It turns out that pairing is a general aspect of fermion systems which serves as a mechanism to lower the energy by condensing pairs of time reversed states into a vacuum of coherent bosons [16, 17]. In the simplest liquid drop model of the nucleus, it was included as an enhancement of the binding energy. However, more sophisticated approaches are required if nuclear observables like spectra, deformations and refined binding energies need to be reproduced better. In this chapter, we introduce the different approaches for describing pairing in the nucleus, some of them inspired in electronic systems along with a mathematical formalism useful for the development of this thesis.

2.1 Quasiparticles and mathematical formalism

In an independent-particle picture of a many-body system, all interactions occur via a one-body mean-field $\mathcal{V}$ involving no particle-particle forces. This first approximation can be described by a Hamiltonian represented as

$$H_{\mathrm{MF}} = \mathcal{T} + \mathcal{V}, \tag{2.1}$$

where $\mathcal{T}$ is the kinetic energy. In the formalism of fermion second quantization where the operators $a_i^\dagger$ and a_j create and destroy fermions in states with quantum numbers i, j respectively, and follow the anticommutation relations

$$\{a_i, a_j^\dagger\} = \delta_{ij}, \tag{2.2}$$

$$\{a_i^\dagger, a_j^\dagger\} = \{a_i, a_j\} = 0, \tag{2.3}$$

so that the Hamiltonian 2.1 terms are given by

$$\mathcal{T} = \sum_{i,j} \tau_{ij} a_i^\dagger a_j, \tag{2.4}$$

$$\mathcal{V} = \sum_{i,j} \nu_{ij} a_i^\dagger a_j, \tag{2.5}$$

$$H_{\mathrm{MF}} = \sum_{i,j} (\tau_{ij} + \nu_{ij}) a_i^\dagger a_j, \tag{2.6}$$

where the indices run over all states of the model space and τ_{ij}, ν_{ij} are the matrix elements of the kinetic energy and mean-field potential, respectively. Part of the success of the independent-particle shell-model in explaining the overall structure of the nucleus relies in the fact that most of the energy is encapsulated in the simpler terms $\mathcal{T}$ and $\mathcal{V}$ [18]. However, a more rigorous approach aiming to describe the emergent richness of nuclear phenomena must include the so called residual interaction $\mathcal{U}$. This involves many-body operators usually restricted to two-, three- [19] or even four-particle conserving interaction [20] terms as

$$\begin{aligned} \mathcal{H}_{\mathrm{MF+RI}} = \sum_{i,j} (\tau_{ij} + \nu_{ij}) a_i^\dagger a_j + \sum_{i,j,k,l} \upsilon'_{ijkl} a_i^\dagger a_j^\dagger a_k a_l \\ + \sum_{i,j,k,l,m,n} \upsilon''_{ijklmn} a_i^\dagger a_j^\dagger a_k^\dagger a_l a_m a_n + ... \end{aligned} \tag{2.7}$$

Because the nuclear interaction is not exactly known, part of the work of the nuclear physicist is trying to figure out the mathematical form that encapsulates best the residual interaction, even though, the introduction of such terms causes the solution of the many-body systems to be highly non-trivial. However, under a suitable manipulation of the creation and destruction operators, it is possible to capture some of the residual interaction in the one-body part of an artificial algebraic structure called the quasi-particle space. In this section we show two approaches to achieve this, focusing in the short-range residual pairing interaction. Before that, we introduce the mathematical formalism and a simple description of pairing called the seniority model.

2.1.1 The Fock space

The Fock space is a convenient formalism to approach a many-body system where an undefined number of particle states can be established for the description of A particles in an N-dimensional space. Given a single-particle Hilbert space denoted as $\mathcal{H}$, the Fock space is defined as the direct sum of tensor products of $\mathcal{H}$ as

$$\mathcal{H}_{\mathrm{Fock}} = \mathcal{H}_0 \oplus \mathcal{H}_1 \oplus \mathcal{H}_2 \oplus \mathcal{H}_3 ... \oplus \mathcal{H}_A, \tag{2.8}$$

where $\mathcal{H}_i$ denotes the tensor product of i one-particle Hilbert spaces $\mathcal{H}_1$. Its associated basis is given by

$$|0\rangle \cup \{|\alpha^1_{k(1)}, ..., \alpha^i_{k(i)}\rangle : i = 1, ..., A, k(i) = 1, ..., N\}, \tag{2.9}$$

where $|\alpha^1_{k(1)}, ..., \alpha^i_{k(i)}\rangle$ is the anti-symmetric state of i fermions occupying a single-particle state configuration $k(1), ..., k(i)$. The dimension of the Fock space is given by the addition of the dimensions of the individual i-fermion spaces as

$$\binom{N}{0} + \binom{N}{1} + \binom{N}{2} + ... + \binom{N}{A} = (1+1)^N = 2^N. \tag{2.10}$$

With this concept we devise operators to act on one of each many-body spaces depending on the number of particles considered on the interaction and in the basis states. Notice for example that the elementary creation and annihilation operators map states in $\mathcal{H}_i$ to $\mathcal{H}_{i+1}$ and $\mathcal{H}_{i-1}$ respectively.

2.1.2 The variational principle in quantum mechanics

In classical and relativistic mechanics, the least action principle in its simplest form is given by

$$\delta S = \int dt\, L\Big(q(t), \dot{q}(t), t\Big) = 0, \tag{2.11}$$

which is a fundamental and universal approach to obtain the equations of motion of a system. In quantum mechanics, its equivalent is given by the minimization of the energy, which can be treated as a functional of a non-normalized ground state wavefunction $|\Psi_0\rangle$ as

$$\delta E[\Psi_0] = \delta \left[\frac{\langle \Psi_0 | \hat{H} | \Psi_0 \rangle}{\langle \Psi_0 | \Psi_0 \rangle} \right] = 0, \tag{2.12}$$

from which we can derive Schrödinger equation as follows. Since $|\Psi_0\rangle$ and $\langle\Psi_0|$ are independent functions, we have that

$$\begin{aligned} \delta E[\Psi_0] &= \frac{\partial E[\Psi_0]}{\partial |\Psi_0\rangle} |\delta\Psi_0\rangle + \langle \Psi_0 | \frac{\partial E[\Psi_0]}{\partial \langle \Psi_0|} \\ &= \langle \Psi_0 | \hat{H} - E | \delta\Psi_0 \rangle + \langle \delta\Psi_0 | \hat{H} - E | \Psi_0 \rangle = 0, \end{aligned} \tag{2.13}$$

where $|\delta\Psi_0\rangle$ and $\langle\delta\Psi_0|$ can themselves be interpreted as a variation of parameters like occupancies of single-particles, amplitudes, densities, etc. Each variational equation is zero independently from where we get Schrödinger equation

$$(\hat{H} - E)|\Psi_0\rangle = 0, \qquad \langle\Psi_0|(\hat{H} - E) = 0. \tag{2.14}$$

The set of equations 2.14 output the ground state energy. For the first excited state $|\Psi_1\rangle$, a constrained minimization guaranteeing orthogonality between excited states

has to be performed for the modified functional

$$\delta E[\Psi_1] = \delta\left[\frac{\langle\Psi_1|\left[\hat{H} - \lambda_1\langle\Psi_0|\Psi_1\rangle\right]|\Psi_1\rangle}{\langle\Psi_1|\Psi_1\rangle}\right] = 0, \tag{2.15}$$

where λ_1 is the associated Lagrange multiplier. It can be generalized for the n^{th} excited state to

$$\delta E[\Psi_n] = \delta\left[\frac{\langle\Psi_n|\left[\hat{H} - \sum_{j=0}^{n-1}\lambda_n\langle\Psi_j|\Psi_n\rangle\right]|\Psi_n\rangle}{\langle\Psi_n|\Psi_n\rangle}\right] = 0, \tag{2.16}$$

This result is used to get the equation of motion of Hartree-Fock, Bardeen-Cooper-Schreiffer and Hartree-Fock-Bogoliubov models.

Similarly, when an observable of the system $\hat{O}$ has to be constrained to a value O_0, then an unconstrained variation has to be performed over

$$\langle\hat{H}'\rangle = \langle\hat{H}\rangle - \lambda(\langle\hat{O}\rangle - O_0), \tag{2.17}$$

where the associated Lagrange parameter λ has to be determined as well. Stronger versions of this method of constraining observables exist via quadratic terms [7] or the extensively implemented augmented Lagrangian method [21].

2.1.3 Density matrix approach in many-body quantum physics

A physical observable that can be equivalently useful for the study of a many-body system is the density operator. As will be shown in section 3.1.1, finding the many-body wavefunction is a problem that can be completely replaced by finding the one-body density of the system. Its introduction also allows the possibility of representing mixed states, giving opportunity for quantum statistical mechanics applications [10, 22]. Consider a basis $\{|\nu\rangle\}$ and associated wavefunctions $\varphi_\nu(\boldsymbol{r}) = \langle\boldsymbol{r}|\nu\rangle$ of a system. The operators that create (destroy) a particle in a position $\boldsymbol{r}$ with discrete quantum numbers σ (like spin and isospin) are given by

$$\begin{aligned} a^\dagger(\boldsymbol{r},\sigma) &= \sum_\nu \varphi^*_\nu(\boldsymbol{r},\sigma)a^\dagger_\nu, \\ a(\boldsymbol{r},\sigma) &= \sum_\nu \varphi_\nu(\boldsymbol{r},\sigma)a_\nu, \end{aligned} \tag{2.18}$$

and hold the anticommutation relations

$$\begin{aligned} \left\{a(\boldsymbol{r},\sigma), a^\dagger(\boldsymbol{r'},\sigma')\right\} &= \delta_{\sigma\sigma'}\delta(\boldsymbol{r}-\boldsymbol{r'}), \\ \left\{a^\dagger(\boldsymbol{r},\sigma), a^\dagger(\boldsymbol{r'},\sigma')\right\} &= 0, \\ \left\{a(\boldsymbol{r},\sigma), a(\boldsymbol{r'},\sigma')\right\} &= 0, \end{aligned} \tag{2.19}$$

so that we can represent the anti-symmetric N-body wavefunction by

$$\Psi_{\mathfrak{n}}(\boldsymbol{r}_1,\sigma_1,...,\boldsymbol{r}_N,\sigma_N) = \frac{1}{\sqrt{N!}}\langle 0|a(\boldsymbol{r}_1,\sigma_1)...a(\boldsymbol{r}_N,\sigma_N)|\Psi_{\mathfrak{n}}\rangle, \tag{2.20}$$

where $|\Psi_{\mathfrak{n}}\rangle$ is the anti-symmetric state with a particular configuration of occupied states in the single-particle space. For an N-body system, the density matrix operator of order $n < N$ is defined as

$$\begin{aligned}\hat{\rho}^{(n)}(\boldsymbol{r}_1,\sigma_1,...,\boldsymbol{r}_n,\sigma_n;\boldsymbol{r}'_1,\sigma'_1,...,\boldsymbol{r}'_n,\sigma'_n)\\ = a^\dagger(\boldsymbol{r}'_n,\sigma'_n)...a^\dagger(\boldsymbol{r}'_1,\sigma'_1)a(\boldsymbol{r}_1,\sigma_1)...a(\boldsymbol{r}_n,\sigma_n).\end{aligned} \tag{2.21}$$

The n-body density matrix is the expectation value of 2.21 with respect to the N-body wavefunction

$$\begin{aligned}\rho^{(n)}(\boldsymbol{r}_1,\sigma_1,...,\boldsymbol{r}_n,\sigma_n;\boldsymbol{r}'_1,\sigma'_1,...,\boldsymbol{r}'_n,\sigma'_n) &= \langle\Psi_{\mathfrak{n}}|\hat{\rho}^{(n)}|\Psi_{\mathfrak{n}}\rangle\\ &= \binom{N}{n}\sum_{\sigma_{n+1},...,\sigma_N}\int \Psi^*_{\mathfrak{n}}(\boldsymbol{r}'_1,\sigma'_1,...,\boldsymbol{r}'_n\sigma'_n,\boldsymbol{r}_{n+1},\sigma_{n+1},...,\boldsymbol{r}_N,\sigma_N)\\ &\qquad\times\Psi_{\mathfrak{n}}(\boldsymbol{r}_1,\sigma_1,...,\boldsymbol{r}_n,\sigma_n,\boldsymbol{r}_{n+1},\sigma_{n+1},...,\boldsymbol{r}_N,\sigma_N)d\boldsymbol{r}_{n+1}...d\boldsymbol{r}_N\\ &= \sum_{\nu_1,...,\nu_{2n}}\rho_{\nu_1,...,\nu_{2n}}\varphi^*_{\nu_1}(\boldsymbol{r}'_n,\sigma'_n)...\varphi^*_{\nu_n}(\boldsymbol{r}'_1,\sigma'_1)\varphi_{\nu_{n+1}}(\boldsymbol{r}_1,\sigma_1)...\varphi_{\nu_{2n}}(\boldsymbol{r}_n,\sigma_n),\end{aligned} \tag{2.22}$$

where

$$\rho_{\nu_1,...,\nu_{2n}} = \langle\Psi_{\mathfrak{n}}|a^\dagger_{\nu_{2n}}...a^\dagger_{\nu_{n+1}}a_{\nu_n}...a_{\nu_1}|\Psi_{\mathfrak{n}}\rangle, \tag{2.23}$$

is the associate matrix element in the basis $\{|\nu\rangle\}$.

In particular, for the one-body density matrix

$$\rho^{(1)}(\boldsymbol{r}_1,\sigma_1;\boldsymbol{r}'_1,\sigma'_1) = \sum_{\mu,\nu}\rho_{\mu\nu}\varphi^*_\nu(\boldsymbol{r}'_1,\sigma'_1)\varphi_\mu(\boldsymbol{r}_1,\sigma_1), \tag{2.24}$$

where

$$\rho_{\mu\nu} = \langle\Psi_{\mathfrak{n}}|a^\dagger_\nu a_\mu|\Psi_{\mathfrak{n}}\rangle. \tag{2.25}$$

It can be seen that ρ is Hermitian, so there exist a basis $\{|\tilde{\nu}\rangle\}$ in which $\rho_{\mu\nu}$ is diagonal

$$\begin{aligned}\rho_{\tilde{\mu}} &= \langle\Psi_{\mathfrak{n}}|a^\dagger_{\tilde{\mu}}a_{\tilde{\mu}}|\Psi_{\mathfrak{n}}\rangle,\\ 0 &\le \rho_{\tilde{\mu}} \le 1,\end{aligned} \tag{2.26}$$

and is called the canonical or natural basis (see Appendix B). We can also construct the space dependent density by adding over all discrete quantum numbers σ

$$\rho^{(1)}(\boldsymbol{r}_1;\boldsymbol{r}'_1) = \sum_{\sigma_1}\rho^{(1)}(\boldsymbol{r}_1,\sigma_1;\boldsymbol{r}'_1,\sigma_1) = \sum_{\sigma_1}\sum_{\mu,\nu}\rho_{\nu\mu}\varphi^*_\nu(\boldsymbol{r}'_1,\sigma_1)\varphi_\mu(\boldsymbol{r}_1,\sigma_1). \tag{2.27}$$

A useful property of the density matrix approach comes from the calculations of expectation values of operators. Consider that $\hat{O}$ is a one-body observable given by

$$\hat{O} = \sum_{\mu,\nu}o_{\mu\nu}a^\dagger_\mu a_\nu, \tag{2.28}$$

then

$$\begin{aligned}\langle\Psi_{\mathfrak{n}}|\hat{O}|\Psi_{\mathfrak{n}}\rangle &= \sum_{\mu,\nu} o_{\mu\nu}\langle\Psi_{\mathfrak{n}}|a^{\dagger}_{\mu}a_{\nu}|\Psi_{\mathfrak{n}}\rangle \\ &= \sum_{\mu,\nu} o_{\mu\nu}\rho_{\nu\mu} = \mathrm{Tr}(\hat{O}\hat{\rho}).\end{aligned} \tag{2.29}$$

A related operator to the density 2.21, is the so-called anomalous pairing tensor of order n, given by

$$\begin{aligned}&\hat{\kappa}^{(n)}(\boldsymbol{r}_1,\sigma_1,...,\boldsymbol{r}_n,\sigma_n;\boldsymbol{r}'_1,\sigma'_1,...,\boldsymbol{r}'_n,\sigma'_n) \\ &\qquad = a(\boldsymbol{r}'_n,\sigma'_n)...a(\boldsymbol{r}'_1,\sigma'_1)a(\boldsymbol{r}_1,\sigma_1)...a(\boldsymbol{r}_n,\sigma_n),\end{aligned} \tag{2.30}$$

and the associated n-body pairing density

$$\begin{aligned}\kappa^{(n)}(\boldsymbol{r}_1,\sigma_1,...,\boldsymbol{r}_n,\sigma_n;\boldsymbol{r}'_1,\sigma'_1,...,\boldsymbol{r}'_n,\sigma'_n) &= \langle\Psi_{\mathfrak{n}}|\hat{\kappa}^{(n)}|\Psi_{\mathfrak{n}}\rangle \\ &= \binom{N}{n}\sum_{\sigma_{n+1},...,\sigma_N}\int \Psi_{\mathfrak{n}}(\boldsymbol{r}'_1,\sigma'_1,...,\boldsymbol{r}'_n,\sigma'_n,\boldsymbol{r}_{n+1},\sigma_{n+1},...,\boldsymbol{r}_N,\sigma_N) \\ &\qquad \times \Psi_{\mathfrak{n}}(\boldsymbol{r}_1,\sigma_1,...,\boldsymbol{r}_n,\sigma_n,\boldsymbol{r}_{n+1},\sigma_{n+1},...,\boldsymbol{r}_N,\sigma_N)d\boldsymbol{r}_{n+1}...d\boldsymbol{r}_N \\ &= \sum_{\nu_1,...,\nu_{2n}} \kappa_{\nu_1,...,\nu_{2n}}\varphi_{\nu_1}(\boldsymbol{r}'_n,\sigma'_n)...\varphi_{\nu_n}(\boldsymbol{r}'_1,\sigma'_1)\varphi_{\nu_{n+1}}(\boldsymbol{r}_1,\sigma_1)...\varphi_{\nu_{2n}}(\boldsymbol{r}_n,\sigma_n),\end{aligned} \tag{2.31}$$

where

$$\kappa_{\nu_1,...,\nu_{2n}} = \langle\Psi_{\mathfrak{n}}|a_{\nu_{2n}}...a_{\nu_1}|\Psi_{\mathfrak{n}}\rangle. \tag{2.32}$$

The Hermitian conjugate $\hat{\kappa}^{\dagger(n)}$ is also a useful and independent operator. Similarly, the one-body pairing tensor is given by

$$\hat{\kappa}^{(1)}(\boldsymbol{r}_1,\sigma_1;\boldsymbol{r}'_1,\sigma'_1) = \sum_{\nu,\mu}\kappa_{\mu\nu}\varphi_{\nu}(\boldsymbol{r}'_1,\sigma'_1)\varphi_{\mu}(\boldsymbol{r}_1,\sigma_1), \tag{2.33}$$

$$\kappa_{\mu\nu} = \langle\Psi_{\mathfrak{n}}|a_{\nu}a_{\mu}|\Psi_{\mathfrak{n}}\rangle. \tag{2.34}$$

Notice that the matrices κ and ρ cannot be diagonal in the same basis.

In a similar way as 2.29, for a two-body operator

$$\hat{F} = \sum_{\mu,\nu} f_{\mu\nu\alpha\beta}a^{\dagger}_{\mu}a^{\dagger}_{\nu}a_{\alpha}a_{\beta}, \tag{2.35}$$

its expectation value is given in terms of the density and pairing tensor matrices as

$$\begin{aligned}\langle\Psi_{\mathfrak{n}}|\hat{F}|\Psi_{\mathfrak{n}}\rangle &= \sum_{\mu,\nu,\alpha,\beta} f_{\mu\nu\alpha\beta}\langle\Psi_{\mathfrak{n}}|a^{\dagger}_{\mu}a^{\dagger}_{\nu}a_{\alpha}a_{\beta}|\Psi_{\mathfrak{n}}\rangle \\ &= \sum_{\mu,\nu,\alpha,\beta} f_{\mu\nu\alpha\beta}\left(\frac{1}{2}\rho_{\alpha\mu}\rho_{\beta\nu} + \frac{1}{4}\kappa^{*}_{\nu\mu}\kappa_{\beta\alpha}\right).\end{aligned} \tag{2.36}$$

Equation 2.29 and the first line of 2.36 always hold, but the second line of 2.36 holds for product states $|\Psi_{\mathfrak{n}}\rangle$ (see appendix B) by means of the Wick theorem (see appendix A).

Consider the specific case of the number operator

$$\hat{N} = \sum_{\mu} a_{\mu}^{\dagger} a_{\mu}, \tag{2.37}$$

which by applying 2.29 we get

$$\langle \Psi_{\mathfrak{n}} | \hat{N} | \Psi_{\mathfrak{n}} \rangle = \mathrm{Tr}(N\rho) = \mathrm{Tr}(\rho) = N. \tag{2.38}$$

Similarly for its variance we get by means of Wick's theorem

$$\sigma_N^2 = \langle \Psi_{\mathfrak{n}} | \hat{N}^2 | \Psi_{\mathfrak{n}} \rangle - \langle \Psi_{\mathfrak{n}} | \hat{N} | \Psi_{\mathfrak{n}} \rangle^2 = 2\mathrm{Tr}(\kappa\kappa^{\dagger}), \tag{2.39}$$

which states that $\kappa = 0$ is equivalent to particle conservation for the state $|\Psi_{\mathfrak{n}}\rangle$. One of the properties of pairing is that its associate wavefunctions violate particle number conservation symmetry and approximately behave as a condensate of bosons.

An important and widely used definition of the density is the local approximation where the position degrees of freedom are reduced to

$$\hat{\rho}(\boldsymbol{r}) = \sum_{i=1}^{N} \delta(\boldsymbol{r}_i - \boldsymbol{r}), \tag{2.40}$$

so that its associated single-particle density is

$$\begin{aligned} \rho^{(n)}(\boldsymbol{r}, \sigma; \boldsymbol{r}, \sigma) = \sum_{\sigma_{n+1}, \ldots, \sigma_N} \binom{N}{n} \int \Psi_{\mathfrak{n}}^{*}(\boldsymbol{r}, \sigma, \boldsymbol{r}_{n+1}, \sigma_{n+1}, \ldots, \boldsymbol{r}_N, \sigma_N) \\ \times \Psi_{\mathfrak{n}}(\boldsymbol{r}, \sigma, \boldsymbol{r}_{n+1}, \sigma_{n+1}, \ldots, \boldsymbol{r}_N, \sigma_N) d\boldsymbol{r}_{n+1} \ldots d\boldsymbol{r}_N, \end{aligned} \tag{2.41}$$

from which we can get the space local density distribution

$$\rho^{(n)}(\boldsymbol{r}) = \sum_{\sigma} \rho(\boldsymbol{r}, \sigma; \boldsymbol{r}, \sigma). \tag{2.42}$$

2.1.4 Time reversal symmetry

We introduce the concept of time reversal here since it is an important property of fermion interactions which show a strong correlation between time reversed counterparts, as observed in electronic systems and nuclei. Time reversal refers to the inversion of the "arrow" of time in the dynamics of physical systems. In the classical sense of dynamical variables, this refers to the transformation $t \to -t$ implying that position $\boldsymbol{r} \to \boldsymbol{r}$ is called time-even while momentum and angular momentum $\boldsymbol{p} \to -\boldsymbol{p}$ and $\boldsymbol{L} \to -\boldsymbol{L}$ are called time-odd. In quantum mechanics, this translates to transformations of the operators $\hat{\boldsymbol{r}} \to \hat{\mathcal{T}}\hat{\boldsymbol{r}}\hat{\mathcal{T}}^{\dagger} = \hat{\boldsymbol{r}}$ and $\hat{\boldsymbol{p}} = -i\hbar\nabla \to \hat{\mathcal{T}}(-i\hbar\nabla)\hat{\mathcal{T}}^{\dagger} = i\hbar\nabla$ so that the canonical commutation relation changes to [23, 24] $[\hat{r}_i, \hat{p}_i] = i\hbar \to [\hat{r}_i, -\hat{p}_i] = -i\hbar$. The angular momentum and spin are also time-odd and transform like $\hat{\boldsymbol{l}} \to \hat{\mathcal{T}}\hat{\boldsymbol{l}}\hat{\mathcal{T}}^{\dagger} = -\hat{\boldsymbol{l}}$ and $\hat{\boldsymbol{s}} \to \hat{\mathcal{T}}\hat{\boldsymbol{s}}\hat{\mathcal{T}}^{\dagger} = -\hat{\boldsymbol{s}}$, respectively, which imply for the total angular momentum $\hat{\boldsymbol{j}} = \hat{\boldsymbol{l}} + \hat{\boldsymbol{s}} \to \hat{\mathcal{T}}\hat{\boldsymbol{j}}\hat{\mathcal{T}}^{\dagger} = -\hat{\boldsymbol{j}}$.

We can formulate an operator for time reversal in quantum mechanics and denote it by $\hat{\mathcal{T}}$. Schrödinger equation must be invariant under time reversal, which requires that the action of the time reversal operator on the constant $i\hbar$ must be the conjugation of it. Such property expressed by

$$\hat{\mathcal{T}}\alpha = \alpha^*\hat{\mathcal{T}}, \tag{2.43}$$

for $\alpha \in \mathbb{C}$ and is called anti-linearity.

Since the spherical symmetry is important in nuclear theory, we are interested in the action of the time-reversal on states of angular momentum j and projection m denoted as $|jm\rangle$. Because $\hat{\boldsymbol{j}} \to -\hat{\boldsymbol{j}}$, time reversal will conserve $\hat{\boldsymbol{j}}^2$ but not $\hat{j}_z$. If $\hat{\mathcal{T}}$ is composed with a rotation around the y-axis by an angle of π, $\hat{j}_z$ will be conserved. Thus, the states $|jm\rangle$ are eigenstates of the composition $\hat{R}_y(\pi)\hat{\mathcal{T}}$ with eigenvalue 1, which defines the standard phase convention for $|jm\rangle$. Given this, the action of $\hat{\mathcal{T}}$ on $|jm\rangle$ can be deduced as

$$\hat{\mathcal{T}}|jm\rangle = \hat{R}_y^{-1}(\pi)\hat{R}_y(\pi)\hat{\mathcal{T}}|jm\rangle = \hat{R}_y^{-1}(\pi)|jm\rangle = (-1)^{j-m}|j-m\rangle, \tag{2.44}$$

since the Wigner-d matrix is

$$\langle jm|\hat{R}_y^{-1}(\pi)|jm'\rangle = d^j_{mm'}(\pi) = (-1)^{j-m}\delta_{mm'}. \tag{2.45}$$

Thus, the action of time reversal in spherical-symmetric or axial-symmetric states will cause the inversion of the projection of the total angular momentum and the appearance of a phase. This property is important for the concepts of pairing in the nucleus and the Bogoliubov transformation as explained below.

2.2 Seniority model of pairing

As mentioned above, the nuclear interaction carries a strong short-range residual component called pairing that is not accounted in the mean-field independent-particle potential. This interaction causes the wavefunctions to not be able to be represented by a single-particle-conserving Slater determinant. The seniority model is one of the elementary approaches to pairing. It considers a system where the interaction is given by a one-body mean-field $\hat{H}_{\mathrm{SP}}$ and the residual interaction comes from a short range pairing term as $\hat{V}_{\mathrm{P}}$

$$\hat{H} = \hat{H}_{\mathrm{SP}} + \hat{V}_{\mathrm{P}}. \tag{2.46}$$

A pair is defined as two nucleons of the same kind (π stands for proton while ν stands for neutron) that form a time reversed pair and couple to total angular momentum $J = 0$. This setup of time reversed pairs have large spatial overlap which is energetically favored and increases the binding energy further. Since it is a residual interaction, it must be expressed as a two-body interaction of pairs which in general can happen across several shells. By adopting a spherical shell model basis, we have a pair $|jm\rangle \otimes |j-m\rangle$ coupled to $|J=0, M=0\rangle$ and denoted as $|jj;00\rangle$. We focus now only in the properties

of $\hat{V}_P$ which in second quantization is given by

$$\hat{V}_P = \frac{1}{2} \sum_{\substack{j,j' \\ m,m'>0}} \langle jj;00|\hat{V}_P|j'j';00\rangle a^\dagger_{jm} a^\dagger_{j-m} a_{j'-m'} a_{j'm'}. \tag{2.47}$$

Usually the matrix element is approximated by a positive constant G called the pairing strength

$$-2G = \langle jj;00|\hat{V}_P|j'j';00\rangle, \tag{2.48}$$

whose phenomenological values are given by

$$\begin{aligned} G_\pi &= \frac{17}{A} \qquad [\text{MeV}], \\ G_\nu &= \frac{23}{A} \qquad [\text{MeV}]. \end{aligned} \tag{2.49}$$

A multi-shell analysis is possible [18], but for simplicity of presentation we will reduce to the case of a single shell $j = j'$ with N particles holding $0 \leq N \leq 2j+1$.

We can rewrite 2.47 as

$$\hat{V}_P = -G\hat{S}^\dagger \hat{S}, \tag{2.50}$$

where $\Omega = \frac{1}{2}(2j+1)$ is the maximum number of pairs in a shell j and

$$\begin{aligned} \hat{S}^\dagger &= \sum_{m>0} a^\dagger_{jm} a^\dagger_{j-m} = \sum_{m>0} \hat{s}^\dagger_m, \\ \hat{S} &= \sum_{m>0} a_{j-m} a_{jm} = \sum_{m>0} \hat{s}_m, \end{aligned} \tag{2.51}$$

are creation and destruction operators of time-reversed pairs. Defining

$$\begin{aligned} \hat{s}^0_m &= \frac{1}{2}(a^\dagger_{jm} a_{jm} + a^\dagger_{j-m} a_{j-m} - 1), \\ \hat{S}^0 &= \frac{1}{2} \sum_{m>0} (a^\dagger_{jm} a_{jm} + a^\dagger_{j-m} a_{j-m} - 1) = \sum_{m>0} \hat{s}^0_m, \end{aligned} \tag{2.52}$$

we can establish that the operators in 2.51 follow the algebra of $\mathfrak{su}(2)$ in their spherical components

$$\begin{aligned} \left[\hat{s}^\dagger_m, \hat{s}_m\right] &= 2\hat{s}^0_m, \\ \left[\hat{s}^0_m, \hat{s}_m\right] &= \hat{s}^\dagger_m, \\ \left[\hat{s}^0_m, \hat{s}^\dagger_m\right] &= -\hat{s}_m, \end{aligned} \tag{2.53}$$

which is called the quasi-spin algebra. $\hat{S}^\dagger$ and $\hat{S}$ behave as the components $+$ and $-$ of a vector operator, respectively, so we can rewrite 2.50 as

$$\hat{V}_P = -G(\hat{\boldsymbol{S}}^2 - (\hat{S}^0)^2 + \hat{S}^0), \tag{2.54}$$

which by the studies of the algebra $\mathfrak{su}(2)$, its eigenvectors are $|S, S_0\rangle$, the eigenvalues

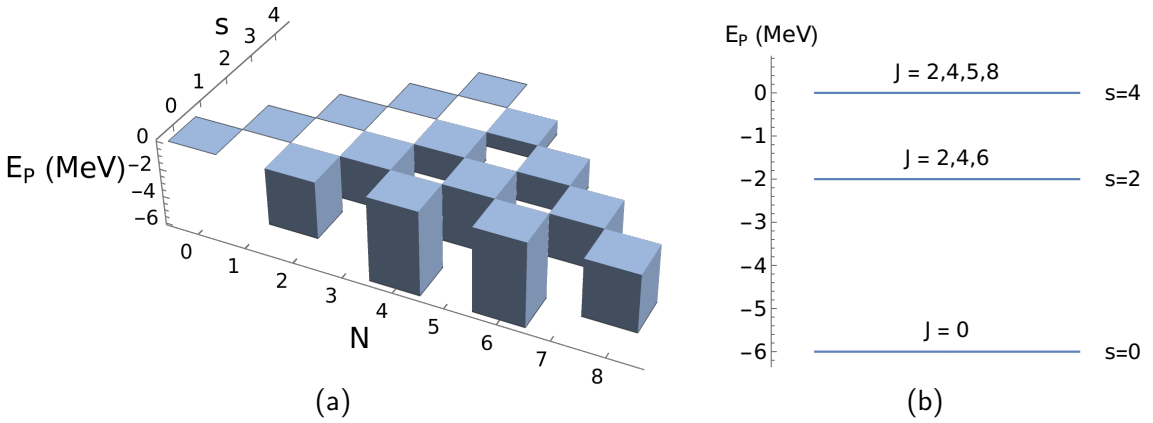

Figure 2.1: (a) Pairing energies of the seniority model for $G = 1$ MeV and a single shell $j = 7/2$ in function of number of particles N and seniority s. (b) Energies and spins of the $j = 7/2$ and $N = 4$ for all allowed seniority values.

of $\hat{V}_P$ are given by

$$E_P(S) = -G(S(S+1) - S_0^2 + S_0), \tag{2.55}$$

and the quasi-spin quantum number adopts the values

$$S = \begin{cases} \frac{\Omega}{2}, \frac{\Omega}{2} - 1, \frac{\Omega}{2} - 2, ..., \frac{|\Omega - N|}{2}, & \text{for } N \text{ even}, \\ \frac{\Omega}{2} - \frac{1}{2}, \frac{\Omega}{2} - \frac{3}{2}, \frac{\Omega}{2} - \frac{5}{2}, ..., \frac{|\Omega - N|}{2}, & \text{for } N \text{ odd}, \end{cases} \tag{2.56}$$

interpreted as proportional to the total number of pair-particle and pair-holes in a given configuration in shell j. We can now introduce the seniority quantum number s given by

$$\begin{aligned} s &= \Omega - 2S, \\ s &= \begin{cases} 0, 2, 4, ..., \Omega, & \text{for } N \text{ even}, \\ 1, 3, 5, ..., \Omega - 1, & \text{for } N \text{ odd}, \end{cases} \end{aligned} \tag{2.57}$$

which quantifies the number of unpaired nucleons and defines a new basis $|N, s\rangle$. Rewriting 2.55 in terms of s we get

$$E_P(N, s) = -\frac{G}{4}(N - s)(2\Omega - s - N + 2). \tag{2.58}$$

Fig. 2.1 shows the dependence of pairing energy with respect to s and N for a shell $j = 7/2$ with $G = 1$ MeV. The lowest energy configurations are given by the smallest possible values of s, namely $s = 0$ for even N nuclei and $s = 1$ for odd N.

The degeneracy D for a given state of seniority s is given by

$$D(s) = \begin{cases} \binom{2\Omega}{s}, & \text{for } s < 2, \\ \binom{2\Omega}{s} - \binom{2\Omega}{s-2}, & \text{for } s \geq 2, \end{cases} \tag{2.59}$$

which is a useful expression for assigning the angular momentum values of each seniority eigenstate. The validity of equation 2.59 is constrained to $N + s \leq 2j + 1$ which arises

from the $m-$scheme of allowed angular momentum states degeneracy that cannot be surpassed [25, 26].

For odd-A nuclei the unpaired nucleon will not contribute to the pairing interaction and it will result in the lowest state ($s = 1$) while for even-even nuclei the lowest configuration is the one where all nucleons are paired ($s = 0$). Even though it can become very complex via the incorporation of several shells and the introduction of broken pairs, its relative simplicity cannot account for the full pair interactions in the nucleus. However, many of its qualitative features remain valid in more realistic cases.

2.3 The special Bogoliubov transformation

Following the idea of section 2.1, we aim now to perform transformations on the fermion space to capture part of the residual interaction in a simpler fermion quasiparticle algebraic structure. The simplest transformation that can be formulated in the fermion space involves a linear combination of creation and annihilation operators. This is called the Bogoliubov transformation and is given by

$$\begin{aligned} \alpha_i^\dagger &= u_i a_i^\dagger - v_i a_{\bar{i}}, \\ \alpha_i &= -v_i a_{\bar{i}}^\dagger + u_i a_i, \end{aligned} \tag{2.60}$$

where $\alpha_i^\dagger$ and α_i are the quasiparticle creation and annihilation operators for all states i in the original fermion space and the coefficients u_i, $v_i \in \mathbb{R}$ are called the Bogoliubov amplitudes. These follow $u_i = u_{\bar{i}}$ and $v_i = -v_{\bar{i}}$. The symbol $\bar{i}$ denotes the time reversed state of i. This condition is not mandatory in the transformation rule, it suffices that the model space states are paired in any way, but it is a standard to pair time reversed counterparts in nuclear physics. The quasiparticles in 2.61 have a nature intermediate between particles and holes in the shell-model sense. Inverse relations of 2.61 read

$$\begin{aligned} a_i^\dagger &= u_i \alpha_i^\dagger + v_i \alpha_{\bar{i}}, \\ a_i &= v_i \alpha_{\bar{i}}^\dagger + u_i \alpha_i. \end{aligned} \tag{2.61}$$

This newly defined set of quasiparticle operators need to hold all anti-commutation rules of the original space, from where we can deduce the normalization conditions

$$\begin{aligned} &\{\alpha_i^\dagger, \alpha_j\} = (u_i u_j + v_i v_j)\delta_{ij} = \delta_{ij}, \\ &\implies \begin{cases} u_i^2 + v_i^2 & = 1, \qquad i = j \\ u_i u_j + v_i v_j & = 0, \qquad i \neq j. \end{cases} \end{aligned} \tag{2.62}$$

Also, the fermion vacuum $|0\rangle$ is transformed to a quasiparticle vacuum $|\Phi\rangle$ such that the condition

$$\alpha_i |\Phi\rangle = a_i |0\rangle = 0 \qquad \forall i, \tag{2.63}$$

is fulfilled.

The entire set of observables is mapped to the quasiparticle space according to 2.61.

Taking the Hamiltonian with mean-field and two-body particle conserving residual interaction

$$H = \sum_{i,j} t_{ij} a_i^\dagger a_j + \frac{1}{4} \sum_{i,j,k,l} \bar{v}_{ijkl} a_i^\dagger a_j^\dagger a_l a_k, \tag{2.64}$$

$$\bar{v}_{ijkl} = v_{ijkl} - v_{ijlk}, \tag{2.65}$$

we obtain the following form in the normal-ordered quasiparticle space

$$\begin{aligned} H =& H^{(00)} + \sum_{i,j} H_{ij}^{(11)} \alpha_i^\dagger \alpha_j + \sum_{i,j} \Big(H_{ij}^{(20)} \alpha_i^\dagger \alpha_j^\dagger + h.c. \Big) \\ &+ \sum_{i,j,k,l} \Big(H_{ijkl}^{(22)} \alpha_i^\dagger \alpha_j^\dagger \alpha_k \alpha_l + h.c. \Big) + \sum_{i,j,k,l} \Big(H_{ijkl}^{(31)} \alpha_i^\dagger \alpha_j^\dagger \alpha_k^\dagger \alpha_l + h.c. \Big) \\ &+ \sum_{i,j,k,l} \Big(H_{ijkl}^{(40)} \alpha_i^\dagger \alpha_j^\dagger \alpha_k^\dagger \alpha_l^\dagger + h.c. \Big) \\ =& H^{\text{q.p.}} + H_{\text{RI}}^{\text{q.p.}}, \end{aligned} \tag{2.66}$$

where the only terms we are concerned about after the transformation are $H^{(00)}$, $H^{(11)}$ and $H^{(20)}$. The explicit form of $H^{(00)}$ is given by

$$H^{(00)} = \sum_i t_{ii} v_i^2 + \frac{1}{4} \sum_{i,j} \Big(\bar{v}_{i\bar{i}\bar{j}j} u_i v_i u_j v_j + 2 \bar{v}_{ijij} v_i^2 v_j^2 \Big), \tag{2.67}$$

and is the only term that survives after calculating expectation values in the quasiparticle space. The terms $H^{(22)}$, $H^{(31)}$ and $H^{(40)}$ will be considered as residual quasiparticle interaction $H_{\text{RI}}^{\text{q.p.}}$. Notice how $H^{(00)}$ and $H^{(11)}$ contain terms of the original residual interaction in the one-body quasiparticle scheme, as was initially aimed. A useful computer library to obtain explicit forms of the terms in 2.66 is the Mathematica package `SNEG` [27].

2.3.1 Bardeen-Cooper-Schreiffer (BCS) theory

A more sophisticated approach to pairing is given in this section. The BCS theory was originally devised for solid state physics as an explanation for superconductivity [13], where pairs of electrons interact via a long range attractive force forming a boson-like condensate that manifests as zero resistance to current of certain materials under specific conditions. The effects of pairing had been known for a while in the nucleus, so the physicist of the time quickly adapted the BCS model to the atomic nucleus [14] finding it fructiferous in explaining several aspects of it.

As described in the appendix B, the product state of an even particle system can adopt a particular mathematical form via the Thouless theorem as

$$|\Phi\rangle_{\text{even}} = \mathcal{A} \exp\Big(-\frac{1}{2} \sum_{i,j} Z_{ij}^\dagger a_i^\dagger a_j^\dagger \Big) |0\rangle, \tag{2.68}$$

where Z_{ij} is the Thouless matrix and $\mathcal{A}$ denotes the normalization factor. In the

canonical basis, it can be rewritten as

$$|\Phi\rangle_{\text{even}} = \mathcal{A} \exp\Big(\sum_{i>0} s_i^* z_i \bar{a}_{\bar{i}}^\dagger \bar{a}_i^\dagger \Big) |0\rangle, \tag{2.69}$$

where the bar in the creation operators $\bar{a}^\dagger$ denote the canonical basis and $\bar{i}$ denotes a canonically conjugated state, usually corresponding to the time reversed state. The summation $i > 0$ denotes sum over half of the space, *i.e.*, only over one state representative of the pair. Being aware of the Baker–Campbell–Hausdorff (BCH) theorem and because the square of any creation fermion operator vanishes, we can rewrite 2.69 as a product of exponentials

$$|\Phi\rangle_{\text{even}} = \mathcal{A} \prod_{i>0} \exp(s_i^* z_i \bar{a}_{\bar{i}}^\dagger \bar{a}_i^\dagger)|0\rangle = \mathcal{A} \prod_{i>0} (1 + s_i^* z_i \bar{a}_{\bar{i}}^\dagger \bar{a}_i^\dagger)|0\rangle. \tag{2.70}$$

By means of the Onishi theorem (see appendix B), the normalization factor is given by

$$\mathcal{A} = \frac{1}{\prod_{i>0} \sqrt{(1 + z_i^2)}}, \tag{2.71}$$

after replacing 2.71 into 2.70 we get

$$|\Phi\rangle_{\text{even}} = \prod_{i>0} (u_i + v_i \bar{a}_{\bar{i}}^\dagger \bar{a}_i^\dagger)|0\rangle = |\text{BCS}\rangle_{\text{even}}, \tag{2.72}$$

which is the so called BCS ground state ansatz in the canonical basis. The product state described above belongs to the Fock space, which means it has no fixed number of particles, but instead it is a superposition of even-particle states.

The state 2.72 is the starting point of the BCS theory as the coefficients u_i and v_i which are the same of the Bogoliubov transformation 2.61 play the role of variational parameters. Following 2.63, the associate BCS quasiparticle operators hold

$$\alpha_i |\text{BCS}\rangle = 0 \qquad \forall i. \tag{2.73}$$

Let us remove from now on the bar on the creation and destruction operators for simplicity in the notation. The expectation value of the number operator with respect to the BCS state is

$$\langle \text{BCS}|\hat{N}|\text{BCS}\rangle = 2 \sum_{i>0} v_i^2, \tag{2.74}$$

so that the interpretation of the coefficients v_i^2 are the occupations of state $|i\rangle$ while the u_i^2 denote the corresponding vacancies. Because the particle number is no longer conserved, the standard deviation of the operator will be non-zero and has a value of

$$\Delta N^2 = 4 \sum_{i>0} u_i^2 v_i^2. \tag{2.75}$$

We constrain the particle number in the Hamiltonian $H^{\text{q.p.}}$ of 2.66 by

$$H' = H - \lambda(N - N_0), \tag{2.76}$$

and its expectation value following 2.67 is given by

$$\langle H' \rangle = \sum_i \left[(t_{ii} - \lambda) v_i^2 + \frac{1}{2} \sum_j \bar{v}_{ijij} v_i^2 v_j^2 \right] + \frac{1}{4} \sum_{ij} \bar{v}_{i\bar{i}j\bar{j}} u_i v_i u_j v_j, \tag{2.77}$$

over which we perform a non-constrained variation, where λ is a Lagrange multiplier called the Fermi energy. The variation is given by

$$\delta\langle H' \rangle = \sum_i \left(\frac{\partial \langle H' \rangle}{\partial u_i} \delta u_i + \frac{\partial \langle H' \rangle}{\partial v_i} \delta v_i \right) + \frac{\partial \langle H' \rangle}{\partial \lambda} \delta\lambda = 0, \tag{2.78}$$

because of condition 2.62, we have

$$\begin{aligned} \delta\langle H' \rangle &= \sum_i \left(1 + \frac{\partial v_i}{\partial u_i} \right) \frac{\partial \langle H' \rangle}{\partial v_i} \delta v_i + (N - N_0) \delta\lambda \\ &= \sum_i \left(1 - \frac{u_i}{v_i} \right) \frac{\partial \langle H' \rangle}{\partial v_i} \delta v_i + (N - N_0) \delta\lambda = 0, \end{aligned} \tag{2.79}$$

each variation must vanish independently so that for the variation δv_i after calculating $\partial\langle H' \rangle / \partial v_i$ we get the BCS equation

$$2\tilde{\epsilon}_i u_i v_i + \Delta_i (v_i^2 + u_i^2) = 0, \tag{2.80}$$

where

$$\begin{aligned} \tilde{\epsilon}_i &= \frac{1}{2} \left(t_{ii} + t_{\bar{i}\bar{i}} + \sum_j \left(\bar{v}_{ijij} + \bar{v}_{\bar{i}j\bar{i}j} \right) v_j^2 \right) - \lambda, \\ \Delta_i &= -\sum_{j>0} \bar{v}_{i\bar{i}j\bar{j}} u_j v_j, \end{aligned} \tag{2.81}$$

are called the modified single-particle energy and pairing gap respectively. The non-trivial solution ($v_i u_i \neq 0$) [28] of equation 2.80 results in

$$\begin{aligned} v_i^2 &= \frac{1}{2} \left(1 - \frac{\tilde{\epsilon}_i}{\sqrt{\tilde{\epsilon}_i^2 + \Delta_i^2}} \right), \\ u_i^2 &= \frac{1}{2} \left(1 + \frac{\tilde{\epsilon}_i}{\sqrt{\tilde{\epsilon}_i^2 + \Delta_i^2}} \right), \end{aligned} \tag{2.82}$$

these are physically interpreted as the occupancies and vacancies of single quasiparticle states i, respectively. The quantity

$$\tilde{E}_i = \sqrt{\tilde{\epsilon}_i^2 + \Delta_i^2}, \tag{2.83}$$

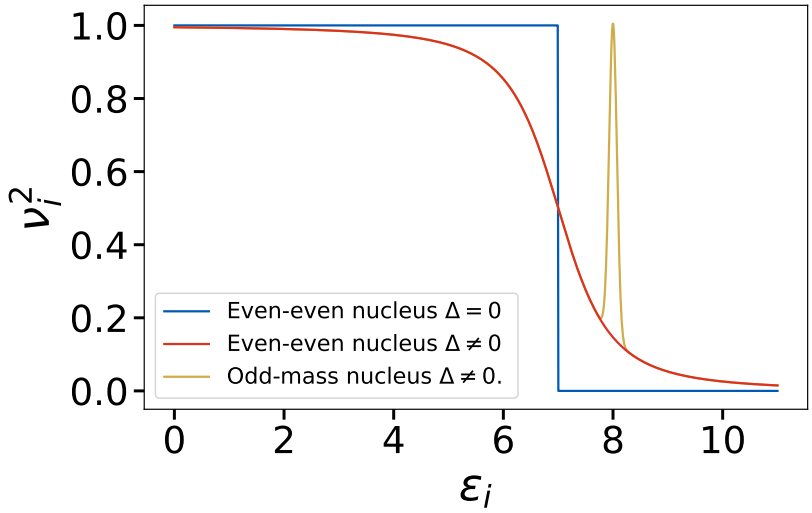

Figure 2.2: Effects of pairing interaction and blocking in nuclear single-particle occupations.

is called the quasiparticle energy as it can be identified as the expression for $\mathcal{H}_{ii}^{(11)}$ of 2.67 in the basis in which $h_{ij} = t_{ij} + \sum_k v_{ikjk} v_j^2$ is diagonal.

If the solutions 2.82 are replaced in 2.81, then we obtain the so called gap equation

$$\Delta_i = -\frac{1}{2} \sum_{j>0} \bar{v}_{i\bar{i}j\bar{j}} \frac{\Delta_j}{\sqrt{\tilde{\epsilon}_j^2 + \Delta_j^2}} \tag{2.84}$$

which shows explicitly the non-linear coupling of the equations and thus the need to solve them via numerical iterative methods.

In a simplified case where the residual interaction is just the pairing term of the form 2.47 with constant matrix elements and the one-body term is diagonal as

$$H_P = \sum_i \epsilon_i (a_i^\dagger a_i + a_{\bar{i}}^\dagger a_{\bar{i}}) - \frac{G}{2} \sum_{i,j} a_i^\dagger a_{\bar{i}}^\dagger a_{\bar{j}} a_j, \tag{2.85}$$

then, equation 2.77 reduces to

$$\langle H_P \rangle = 2 \sum_{i>0} \left(\tilde{\epsilon}_i v_i^2 + \frac{1}{2} G v_i^4 \right) - \frac{\Delta^2}{G}, \tag{2.86}$$

where the gap parameter looses its dependence on a particular state as

$$\begin{aligned} \Delta &= G \sum_{j>0} u_j v_j, \\ \tilde{\epsilon}_i &= \epsilon_i - G v_i^2 - \lambda. \end{aligned} \tag{2.87}$$

The terms Gv_i^2 and Gv_i^4 are usually neglected. Equations 2.82 and 2.84 now read as

$$\begin{aligned} v_i^2 &= \frac{1}{2}\left(1 - \frac{\epsilon_i - \lambda}{\sqrt{(\epsilon_i - \lambda)^2 + \Delta^2}}\right), \\ u_i^2 &= \frac{1}{2}\left(1 + \frac{\epsilon_i - \lambda}{\sqrt{(\epsilon_i - \lambda)^2 + \Delta^2}}\right), \end{aligned} \tag{2.88}$$

$$\Delta = \frac{G}{2}\sum_{j>0}\frac{\Delta}{\sqrt{\epsilon_j^2 + \Delta^2}} \tag{2.89}$$

The quantity Δ quantifies the strength of the pairing interaction and influences the single-particle orbital occupation by softening its values around the Fermi surface by partially occupying orbitals above and partially emptying orbitals below in an analogous situation as in finite temperature Fermi gases [29]. This phenomenon can be seen in Fig. 2.2 where the trivial solution ($u_i v_i = 0\ \forall i$) and a non-zero pairing gap situation is shown. Naturally, a different pairing gap exists for neutrons Δ_ν and protons Δ_π. Experimentally, the pairing gap is evidenced via the so called odd-even mass staggering where the mass of an odd-even nucleus is larger than the mean of its even-even neighbours following

$$M(A) = \frac{1}{2}(M(A-1) + M(A+1)) + \Delta, \tag{2.90}$$

this expression is used to fit the values of Δ_π and Δ_ν in theoretical applications. It is worth noticing that theoretically for full shells we have $\Delta \to 0$ (see chapter 5), which implies that the condensate is not realized and a trivial solution is obtained. However, the contribution from pairing to the total energy is still non-zero. An empirical formula for the pairing gap is

$$\Delta = \frac{12}{A^{\frac{1}{2}}}\ \text{MeV}, \tag{2.91}$$

Blocking

In the previous section, the case of even particle number systems was analysed. When the total number of fermions is large this issue becomes irrelevant, but in few fermion systems it is crucial to study the unpaired or odd-particle number case for the understanding of the single-particle influence in the hole system and its interaction with the rest of it. The ground state is given by

$$|\Phi\rangle_{\text{odd}} = \alpha_j^\dagger |\text{BCS}\rangle_{\text{even}} = a_j^\dagger \prod_{i\neq j>0}(u_i + v_i \tilde{a}_{\bar{i}}^\dagger \tilde{a}_i^\dagger)|0\rangle = |\text{BCS}\rangle_{\text{odd}}, \tag{2.92}$$

where the particle created in orbital j on top of the even system does not participate in the pairing. The mathematical form of 2.92 constrains the occupancies $v_j = 1$ and $v_{\bar{j}} = 0$ simultaneously. This is illustrated in Fig. 2.2 and is the effect of blocking where the j^{th} column and row of the corresponding Thouless matrix (see B.0.2) are zero.

This is an essential aspect for the description of odd and odd-odd mass nuclei, which

in practice is realized by blocking a given eigenstate of the Hamiltonian in every step of the self-consistent iteration. Such state can be selected by calculating the overlap between all the quasiparticle orbitals and a fixed eigenstate of H followed across the iterations. This methodology has been implemented in [30] and extensively applied for example in [31, 32, 33] and this work. The initial blocked eigenstate of H should be constrained to a specific set of single-particle properties that are aimed to be conserved accordingly to the symmetries of the system and that will reproduce its observables. In the case of this work, the axiality is a conserved symmetry for which the Nilsson states $|[Nn_z\Lambda]\Omega\rangle$ [34, 35] serve to track the blocked quasiparticles (see chapter 5). These results also hold for next section where the HFB generalization of BCS is presented.

2.4 The general Bogoliubov transformation

The aim of this section is presenting the Hartree-Fock-Bogoliubov (HFB) theory as an extension of the BCS approach, where a generalization of the Bogoliubov transformation is implemented involving all n states in the model space as

$$\begin{aligned} \alpha_i^\dagger &= \sum_j \Big(u_{ji} a_j^\dagger + v_{ji} a_j \Big), \\ \alpha_i &= \sum_j \Big(v_{ji}^* a_j^\dagger + u_{ji}^* a_j \Big), \end{aligned} \tag{2.93}$$

thus, we introduce now the doubled dimension representation to facilitate derivations. We define a $2n$ dimensional vector of operators as

$$c = \begin{pmatrix} a \\ a^\dagger \end{pmatrix} = (a_1 ... a_n \; a_1^\dagger ... a_n^\dagger)^T \tag{2.94}$$

so that the transformation 2.93 can be expressed via a $2n \times 2n$ matrix

$$\mathcal{W} = \begin{pmatrix} U & V^* \\ V & U^* \end{pmatrix}, \tag{2.95}$$

$$\begin{pmatrix} \alpha \\ \alpha^\dagger \end{pmatrix} = \begin{pmatrix} U^\dagger & V^\dagger \\ V^T & U^T \end{pmatrix} \begin{pmatrix} a \\ a^\dagger \end{pmatrix} = \mathcal{W}^\dagger \begin{pmatrix} a \\ a^\dagger \end{pmatrix}, \tag{2.96}$$

and the anti-commutation rules of the quasiparticles 2.93 imply

$$\begin{aligned} U^\dagger U + V^\dagger V = \mathbb{I}, \qquad & UU^\dagger + V^* V^T = \mathbb{I} \\ U^T V + V^T U = 0, \qquad & UV^\dagger + V^* U^T = 0, \end{aligned} \tag{2.97}$$

which also guarantees the unitarity of $\mathcal{W}$. We know from the Bloch-Messiah-Zumino theorem [36, 37], that a unitary matrix of the form 2.95 can be decomposed as

$$\mathcal{W} = \begin{pmatrix} D & 0 \\ 0 & D^* \end{pmatrix} \begin{pmatrix} \bar{U} & \bar{V} \\ \bar{V} & \bar{U} \end{pmatrix} \begin{pmatrix} C & 0 \\ 0 & C^* \end{pmatrix} \tag{2.98}$$

where $\mathcal{C}$, $\mathcal{D}$ are unitary matrices and $\bar{U}$, $\bar{V}$ are the Bogoliubov amplitudes in the canonical basis given by the block diagonal form

$$\bar{U} = \begin{pmatrix} 0 & & & & & & & & 0 \\ & \ddots & & & & & & & \\ & & 0 & & & & & & \\ & & & \boxed{\begin{matrix} u_1 & 0 \\ 0 & u_1 \end{matrix}} & & & & & \\ & & & & \ddots & & & & \\ & & & & & \boxed{\begin{matrix} u_k & 0 \\ 0 & u_k \end{matrix}} & & & \\ & & & & & & 1 & & \\ & & & & & & & \ddots & \\ 0 & & & & & & & & 1 \end{pmatrix}, \tag{2.99}$$

$$\bar{V} = \begin{pmatrix} 1 & & & & & & & & 0 \\ & \ddots & & & & & & & \\ & & 1 & & & & & & \\ & & & \boxed{\begin{matrix} 0 & v_1 \\ -v_1 & 0 \end{matrix}} & & & & & \\ & & & & \ddots & & & & \\ & & & & & \boxed{\begin{matrix} 0 & v_k \\ -v_k & 0 \end{matrix}} & & & \\ & & & & & & 0 & & \\ & & & & & & & \ddots & \\ 0 & & & & & & & & 0 \end{pmatrix}, \tag{2.100}$$

thus, the function of matrix $\mathcal{D}$ is the change of basis from an arbitrary to the canonical basis, $\bar{U}$ and $\bar{V}$ constitute a special Bogoliubov transformations of the type in section 2.3 and $\mathcal{C}$ performs a linear unitary transformation between the quasiparticle operators.

The vacuum of the quasiparticle operators α will be denoted as $|\text{HFB}\rangle$ and follows condition 2.63, namely

$$\alpha_i|\text{HFB}\rangle = 0, \tag{2.101}$$

thus we can calculate one-body density matrix and anomalous pairing tensor by means of 2.93 and 2.101 as

$$\begin{aligned} \rho =& \langle \text{HFB}|a^\dagger a|\text{HFB}\rangle = V^* V^T, \\ \kappa =& \langle \text{HFB}|aa|\text{HFB}\rangle = V^* U^T = -UV^\dagger. \end{aligned} \tag{2.102}$$

We postulate these now as it can be proved that different Bogoliubov transformations lead to different density matrices but there is a one-to-one correspondence between ρ and $|\text{HFB}\rangle$ (see chapter 3). Furthermore, using the Bloch-Messiah-Zumino decomposition we can show that

$$\begin{aligned} \rho =& D\bar{V}D^\dagger, \\ \kappa =& D\bar{U}\bar{V}D^T, \end{aligned} \tag{2.103}$$

which implies that in the canonical basis ρ is diagonal while κ is skew-symmetric

composed by blocks as

$$\rho = \begin{pmatrix} 1 & & & & 0 \\ & \ddots & & & \\ & & \boxed{\begin{matrix} -v_i^2 & 0 \\ 0 & -v_{\bar{i}}^2 \end{matrix}} & & \\ & & & \ddots & \\ 0 & & & & 0 \end{pmatrix}, \qquad \kappa = \begin{pmatrix} 0 & & & & 0 \\ & \ddots & & & \\ & & \boxed{\begin{matrix} 0 & u_i v_i \\ -u_i v_i & 0 \end{matrix}} & & \\ & & & \ddots & \\ 0 & & & & 0 \end{pmatrix}. \tag{2.104}$$

From 2.97 and 2.102 the following relations hold

$$\begin{aligned} \rho^2 + \kappa\kappa^\dagger &= \rho, \\ \rho\kappa - \kappa\rho^* &= 0, \end{aligned} \tag{2.105}$$

which demonstrate that the pairing tensor deviates ρ from being a projective matrix, *i.e*, $\rho^2 = \rho$. This case is realized for example when the particle number is fixed so that $\kappa = 0$.

It is natural to extend the density matrix to the doubled dimension representation where it is generalized by the so-called Valatin matrix given by

$$\mathcal{R} = \begin{pmatrix} \rho & \kappa \\ -\kappa^* & 1 - \rho^* \end{pmatrix} = \begin{pmatrix} V^* V^T & V^* U^T \\ U^* V^T & U^* U^T \end{pmatrix}, \tag{2.106}$$

so that

$$\mathcal{R} = \mathcal{R}^2, \tag{2.107}$$

and

$$\tilde{\mathcal{R}} = \mathcal{W}^\dagger \mathcal{R} \mathcal{W} = \begin{pmatrix} 0 & 0 \\ 0 & \mathbb{I}, \end{pmatrix} \tag{2.108}$$

meaning that its eigenvalues are 0 and 1 for the eigenstates $(U, V)_k^T$ and $(V^*, U^*)_k^T$, respectively for column k of U and V.

2.4.1 Hartree-Fock-Bogoliubov (HFB) theory

In the previous section we presented the BCS theory in which we assume that the Hartree-Fock (HF) solutions have been already obtained and pairing is added as a post self consistent calculation. Here we introduce the HFB theory in which both mean-field and pairing are treated simultaneously. Similarly as for the BCS case, we begin with

the particle conserving Hamiltonian 2.64 but now replace the generalized Bogoliubov transformation 2.93 leading to a form like 2.66, where after constraining the particle number we get

$$H^{(00)}_{\rm HFB} = {\rm Tr}((t-\lambda)\rho + \frac{1}{2}\Gamma\rho + \frac{1}{2}\Delta\kappa^*) = \langle {\rm HFB}|\hat{H}|{\rm HFB}\rangle = E_{\rm HFB}[\rho,\kappa,\kappa^*], \tag{2.109}$$

which encapsulates again part of the residual interaction in the terms

$$\begin{aligned}
\Gamma_{ij} &= \sum_{k,l} \bar{v}_{ikjl}\rho_{kl}, \\
\Delta_{ij} &= \frac{1}{2}\sum_{k,l} \bar{v}_{ijkl}\kappa_{kl} = 2\frac{\partial E_{\rm HFB}}{\partial \kappa_{ij}} = 2\frac{\partial E_{\rm HFB}}{\partial \kappa^*_{ji}}, \\
h_{ij} &= t_{ij} + \Gamma_{ij} - \lambda\delta_{ij} = \frac{\partial E_{\rm HFB}}{\partial \rho_{ji}},
\end{aligned} \tag{2.110}$$

where such matrix elements are given in an arbitrary basis. Γ serves to describe the HF potential while Δ determines the pairing correlations. Notice that the case $\Delta \to 0$ reduces HFB to HF theory. For the doubled basis we define the generalized HFB matrix as

$$\mathcal{H}' = \begin{pmatrix} h & \Delta \\ -\Delta^* & -h^* \end{pmatrix}, \tag{2.111}$$

whose $2n$ eigenvalues are the generalized quasiparticle energies E_k, $-E_k$ for the $2n$ eigenstates $(U,V)^T_k$ and $(V^*,U^*)^T_k$, respectively. The HFB equations are a set of non-linear equations which read

$$\mathcal{H}'\begin{pmatrix} U \\ V \end{pmatrix}_k = \begin{pmatrix} h & \Delta \\ -\Delta^* & -h^* \end{pmatrix}\begin{pmatrix} U \\ V \end{pmatrix}_k = E_k \begin{pmatrix} U \\ V \end{pmatrix}_k, \tag{2.112}$$

Because 2.106 and 2.112 have a common basis, then it must happen that

$$[\mathcal{H}', \mathcal{R}] = 0. \tag{2.113}$$

The HFB equations 2.112 must be solved in an iterative self consistent way like the Hartree-Fock approach. A practical implementation begins with a trial of the vector $(U,V)^T_{k,0}$ for all k which is used to calculate ρ and κ using 2.102. Then the HFB matrix 2.112 is calculated and diagonalized to obtain the eigenvalues $E_{k,1}$ and eigenvectors $(U,V)^T_{k,1}$. This is repeated iteratively until a self consistent solution is attained. It is worth mentioning the behaviour of the HFB equations in the canonical basis employing 2.103. The HFB equations reduce to a BCS form

$$u_i v_i (h_{ii} + h_{\bar{i}\bar{i}}) + \Delta_{i\bar{i}}(u_i^2 - v_i^2) = 0, \tag{2.114}$$

with solutions for occupations and vacancies

$$v_i^2 = \frac{1}{2}\left(1 - \frac{h_{ii} + h_{\bar{i}\bar{i}}}{\sqrt{(h_{ii} + h_{\bar{i}\bar{i}})^2 + 4\Delta_{i\bar{i}}^2}}\right), \tag{2.115}$$

$$u_i^2 = \frac{1}{2}\left(1 + \frac{h_{ii} + h_{\bar{i}\bar{i}}}{\sqrt{(h_{ii} + h_{\bar{i}\bar{i}})^2 + 4\Delta_{i\bar{i}}^2}}\right), \tag{2.116}$$

and quasiparticle energies

$$\tilde{E} = \sqrt{h_{ii}^2 + \Delta_{i\bar{i}}^2}. \tag{2.117}$$

3 Density functional theory

In quantum mechanics, the wavefunction is the mathematical object that encapsulates all degrees of freedom of a system and describes all that can be known about it. Thus, the solution of Schrödinger equation (or its relativistic extensions) is the most important step to model all observables and properties of a system. Density functional theory is an alternative approach to the solution of many-body quantum systems where the main mathematical object to obtain is no longer the wavefunction but the one-body local space density of the system given by

$$\rho(\boldsymbol{r}) = \langle\Psi|\hat{\rho}^{(1)}|\Psi\rangle = N \int d\boldsymbol{r}_2 ... d\boldsymbol{r}_N \, |\Psi(\boldsymbol{r}, \boldsymbol{r}_2, \boldsymbol{r}_3, ..., \boldsymbol{r}_N)|^2, \tag{3.1}$$

where $|\Psi\rangle$ is the exact N-body ground state (g.s.) wavefunction. This strategy reduces the N-body problem from finding a complex-valued wavefunction $|\Psi\rangle$ of $3N$ coordinates to a real-valued function $\rho(\boldsymbol{r})$ dependent of three position coordinates obtained via minimization of the energy density functional $E[\rho]$ that holds non-negativity ($0 \leq \rho(\boldsymbol{r})$), normalization ($\int d\boldsymbol{r}\rho(\boldsymbol{r}) \leq \infty$) and is continuously differentiable ($\rho(\boldsymbol{r}) \in C^\infty$). This apparent advantageous approach does not come without cost, as it represents a trade-off where inherent complexities eventually manifest. In this section we present its original foundation for solid state systems and then extend the theory to non-relativistic nuclear physics where we present the available energy density functionals along with some of their properties.

3.1 General density functional theory

We review the main theorems and foundational results that support the density functional theory (DFT) framework for studying many-body systems. Although these theoretical developments originated primarily within the context of solid state physics, their applicability extends to many other fields, including nuclear physics as is our case of interest.

3.1.1 The Hohenberg-Kohn (HK) theorem and the Kohn-Sham (KS) equations

The proposal of DFT relies in the important HK theorem and KS equations, originally stated in a series of papers for electron gases [8, 9]. These demonstrate that

densities, wavefunctions and the external potentials for N-body systems are in a one-to-one correlation and that this mappings allow a simplification of the N-body to an independent-particle mean-field, respectively. In the original formulation, the Hamiltonian of the system is

$$\hat{H} = \hat{T} + \hat{W} + \hat{V}_{\text{ext}}, \tag{3.2}$$

where $\hat{T}$ is the kinetic energy, $\hat{W}$ is an universal particle-particle potential interaction common to all electronic systems and $\hat{V}_{\text{ext}}$ is an external field that can be expressed as

$$\hat{W} = \sum_{i<j}^{N} \hat{w}(\mathbf{r}_i, \mathbf{r}_j) = \int d\mathbf{r} \int d\mathbf{r}' \; \hat{\rho}(\mathbf{r}') w(\mathbf{r}, \mathbf{r}') \hat{\rho}(\mathbf{r}), \tag{3.3}$$

$$\hat{V}_{\text{ext}} = \sum_{i=1}^{N} \hat{v}_{\text{ext}}(\mathbf{r}_i) = \int d\mathbf{r} \; v_{\text{ext}}(\mathbf{r}) \hat{\rho}(\mathbf{r}), \tag{3.4}$$

In principle, $\hat{H}$ is non-relativistic, zero temperature and time independent, even though extensions to these regimes have been developed in dedicated research [10]. Below we sketch the approach of [38, 39], where rigorous proofs of the HK theorem can be found in [40, 41]. If we define the following sets

$$\mathscr{V} = \{v_{\text{ext}}(\mathbf{r}) \mid v_{\text{ext}}(\mathbf{r}) \neq v'_{\text{ext}}(\mathbf{r}) + \text{const.} \;\; \forall v'_{\text{ext}}(\mathbf{r}) \in \mathscr{V}\}, \tag{3.5}$$

$$\mathscr{G} = \{|\Psi\rangle \mid |\Psi\rangle \neq e^{\phi}|\Psi\rangle \text{ are non-degenerate g. s. associated to } v_{\text{ext}} \in \mathscr{V}\}, \tag{3.6}$$

$$\mathscr{N} = \{\rho(\boldsymbol{r}) \; | \rho(\boldsymbol{r}) = \langle\Psi|\hat{\rho}(\boldsymbol{r})|\Psi\rangle, \; |\Psi\rangle \in \mathscr{G}\}, \tag{3.7}$$

and the maps

$$\mathscr{A} : \mathscr{V} \to \mathscr{G}, \tag{3.8}$$

$$\mathscr{B} : \mathscr{G} \to \mathscr{N}, \tag{3.9}$$

which are operationally defined as the solution of Schrödinger equation and calculation of $\langle\Psi|\hat{\rho}^{(1)}|\Psi\rangle$, respectively. The thesis that the HK theorem addresses concerns the injectivity of $\mathscr{A}$ and $\mathscr{B}$. In other words, if once fixed $v_{\text{ext}}(\boldsymbol{r})$, then the associated ground state and densities $|\Psi\rangle$ and $\rho(\boldsymbol{r})$ are unambiguously defined as well up to a constant. A graphical representation of the HK theorem is shown in Fig. 3.1. It turns out that the HK theorem can be proved and thus the injectivity of the maps $\mathscr{A}$ and $\mathscr{B}$ is guaranteed.

What was presented above assumed that the ground state is non-degenerate, but proofs for degenerate states can also be formulated in which these partition the whole space so that the theorem is extended to single representatives of each partition. A corollary of this result is that the state $|\Psi\rangle$ can be uniquely parametrized as a functional of the density $\rho(\boldsymbol{r})$, denoted by $|\Psi\rangle = |\Psi[\rho]\rangle$, and it can be interpreted as a realization of the map $\mathscr{B}^{-1}$ (which exists since the injectivity is guaranteed). The same can be said for any observable O expressed as

$$O[\rho] = \langle\Psi[\rho]|\hat{O}|\Psi[\rho]\rangle, \tag{3.10}$$

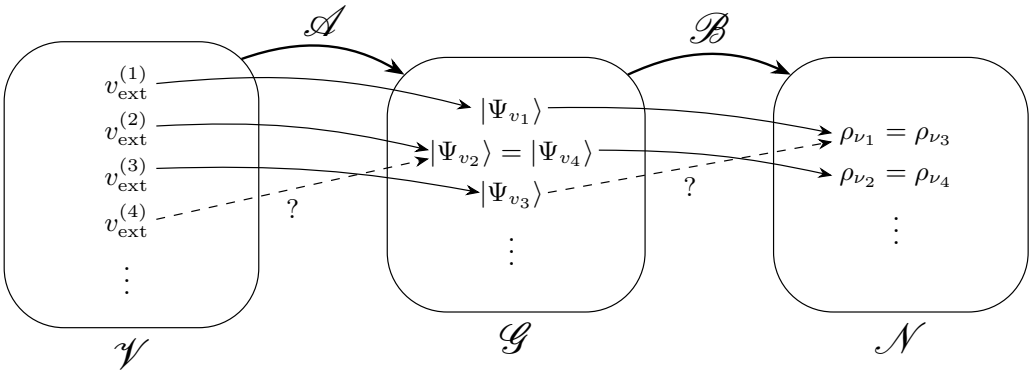

Figure 3.1: Schematic representation of the HK theorem as maps between the spaces of external fields $\mathscr{V}$, wavefunctions $\mathscr{G}$ and densities $\mathscr{N}$.

in particular the energy density functional (EDF) is

$$E[\rho] = \langle \Psi[\rho] | \hat{H} | \Psi[\rho] \rangle, \tag{3.11}$$

which is the essential functional of the DFT. Without mentioning some crucial formalities, DFT postulates the variational principle

$$\frac{\delta}{\delta \rho} \left\{ E[\rho] - \mu \Big[\int d\boldsymbol{r} \rho(\boldsymbol{r}) - N \Big] \right\} \Bigg|_{\rho_0(\boldsymbol{r})} = 0, \tag{3.12}$$

which expresses that the energy functional has a stationary point in the density $\rho_0(\boldsymbol{r})$ of the associated ground state $|\Psi\rangle$ constrained to a finite number of particles, being μ the Lagrange multiplier associated to the chemical potential. Equation 3.12 is the equivalent of Schrödinger equation for the DFT formulation. The HK theorem however is just an existence proof, no computational procedure is established for finding the appropriate functional $E[\rho]$. In section 3.2 we will describe few strategies to figure out $E[\rho]$ in the context of nuclear physics with potentials used in nuclear structure applications.

Another motivation for the formulation of the DFT is the possibility of mapping an interacting N-body system into a non-interacting system described by a Slater determinant in the fermion case. This is the main thesis that the KS equations aim to solve and is also called the non-interacting v-representability (standing for v_{ext}). In principle, the densities obtained are exact solutions of the many-body problem constrained to the exact expression of the kinetic and potential functionals.

Consider a system of non-interacting fermions so that its Hamiltonian and external potentials are given by

$$\begin{aligned} \hat{H}_{\text{KS}} &= \hat{T} + \hat{V}_{\text{KS}}, \\ \hat{V}_{\text{KS}} &= \int d\boldsymbol{r}\ v_{\text{KS}}(\boldsymbol{r}) \hat{\rho}(\boldsymbol{r}), \end{aligned} \tag{3.13}$$

and its ground state $|\Phi_{\mathrm{KS}}\rangle$ holds

$$\hat{H}_{\mathrm{KS}}|\Phi_{\mathrm{KS}}\rangle = E_{\mathrm{KS}}|\Phi_{\mathrm{KS}}\rangle, \tag{3.14}$$

which is a Slater determinant of single-particle states $|\phi_i\rangle$ in the space representation given by

$$\langle \boldsymbol{r}_1, ..., \boldsymbol{r}_n|\Phi_{\mathrm{KS}}\rangle = \Phi_{\mathrm{KS}}(\boldsymbol{r}_1, ..., \boldsymbol{r}_n) = \frac{1}{\sqrt{N!}}\begin{vmatrix} \phi_1(\boldsymbol{r}_1) & \dots & \phi_N(\boldsymbol{r}_1) \\ \vdots & \ddots & \vdots \\ \phi_1(\boldsymbol{r}_N) & \dots & \phi_N(\boldsymbol{r}_N) \end{vmatrix},$$

with each one a solution of

$$\left(-\frac{\hbar^2}{2m}\nabla^2 + v_{\mathrm{KS}}(\boldsymbol{r}) \right)\phi_i(\boldsymbol{r}) = \epsilon_i\phi_i(\boldsymbol{r}), \tag{3.15}$$

where

$$\begin{aligned} \epsilon_1 \leq \epsilon_2 \leq ...\epsilon_N = \epsilon_F, \\ E_{\mathrm{KS}} = \sum_{i=1}^{N} \epsilon_i, \end{aligned} \tag{3.16}$$

for Fermi energy ϵ_F. The density for the non-interacting case has a simple form

$$\rho_{\mathrm{KS}}(\boldsymbol{r}) = \sum_{i=1}^{N} |\phi_i(\boldsymbol{r})|^2. \tag{3.17}$$

From the HK theorem we have that $|\Phi_{\mathrm{KS}}\rangle = |\Phi_{\mathrm{KS}}[\rho_{\mathrm{KS}}]\rangle$. The question now reduces to finding the density of non-interacting fermions $\rho_{\mathrm{KS}}(\boldsymbol{r})$ that equals the density of the interacting system $\rho(\boldsymbol{r})$. As proved in reference [42], this is possible for any non-negative normalized density for which 3.17 holds for a set of orthonormal single-particle states. One can therefore write an external field

$$v_{\mathrm{KS}}(\boldsymbol{r}) = v_{\mathrm{ext}}(\boldsymbol{r}) + v_{\mathrm{H}}[\rho_{\mathrm{KS}}](\boldsymbol{r}) + v_{\mathrm{xc}}[\rho_{\mathrm{KS}}](\boldsymbol{r}), \tag{3.18}$$

where

$$\begin{aligned} v_{\mathrm{H}}[\rho_{\mathrm{KS}}](\boldsymbol{r}) =& \int d\boldsymbol{r'} w(\boldsymbol{r}, \boldsymbol{r'})\rho_{\mathrm{KS}}(\boldsymbol{r'}), \\ v_{\mathrm{xc}}[\rho_{\mathrm{KS}}](\boldsymbol{r}) =& \frac{\delta E_{\mathrm{xc}}[\rho]}{\delta\rho(\boldsymbol{r})} \end{aligned} \tag{3.19}$$

and $E_{\mathrm{xc}}[\rho]$ represents the exchange energy which is one of the unknowns of the KS approach whose role is to correct the total potential so that the independent-particle system represents exactly the interacting system. Thus we formulate the KS equations explicitly from 3.15 as

$$\left(-\frac{\hbar^2}{2m}\nabla^2 + v_{\mathrm{ext}}(\boldsymbol{r}) + v_H[\rho](\boldsymbol{r}) + v_{\mathrm{xc}}[\rho](\boldsymbol{r}) \right)\phi_i(\boldsymbol{r}) = \epsilon_i\phi_i(\boldsymbol{r}), \tag{3.20}$$

which are to be solved iteratively in a self-consistent fashion like the Hartree-Fock method. The independent-particle orbitals are interpreted as purely mathematical constructs to solve the many-body density since the KS equations guarantee that the energies and densities are reproduced but not the ground states themselves. A difficulty of the DFT approach is now apparent, that is, the non-linearity of the KS equations 3.20 which lead to non-convergence, instabilities and impossibilities to attain a solution [43].

3.2 Density functional theory in the nuclear case

The nucleus is a self bounded system, so in principle there is no external field in its Hamiltonian. In addition, the particle-particle potential $\hat{W}$ is not only two-body but also three-body and possibly four-body terms should be included [19, 20]. However the results of DFT still hold for the nuclear case. In general the EDF can be separated into kinetic, nuclear potential, pairing and Coulomb as

$$E[\rho,\kappa,\kappa^\dagger] = E_{\text{kin.}}[\rho] + E_{\text{pot.}}[\rho] + E_{\text{pair.}}[\rho,\kappa,\kappa^\dagger] + E_{\text{Coul.}}[\rho,\kappa,\kappa^\dagger], \tag{3.21}$$

The one-body density operators act in the space of spin and isospin, and thus can be expanded in scalar and vector components of each of these spaces as

$$\hat{\rho}(\boldsymbol{r},\boldsymbol{r'}) = \frac{1}{4}\rho_{0,0}(\boldsymbol{r},\boldsymbol{r'}) + \frac{1}{4}\rho_{0,1}(\boldsymbol{r},\boldsymbol{r'})\hat{\boldsymbol{\tau}} + \frac{1}{4}\boldsymbol{s}_{1,0}(\boldsymbol{r},\boldsymbol{r'})\hat{\boldsymbol{\sigma}} + \frac{1}{4}\boldsymbol{s}_{1,1}(\boldsymbol{r},\boldsymbol{r'})\hat{\boldsymbol{\sigma}}\hat{\boldsymbol{\tau}}, \tag{3.22}$$

implying that the densities and thus the EDF of 3.21 can be separated into scalar and vector components in spin and isospin as well.

Additionally, we can also establish that the nuclear EDF is the integral over the volume of the energy density $\mathfrak{H}$ as

$$E_{\text{pot.}}[\rho] = \int dV \mathfrak{H}(\rho), \tag{3.23}$$

which itself is given by the expectation value of some nuclear interaction operator called the pseudo-potential $\hat{\mathfrak{v}}$ as

$$\mathfrak{H}(\rho) = \langle\Psi|\hat{\mathfrak{v}}|\Psi\rangle. \tag{3.24}$$

This approach requires a physical formulation of $\hat{\mathfrak{v}}$, which is mostly abandoned nowadays for phenomenological constructions of $\mathfrak{H}$ from one-body isoscalar ($t=0$) and isovector ($t=1$), local and non-local densities given by [22, 44]

$$\begin{aligned}
\rho_{0,0}(\boldsymbol{r},\boldsymbol{r'}) &= \sum_{\sigma,\tau}\sum_{\nu,\mu}\rho_{\mu\nu}\varphi^*_\nu(\boldsymbol{r'},\sigma,\tau)\varphi_\mu(\boldsymbol{r},\sigma,\tau),\\
\rho_{1,k}(\boldsymbol{r},\boldsymbol{r'}) &= \sum_{\sigma,\tau}\sum_{\nu,\mu}\rho_{\mu\nu}\varphi^*_\nu(\boldsymbol{r'},\sigma,\tau)\hat{\tau}_k\varphi_\mu(\boldsymbol{r},\sigma,\tau),\\
\rho_{t,k}(\boldsymbol{r}) &= \rho_{t,k}(\boldsymbol{r},\boldsymbol{r'})\Big|_{\boldsymbol{r}=\boldsymbol{r'}},
\end{aligned} \tag{3.25}$$

spin densities

$$\begin{aligned}
\boldsymbol{s}_{0,0}(\boldsymbol{r},\boldsymbol{r}') &= \sum_{\sigma,\tau}\sum_{\nu,\mu}\rho_{\mu\nu}\varphi^*_\nu(\boldsymbol{r}',\sigma,\tau)\hat{\boldsymbol{\sigma}}\varphi_\mu(\boldsymbol{r},\sigma,\tau),\\
\boldsymbol{s}_{1,k}(\boldsymbol{r},\boldsymbol{r}') &= \sum_{\sigma,\tau}\sum_{\nu,\mu}\rho_{\mu\nu}\varphi^*_\nu(\boldsymbol{r}',\sigma,\tau)\hat{\boldsymbol{\sigma}}\hat{\tau}_k\varphi_\mu(\boldsymbol{r},\sigma,\tau),\\
\boldsymbol{s}_{t,k}(\boldsymbol{r}) &= \boldsymbol{s}_{t,k}(\boldsymbol{r},\boldsymbol{r}')\Big|_{\boldsymbol{r}=\boldsymbol{r}'},
\end{aligned} \tag{3.26}$$

kinetic and spin-kinetic densities

$$\begin{aligned}
\tau_{t,k}(\boldsymbol{r}) &= \nabla\cdot\nabla'\rho_{t,k}(\boldsymbol{r},\boldsymbol{r}')\Big|_{\boldsymbol{r}=\boldsymbol{r}'},\\
\boldsymbol{T}_{t,k}(\boldsymbol{r}) &= \nabla\cdot\nabla'\boldsymbol{s}_{t,k}(\boldsymbol{r},\boldsymbol{r}')\Big|_{\boldsymbol{r}=\boldsymbol{r}'},
\end{aligned} \tag{3.27}$$

and current densities

$$\begin{aligned}
\boldsymbol{j}_{t,k}(\boldsymbol{r}) &= -\frac{i}{2}(\nabla-\nabla')\rho_{t,k}(\boldsymbol{r},\boldsymbol{r}')\Big|_{\boldsymbol{r}=\boldsymbol{r}'},\\
\mathbb{J}_{t,k}(\boldsymbol{r}) &= -\frac{i}{2}(\nabla-\nabla')\boldsymbol{s}_{t,k}(\boldsymbol{r},\boldsymbol{r}')\Big|_{\boldsymbol{r}=\boldsymbol{r}'},\\
\mathbf{F}_{t,k}(\boldsymbol{r}) &= \frac{1}{2}(\nabla\nabla'\cdot\boldsymbol{s}_{t,k}(\boldsymbol{r},\boldsymbol{r}')+\nabla'\nabla\cdot\boldsymbol{s}_{t,k}(\boldsymbol{r},\boldsymbol{r}'))\Big|_{\boldsymbol{r}=\boldsymbol{r}'},
\end{aligned} \tag{3.28}$$

which are accompanied by a small set of parameters (between 5 and 15) whose numerical values are fit from experimental data to reproduce specific features like infinite nuclear matter, nuclear structures, astrophysical environments *etc.*

Further structure of the functionals that can be formulated from 3.25, 3.26, 3.27 and 3.28 can be by figured out by analyzing their time reversal properties. The local densities $\rho_{t,k}(\boldsymbol{r})$, $\tau_{t,k}(\boldsymbol{r})$ and $\mathbb{J}_{t,k}(\boldsymbol{r})$ are time-even while $\boldsymbol{s}_{t,k}(\boldsymbol{r})$, $\boldsymbol{T}_{t,k}(\boldsymbol{r})$, $\boldsymbol{j}_{t,k}(\boldsymbol{r})$ and $\mathbf{F}_{t,k}(\boldsymbol{r})$ are time-odd. Thus we can also separate the nuclear EDF into two terms as

$$E_{\text{pot.}}[\rho] = \int dV\Big(\mathfrak{H}_{\text{Even}}(\rho)+\mathfrak{H}_{\text{Odd}}(\rho)\Big), \tag{3.29}$$

which has to obey invariance under space and isospin rotations, translation, parity, time-reversal and Galilean transformations. It is worth noting that the term $\mathfrak{H}_{\text{Odd}}(\rho)$ is only non-zero for time reversal breaking systems, in the nuclear case this is realized for odd-A nuclei.

3.2.1 The Skyrme functional

The Skyrme interaction [45] is a family of parametrizations of a physically motivated EDF that is in principle non-local, three-body and zero range. It is constructed by considering products of up to two densities and gradients. Its mathematical form is

$$
\begin{aligned}
E^{\text{Skyrme}}_{\text{pot.}}[\rho] = \int dV \sum_t \Big\{ & C_t^{\rho\rho}\rho_t^2 + C_t^{\rho\Delta\rho}\rho_t\Delta\rho_t + C_t^{\rho\tau}(\rho_t\tau_t - \mathbb{J}_t\cdot\mathbb{J}_t) \\
& + C_t^{ss}\boldsymbol{s}_t^2 + C_t^{s\Delta s}\boldsymbol{s}_t\cdot\Delta\boldsymbol{s}_t + C_t^{\rho\nabla J}(\rho_t\nabla\cdot\tilde{\mathbf{J}}_t + \boldsymbol{j}_t\cdot\nabla\times\boldsymbol{s}_t) \\
& + C_t^{s\nabla s}(\nabla\cdot\boldsymbol{s}_t)^2 + C_t^{JJ}\big(\mathbb{J}_t:\mathbb{J}_t - \boldsymbol{s}_t\cdot\boldsymbol{T}_t\big) \\
& + C_t^{J\bar{J}}\Big[(\mathrm{Tr}(\mathbb{J}_t))^2 + \mathbb{J}_t:\mathbb{J}_t^T - 2\mathbf{s}_t\cdot\mathbf{F}_t\Big]\Big\},
\end{aligned}
\tag{3.30}
$$

where : denotes the contraction of tensors, $\tilde{\mathbf{J}}_t = \sum_{\mu,\nu,k}\epsilon_{\mu\nu k}\mathbb{J}_{\mu\nu,t}\boldsymbol{e}_k$ and the coupling constants are denoted by $C_t^{ff'}$. Extensive literature exist for the later quantities and explicit numerical values are given in [46, 47, 48, 49, 50, 51, 52]. The separation of terms into isoscalar and isovector, time-odd and time-even is apparent now in 3.30.

Moreover, the Skyrme interaction is motivated by a physical pseudo potential whose two-body part is separated into three contributions

$$
\hat{\mathfrak{v}}_{\text{Skyrme}}(\mathbf{r}_1,\mathbf{r}_2,\overrightarrow{k},\overleftarrow{k'}) = \left[\hat{\mathfrak{v}}_{\text{centr}} + \hat{\mathfrak{v}}_{\text{LS}} + \hat{\mathfrak{v}}_{\text{tens}}\right](\mathbf{r}_1,\mathbf{r}_2,\overrightarrow{k},\overleftarrow{k'}),
\tag{3.31}
$$

where the central, spin-orbit and tensor components are given by

$$
\begin{aligned}
\hat{\mathfrak{v}}_{\text{centr}}(\mathbf{r}_1,\mathbf{r}_2,\overrightarrow{k},\overleftarrow{k'}) = {} & t_0\left(1 + x_0\hat{P}_\sigma\right)\delta(\mathbf{r}_1-\mathbf{r}_2) \\
& + \frac{1}{2}t_1\left(1 + x_1\hat{P}_\sigma\right)\left[\overleftarrow{k'^2}\delta(\mathbf{r}_1-\mathbf{r}_2) + \delta(\mathbf{r}_1-\mathbf{r}_2)\overrightarrow{k^2}\right] \\
& + t_2\left(1 + x_2\hat{P}_\sigma\right)\overleftarrow{k'}\cdot\delta(\mathbf{r}_1-\mathbf{r}_2)\overrightarrow{k} \\
& + \frac{1}{6}t_3\left(1 + x_3\hat{P}_\sigma\right)\rho^\alpha\Big(\frac{\mathbf{r}_1+\mathbf{r}_2}{2}\Big)\delta(\mathbf{r}_1-\mathbf{r}_2),
\end{aligned}
\tag{3.32}
$$

$$
\hat{\mathfrak{v}}_{\text{LS}}(\mathbf{r}_1,\mathbf{r}_2,\overrightarrow{k},\overleftarrow{k'}) = iW_0[\hat{\boldsymbol{\sigma}}_1 + \hat{\boldsymbol{\sigma}}_2]\cdot\overleftarrow{k'}\times\delta(\boldsymbol{r}_1-\boldsymbol{r}_2)\overrightarrow{k},
\tag{3.33}
$$

$$
\begin{aligned}
\hat{\mathfrak{v}}_{\text{tens}}(\mathbf{r}_1,\mathbf{r}_2,\overrightarrow{k},\overleftarrow{k'}) = {} & \frac{1}{2}t_e\Big\{\Big[3(\hat{\boldsymbol{\sigma}}_1\cdot\overleftarrow{k'})(\hat{\boldsymbol{\sigma}}_2\cdot\overleftarrow{k'}) - (\hat{\boldsymbol{\sigma}}_1\cdot\hat{\boldsymbol{\sigma}}_2)\overleftarrow{k'^2}\Big]\delta(\mathbf{r}_1-\mathbf{r}_2) \\
& + \delta(\mathbf{r}_1-\mathbf{r}_2)\Big[3(\hat{\boldsymbol{\sigma}}_1\cdot\overrightarrow{k})(\hat{\boldsymbol{\sigma}}_2\cdot\overrightarrow{k}) - (\hat{\boldsymbol{\sigma}}_1\cdot\hat{\boldsymbol{\sigma}}_2)\overrightarrow{k^2}\Big]\Big\} \\
& + t_o\Big[\frac{3}{2}(\hat{\boldsymbol{\sigma}}_1\cdot\overleftarrow{k'})\delta(\mathbf{r}_1-\mathbf{r}_2)(\hat{\boldsymbol{\sigma}}_2\cdot\overrightarrow{k}) + \frac{3}{2}(\hat{\boldsymbol{\sigma}}_2\cdot\overleftarrow{k'})\delta(\mathbf{r}_1-\mathbf{r}_2)(\hat{\boldsymbol{\sigma}}_1\cdot\overrightarrow{k}) \\
& - (\hat{\boldsymbol{\sigma}}_1\cdot\hat{\boldsymbol{\sigma}}_2)\overleftarrow{k'}\cdot\delta(\mathbf{r}_1-\mathbf{r}_2)\overrightarrow{k}\Big],
\end{aligned}
\tag{3.34}
$$

where $\overrightarrow{k} = -\frac{i}{2}(\overrightarrow{\nabla_1} - \overrightarrow{\nabla_2})$ is the relative momentum operator acting on the right

while $\overleftarrow{k'}$ is its hermitian conjugate acting on the left. $\hat{P}_\sigma = \frac{1}{2}(1 + \hat{\boldsymbol{\sigma}}_1 \cdot \hat{\boldsymbol{\sigma}}_2)$ is the spin-exchange operator. The parameter set t, x, α and W_0 and have in principle a one-to-one correspondence between the coupling constants $C_t^{f,f'}$. Also, sometimes a three body potential is included which has the form

$$\hat{\mathfrak{v}}_{3\text{-b}}(\mathbf{r}_1, \mathbf{r}_2, \mathbf{r}_3) = t_3 \delta(\mathbf{r}_1 - \mathbf{r}_2)\delta(\mathbf{r}_2 - \mathbf{r}_3). \tag{3.35}$$

The Skyrme functional is a popular choice among theorists of several areas, this is reflected in the fact that over 200 parametrization have been developed. Next we comment in some of the relevant choices for nuclear structure for this work in particular.

Parametrizations of the Skyrme functional for nuclear structure

The different parametrizations of the Skyrme functionals can be clustered in families that aim to reproduce specific nuclear structure features and observables. The parameters change from being zero or changing slightly among the different functionals. The relevant parametrizations for this work are shown in table 3.1, where the parameters are in MeV multiplied by some appropriate power λ of fm$^\lambda$. Additionally, for some functionals the spin-orbit term arises from a single isoscalar parameter W_0 or from a separate isoscalar and isovector parameters b_4 and b'_4, respectively [53].

	UNEDF0[48]	UNEDF1[48]	SIII[54]	SLy4[55]	SkM*[56]	SkO'[57]	SkX_c[58]
t_0	-1883.69	-2078.33	-1128.75	-2488.91	-2645	-2099.42	-1438
t_1	277.50	239.40	395	486.82	410	301.531	244.3
t_2	608.43	1575.12	-95	-546.39	-135	154.781	-133.7
t_3	13901.95	14263.65	14000	13777	15595	13526.46	12116.3
x_0	0.0097	0.054	0.45	0.834	0.09	-0.03	0.288
x_1	-1.78	-5.07	0	-0.344	0	-1.33	0.611
x_2	-1.68	-1.37	0	-1	0	-2.32	0.145
x_3	-0.38	-0.16	0	1.35	0	-0.15	-0.056
b_4	125.16	38.39	-	-	65	144	-
b'_4	-91.26	71.32	-	-	65	-82.89	-
W_0	-	-	120	123	130	180	145.7
α	0.32	0.27	1	1/6	1/6	1/4	1/2

Table 3.1: Parameter sets for the Skyrme potentials used in this work.

The Landau parameters

Before leaving the presentation of Skyrme parametrizations we discuss the Landau parameters. These constrain the values of the time-odd isoscalar and isovector spin-spin and spin-kinetic-spin coupling constants as

$$
\begin{aligned}
g_0 &= N_0 \left(2C_0^{ss} + 2C_0^{JJ}\beta\rho_{\text{sat.}}^{2/3}\right), \\
g_0' &= N_0 \left(2C_1^{ss} + 2C_1^{JJ}\beta\rho_{\text{sat.}}^{2/3}\right), \\
g_1 &= -2N_0 C_0^{JJ}\beta\rho_{\text{sat.}}^{2/3}, \\
g_1' &= -2N_0 C_1^{JJ}\beta\rho_{\text{sat.}}^{2/3},
\end{aligned}
\tag{3.36}
$$

where the normalization factor N_0 and β involve the saturation density $\rho_{\text{sat.}}$ and effective nucleon mass m^* given by

$$
\begin{aligned}
\beta &= (3\pi^2/2)^{2/3}, \\
N_0 &= \pi^{-2}\left(\frac{\hbar^2}{2m}\right)^{-1}\frac{m^*}{m}\left(\frac{3\pi^2\rho_{\text{sat.}}}{2}\right)^{1/3}.
\end{aligned}
\tag{3.37}
$$

The influence of g_0' in the values of magnetic dipole moments has received a lot of attention and has been discussed extensively in the literature, see for example [32, 59, 33, 50] for discussions its optimal values.

3.2.2 The Gogny functional

As mentioned above, the residual nuclear interaction can be separated into short and long range contributions. This concept is absent in the Skyrme potential as in its basic formulation it is a zero range interaction. Thus, a natural extension is the inclusion of a finite range component in the central potential approximated by Gaussian functions of different ranges. This functional is called the Gogny interaction [60] and has the features of being non-local, two-body and finite range. Its mathematical form for two different Gaussian ranges is

$$
\begin{aligned}
E_{\text{pot.}}^{\text{Gogny}}[\rho] = \int dV \int dV' \sum_t \sum_{i=1,2} e^{-(\boldsymbol{r}-\boldsymbol{r}')^2/\mu_i^2} \Big[& A_{it}^{\rho\rho}\rho_t(\boldsymbol{r})\rho_t(\boldsymbol{r}') + A_{it}^{ss}\mathbf{s}_t(\boldsymbol{r})\cdot\mathbf{s}_t(\boldsymbol{r}') \\
& + B_{it}^{\rho\rho}\rho_t(\boldsymbol{r},\boldsymbol{r}')\rho_t(\boldsymbol{r}',\boldsymbol{r}) + B_{it}^{ss}\mathbf{s}_t(\boldsymbol{r},\boldsymbol{r}')\cdot\mathbf{s}_t(\boldsymbol{r}',\boldsymbol{r})\Big] \\
+ \int dV \sum_t \Big[& C_t^{\rho\rho}[\rho_0]\rho_t\rho_t + C_t^{ss}[\rho_0]\mathbf{s}_t\cdot\mathbf{s}_t + C_t^{\rho\nabla J}(\rho_t\nabla\cdot\tilde{\mathbf{J}}_t + \tilde{\mathbf{J}}_t\cdot\nabla\times\boldsymbol{s}_t)\Big],
\end{aligned}
\tag{3.38}
$$

where the coupling constants are A_{it}, B_{it} depend on the Gaussian component and the $C_t^{f,f'}$ are inherited from the Skyrme functional with an explicit density dependence.

Complications are apparent due to the involvement of non-local densities and the algebraic form of the functional. This acquired complexity manifests itself mainly in higher computational costs. Additionally, the separation into the time-even and time-odd contributions cannot be done since the non-local densities do not simply get a phase under time reversal transformation but instead behave as

$$
\begin{aligned}
\rho(\boldsymbol{r},\boldsymbol{r}') &\to \rho^*(\boldsymbol{r},\boldsymbol{r}') = \rho(\boldsymbol{r}',\boldsymbol{r}), \\
s(\boldsymbol{r},\boldsymbol{r}') &\to -s^*(\boldsymbol{r},\boldsymbol{r}') = -s(\boldsymbol{r}',\boldsymbol{r}).
\end{aligned}
\tag{3.39}
$$

The Gogny functional is also inspired in a nucleon-nucleon pseudo potential given by

$$\begin{aligned}\hat{\mathfrak{v}}_{\text{Gogny}}(\mathbf{r}_1,\mathbf{r}_2,\overrightarrow{k},\overleftarrow{k'}) = \sum_{i=1,2}\Big[W_i + B_i\hat{P}_\sigma - H_i\hat{P}_\tau - M_i\hat{P}_\sigma\hat{P}_\tau\Big]\, e^{-(\boldsymbol{r}_1-\boldsymbol{r}_2)^2/\mu_i^2} \\ + t_0(1+x_0\hat{P}_\sigma)\rho^\alpha\Big(\frac{\boldsymbol{r}_1+\boldsymbol{r}_2}{2}\Big)\delta(\mathbf{r}_1-\mathbf{r}_2) \\ + iW_{LS}(\hat{\boldsymbol{\sigma}}_1+\hat{\boldsymbol{\sigma}}_2)\overleftarrow{k'}\times\delta(\mathbf{r}_1-\mathbf{r}_2)\overrightarrow{k}.\end{aligned} \tag{3.40}$$

Parametrizations of the Gogny functional for nuclear structure

Although the finite range functionals are not applied in this work, we include for completeness one of its most used set of parameters, the D1S functional [61].

i	μ_i	W_i	B_i	H_i	M_i
1	0.7	-1720.30	1300	-1813.53	1397.60
2	1.2	103.64	-163.48	162.81	-223.93

t_0	x_0	α	W_{LS}
1390.6	1	1/3	-130

Table 3.2: Parameters of the Gogny D1S interaction.

3.2.3 Kinetic, Coulomb and Pairing functionals

Most of the energy is carried by the kinetic and nuclear potential for which most of the efforts are dedicated, however, the other three terms included in 3.21 play an important role in determining the nuclear structure, especially the pairing and Coulomb interactions. The kinetic functional is simply given by the isoscalar density

$$E_{\text{kin.}}[\rho] = \frac{\hbar^2}{2m}\Big(1-\frac{1}{A}\Big)\int dV\,\tau_{0,0}(\boldsymbol{r}), \tag{3.41}$$

where the factor $1-\frac{1}{A}$ serves as an approximation for the centre-of-mass energy correction [54].

For the pairing term, since it is part of the nuclear interaction in principle should be contained in $E_{\text{pot.}}[\rho]$, however, in practice this is not the case as in the BCS and seniority models. Only in the Gogny type potentials where a finite range is considered it is possible to include the pairing interaction within the nucleon-nucleon EDF. One way to do this is via the expectation value of the pseudo-potential where the collection of all terms proportional to κ and $\kappa^\dagger$ constitute the pairing. A standard form obtained from this for the pairing EDF reads as

$$E_{\text{pair.}}[\rho,\kappa,\kappa^\dagger] = \int dV\, A^{\kappa\kappa}[\rho]\sum_n \tilde{\rho}_n^\dagger(\boldsymbol{r})\tilde{\rho}_n(\boldsymbol{r}), \tag{3.42}$$

where $n = \pi, \nu$, the coupling function $A^{\kappa\kappa}[\rho]$ and the local pairing density $\tilde{\rho}_n(\boldsymbol{r})$ are given by

$$\tilde{\rho}_n(\boldsymbol{r}) = -2\sum_{\sigma} \sigma\kappa_n(\boldsymbol{r}, \sigma; \boldsymbol{r}, -\sigma), \tag{3.43}$$

$$A^{\kappa\kappa}[\rho] = \frac{V_{0,n}}{4}\left[1 - \eta\left(\frac{\rho(\boldsymbol{r})}{\rho_{sat}}\right)^{\alpha}\right]\delta(\boldsymbol{r}_1 - \boldsymbol{r}_2), \tag{3.44}$$

where the parameter η controls the distribution of the pairing force across the nuclear volume and $V_{0,n}$ is fit to mass staggering in some applications. The functional in 3.42 can be obtained from the pseudo-potential

$$\mathfrak{v}_{\text{pair., n}}(\boldsymbol{r}_1, \boldsymbol{r}_2) = \frac{V_{0,n}}{2}(1 - \hat{P}_{\sigma})\left[1 - \eta\left(\frac{\rho((\boldsymbol{r}_1 + \boldsymbol{r}_2)/2)}{\rho_{sat}}\right)^{\alpha}\right]\delta(\boldsymbol{r}_1 - \boldsymbol{r}_2). \tag{3.45}$$

Alternatively, in a BCS framework, the pairing EDF has an explicit dependence on the Bogoliubov parameters as

$$E^{\text{BCS}}_{\text{pair.}} = -\sum_{n} \frac{G_n}{4}\left(\sum_{i} u_{i\sigma} v_{i\sigma}\right)^2, \tag{3.46}$$

where G_n is the pairing strength of 2.49. Notice that the contributions from proton-neutron pairing are neglected in the functionals above which might be crucial in some applications.

The last term that completes the nuclear EDF comes from the Coulomb interaction whose mathematical form is well know. Three main terms constitute the Coulomb EDF which quantify the direct local, non-local exchange and pairing contributions are given respectively by

$$E^{\text{dir.}}_{\text{Coul.}}[\rho] = \frac{e^2}{2}\int dV \int dV' \frac{\rho_{\pi}(\boldsymbol{r})\rho_{\pi}(\boldsymbol{r}')}{|\boldsymbol{r} - \boldsymbol{r}'|}, \tag{3.47}$$

$$E^{\text{xc.}}_{\text{Coul.}}[\rho] = -\frac{e^2}{4}\int dV \int dV' \Big[\frac{\rho_{\pi}(\boldsymbol{r}, \boldsymbol{r}')\rho_{\pi}(\boldsymbol{r}', \boldsymbol{r})}{|\boldsymbol{r} - \boldsymbol{r}'|} + \frac{\boldsymbol{s}_{\pi}(\boldsymbol{r}, \boldsymbol{r}') \cdot \boldsymbol{s}_{\pi}(\boldsymbol{r}', \boldsymbol{r})}{|\boldsymbol{r} - \boldsymbol{r}'|}\Big], \tag{3.48}$$

$$E^{\text{pair.}}_{\text{Coul.}}[\rho, \kappa, \kappa^{\dagger}] = \frac{e^2}{2}\int dV \int dV' \sum_{\sigma,\sigma'} \frac{\kappa^{\dagger}_{\pi}(\boldsymbol{r}, \sigma; \boldsymbol{r}', \sigma')\kappa_{\pi}(\boldsymbol{r}, \sigma; \boldsymbol{r}', \sigma')}{|\boldsymbol{r} - \boldsymbol{r}'|}. \tag{3.49}$$

3.3 Post mean-field or multi-reference density functional theory (MR-EDF)

In chapter 2 we presented the pairing interaction and its effects in the nuclear wave-function. Among several properties, the particle number breaking is one of the most remarkable for both BCS and HFB models. These approaches comprehend what is known as the single reference density functional theory (SR-DFT) where we obtain a

single symmetry breaking solution and use it to describe the nucleus. However, many fundamental observables need to be computed for the symmetry-conserving states, like for example multipole moments and transitions. Thus, it becomes a necessity to go beyond this mean-field approaches and consider several configurations that serve as references to restore the symmetry in these already complicated solutions. This is the main focus of the multi reference energy density functional theory (MR-EDF) which we introduce based mostly on references [62, 1, 7, 10, 43, 63].

Reference [10] establishes two main approaches to nuclear physics: the vertical and horizontal philosophies. The former focuses on implementing numerous symmetry-conserving configurations to represent the nuclear state, while the latter seeks to describe the nucleus as a mixture of symmetry breaking wave functions. The later is also the framework in which DFT is formulated. In this section we review the horizontal philosophy approach focusing on the beyond symmetry breaking mean-field theory aiming at the methods of restoration of symmetry.

3.3.1 Symmetries and spontaneous symmetry breaking

Symmetries are essential properties of physical systems, both classical and quantum. They express conserved quantities which in the later case, provide the quantum numbers that determine selection rules and several properties of the system. Here we introduce some of the general theory of symmetries and the spontaneous breaking in the quantum context. We scattered particular symmetry concepts across the chapters as considered necessary for the narrative in sections 2.1.4 and 4.1.

The mathematical structure of symmetries is described by group theory [64, 65, 66, 67], in particular, Lie groups are used for continuous symmetries like rotations and translations, while finite groups are used for discrete symmetries like parity and time reversal. A system possesses a symmetry $\mathcal{S}$ if the commutator of the Hamiltonian of the system $\hat{H}$ with the generators $\hat{S}_i$ of the associated symmetry group follows

$$[\hat{H}, \hat{S}_i] = 0. \tag{3.50}$$

Since the group elements are obtained via the exponential map

$$\hat{R}(\boldsymbol{q}) = \prod_i e^{-iq_i\hat{S}_i}, \tag{3.51}$$

for a set of parameters q_i, we have from 3.50 the invariance

$$\hat{R}(\boldsymbol{q})\hat{H}\hat{R}(\boldsymbol{q})^\dagger = \hat{H}. \tag{3.52}$$

Because of 3.50, the generators and energy eigenstates have a common basis denoted as $|\lambda\mu\rangle$, where λ is the quantum number associated to $\mathcal{S}$ and μ is associated to subalgebras of $\mathcal{S}$ that serve to quantify multiplicities of λ. Table 3.3 summarizes some symmetries relevant to nuclear theory.

The notion of spontaneous symmetry breaking comes from situations where the Hamiltonian of a system $\hat{H}$ holds 3.50 for a given symmetry $\mathcal{S}$ but the ground state $|\Psi\rangle$

Symmetry	Parameters	Generators	Group
3D space rotations	Euler angles: α,β,γ	$\hat{I}_x$, $\hat{I}_y$, $\hat{I}_z$	SU(2) $\cong$ SO(3)
3D isospin rotations	Isospin Euler angles: α_T,β_T,γ_T	$\hat{T}_x$, $\hat{T}_y$, $\hat{T}_z$	SU(2)
Particle number	Gauge angle: ϕ	$\hat{N}$	U(1)
Parity	Orientation angle: $\varphi = 0, \pi$	$\hat{N}_-$	$\mathbb{Z}_2$

Table 3.3: Survey of some symmetries relevant to nuclear physics. $\hat{N}$ denotes the particle number operator and $\hat{N}_- = \sum_k a_k^\dagger a_k$ such that states k are of negative parity only. See [1] for more detail.

does not share such symmetry. A necessary condition for this to happen is the presence of degenerate ground states connected by actions of the symmetry generators $\hat{S}_i|\Psi\rangle$. In the nuclear case this is manifested in the collective phenomena where nuclei develop for example shape deformation and particle condensates that violate rotational and particle-number symmetries (like HFB and BCS theories) respectively, even though the forces involved conserve them. This concept is essential for interpreting several collective phenomena observed in the nucleus like rotational bands, spectra, pairing and transition strengths.

3.3.2 The generator coordinate method (GCM)

In this section, we present the GCM framework, which enables one to restore symmetries after mean-field calculations and describes the mixing of different deformations and single-particle configurations. To quantify the degree of symmetry breaking, we introduce the collective or generator coordinate $\boldsymbol{q}$, which encompasses all information about the degree of deviation from a symmetric state like parameters of shape deformation, gauge angles, Euler angles *etc.* Thus, the GCM wavefunction is defined as a superposition of the (continuous or discrete) collective degrees of freedom $\boldsymbol{q}$ as

$$|\Psi_\mu\rangle = \int d\boldsymbol{q}\, f_\mu(\boldsymbol{q})\, |\Phi(\boldsymbol{q})\rangle, \tag{3.53}$$

where the weight functions (amplitudes) $f_\mu(\boldsymbol{q})$ labelled by quantum numbers μ need to be determined. One of the motivations for 3.53 is the non-orthogonality of the mixing components $|\Phi(\boldsymbol{q})\rangle$ which may contribute to the full description of the system. It represents clearly the horizontal philosophy, where we construct a total wavefunction from a superposition of symmetry breaking states instead than from symmetry conserving, like in the vertical approach. The energy of $|\Psi_\mu\rangle$ is given by the expectation value of the same Hamiltonian $\hat{H}$ that describes the symmetry breaking mean-field wavefunction $|\Phi(\boldsymbol{q})\rangle$ (which can be from the HF, BCS or HFB type) in the form

$$E_\mu = \frac{\langle\Psi_\mu|\hat{H}|\Psi_\mu\rangle}{\langle\Psi_\mu|\Psi_\mu\rangle}, \tag{3.54}$$

thus the variational equation is

$$\delta E_\mu = \frac{\partial E_\mu}{\partial |\Psi_\mu\rangle}|\delta\Psi_\mu\rangle + \langle\delta\Psi_\mu|\frac{\partial E_\mu}{\partial\langle\Psi_\mu|}, \tag{3.55}$$

from the term of $|\delta\Psi_\mu\rangle$ where

$$|\delta\Psi_\mu\rangle = \frac{\partial|\Psi_\mu\rangle}{\partial f_\mu}\delta f_\mu = \delta f_\mu \int d\boldsymbol{q}\,|\Phi(\boldsymbol{q})\rangle, \tag{3.56}$$

we get the Hill-Wheeler-Griffin equation [68, 69, 70]

$$\int d\boldsymbol{q}\left[\mathcal{H}(\boldsymbol{q}',\boldsymbol{q}) - E_\mu\mathcal{N}(\boldsymbol{q}',\boldsymbol{q})\right] f_\mu(\boldsymbol{q}) = 0 \tag{3.57}$$

where

$$\mathcal{H}(\boldsymbol{q}',\boldsymbol{q}) = \langle\Phi(\boldsymbol{q}')|\hat{H}|\Phi(\boldsymbol{q})\rangle \tag{3.58}$$

$$\mathcal{N}(\boldsymbol{q}',\boldsymbol{q}) = \langle\Phi(\boldsymbol{q}')|\Phi(\boldsymbol{q})\rangle \tag{3.59}$$

are called the energy and norm kernels, respectively. The latter along with

$$\rho_{ij}(\boldsymbol{q}',\boldsymbol{q}) = \frac{\langle\Phi(\boldsymbol{q}')|c_j^\dagger c_i|\Phi(\boldsymbol{q})\rangle}{\langle\Phi(\boldsymbol{q}')|\Phi(\boldsymbol{q})\rangle}, \tag{3.60}$$

$$\kappa_{ij}(\boldsymbol{q}',\boldsymbol{q}) = \frac{\langle\Phi(\boldsymbol{q}')|c_j c_i|\Phi(\boldsymbol{q})\rangle}{\langle\Phi(\boldsymbol{q}')|\Phi(\boldsymbol{q})\rangle}, \tag{3.61}$$

$$\kappa_{ij}^*(\boldsymbol{q}',\boldsymbol{q}) = \frac{\langle\Phi(\boldsymbol{q})|c_i^\dagger c_j^\dagger|\Phi(\boldsymbol{q}')\rangle}{\langle\Phi(\boldsymbol{q})|\Phi(\boldsymbol{q}')\rangle}. \tag{3.62}$$

are the main quantities for any GCM calculation since we can express any observable in terms of them.

In practical applications, $\boldsymbol{q}$ is a discrete variable so we will present from now on the discrete version of it from which the continuous case can be recovered straightforwardly. We have instead

$$\sum_l \left[\mathcal{H}_{kl} - E_\mu\mathcal{N}_{kl}\right] f_{l,\mu} = 0 \tag{3.63}$$

where

$$\mathcal{H}_{kl} = \mathcal{H}(q_k, q_l), \tag{3.64}$$

$$\mathcal{N}_{kl} = \mathcal{N}(q_k, q_l). \tag{3.65}$$

Equation 3.63 is almost an eigenvalue problem except for the presence of the norm kernel $\mathcal{N}$. A method for dealing with this inconvenience is called symmetric orthogonalization which assumes that $\mathcal{N}$ can be decomposed into invertible matrices $\mathcal{N}^{1/2}$ that follow

$$\sum_m \mathcal{N}_{km}^{1/2}\mathcal{N}_{ml}^{1/2} = \mathcal{N}_{kl}, \tag{3.66}$$

$$\sum_m \mathcal{N}_{km}^{-1/2}\mathcal{N}_{ml}^{1/2} = \delta_{kl}, \tag{3.67}$$

$$\sum_{mn} \mathcal{N}_{km}^{-1/2}\mathcal{N}_{mn}\mathcal{N}_{nl}^{-1/2} = \delta_{kl}. \tag{3.68}$$

After applying property 3.68 to 3.63 we get the eigenvalue problem

$$\sum_l \left[\tilde{\mathcal{H}}_{kl} - E_\mu \delta_{kl}\right] g_{l,\mu} = 0, \tag{3.69}$$

with the modified kernel and weight functions

$$\tilde{\mathcal{H}}_{kl} = \sum_{mn} \mathcal{N}_{km}^{-1/2}\mathcal{H}_{mn}\mathcal{N}_{nl}^{-1/2}, \tag{3.70}$$

$$g_{k,\mu} = \sum_l \mathcal{N}_{kl}^{1/2} f_{l,\mu}. \tag{3.71}$$

Having solved for g_μ and $\mathcal{N}^{1/2}$, the expectation values of any one-body operator $\hat{O}$ can be calculated using 3.67 as

$$\langle \Psi_\mu | \hat{O} | \Psi_\nu \rangle = \sum_{kl} f_{k,\mu}^* \langle \Phi(\boldsymbol{q}_k) | \hat{O} | \Phi(\boldsymbol{q}_l) \rangle f_{l,\nu} = \sum_{kl} g_{k,\mu}^* \tilde{O}_{kl}\, g_{l,\nu}, \tag{3.72}$$

where

$$\tilde{O}_{kl} = \sum_{mn} \mathcal{N}_{mk}^{-1/2} \langle \Phi(\boldsymbol{q}_m) | \hat{O} | \Phi(\boldsymbol{q}_n) \rangle \mathcal{N}_{nl}^{-1/2}. \tag{3.73}$$

3.3.3 Restoration of symmetries: projection theory

The projection theory is one of the applications of the GCM to restore broken symmetries. Together with the mean-field calculations, this approach has been developed in two ways depending on the order of these two operations. Minimization of the energy from symmetry restored wavefunctions is called variation after projection (VAP), while the projection of minimum energy states is the projection after variation (PAV) [7]. In this section we present only the PAV method which was applied for calculations in chapter 5.

For a continuous symmetry characterized by quantum numbers λ we need to construct a projection operator $\hat{P}^\lambda$ that extracts the component that transforms like the irreducible representation $|\lambda\rangle$ of a general state $|\Psi\rangle$. To achieve this consider the action of the group operator $\hat{R}(\boldsymbol{q})$ in the symmetry multiplet state $|\lambda\mu\rangle$ given by

$$\hat{R}(\boldsymbol{q})\,|\lambda\mu\rangle = \sum_{\rho\sigma} \langle \rho\sigma | \hat{R}(\boldsymbol{q})\,|\lambda\mu\rangle | \rho\sigma \rangle = \sum_\sigma D_{\sigma\mu}^\lambda(\boldsymbol{q}) | \lambda\sigma \rangle, \tag{3.74}$$

where $D_{\sigma\mu}^\lambda(\boldsymbol{q})$ are the continuous single valued representations of the group. In the case of the group of rotations these are the well-known Wigner functions. These functions

follow the orthogonality

$$\int d\boldsymbol{q}\, D^{\lambda *}_{\mu\nu}(\boldsymbol{q}) D^{\lambda'}_{\mu'\nu'}(\boldsymbol{q}) = \frac{V}{n}\delta_{\lambda\lambda'}\delta_{\mu\mu'}\delta_{\nu\nu'}, \tag{3.75}$$

where the volume is $V = \int d\boldsymbol{q}$ and n is the dimension of the irreducible representation $|\lambda\mu\rangle$. In the case of rotational symmetry for states $|IM\rangle$ we have $V = 8\pi^2$ (as long as both λ and λ' are both integers or half-integers [25]) and $n = 2I + 1$. Multiplying 3.74 by $D^{\gamma *}_{\alpha\beta}(\boldsymbol{q})$, integrating over $\boldsymbol{q}$ and applying 3.75 results in

$$\int d\boldsymbol{q}\, D^{\gamma *}_{\alpha\beta}(\boldsymbol{q}) \hat{R}(\boldsymbol{q}) \,|\lambda\mu\rangle = \delta_{\gamma\lambda}\delta_{\beta\mu}\frac{V}{n}|\gamma\alpha\rangle, \tag{3.76}$$

where the resemblance of the left hand side with the GCM state 3.53 is apparent having the parameters of the Lie algebra play the role of the generator coordinate. From 3.76 we define the projection operator onto state $|\lambda\mu\rangle$ as

$$\hat{P}^{\lambda}_{\mu\nu} = \frac{n}{V}\int d\boldsymbol{q}\, D^{\lambda *}_{\mu\nu}(\boldsymbol{q})\hat{R}(\boldsymbol{q}), \tag{3.77}$$

such that

$$\hat{P}^{\lambda}_{\mu\nu}|\alpha\beta\rangle = \delta_{\alpha\lambda}\delta_{\nu\beta}|\lambda\mu\rangle, \qquad \hat{P}^{\lambda\dagger}_{\mu\nu} = \hat{P}^{\lambda}_{\nu\mu}, \tag{3.78}$$

and thus we can establish the projected state with good quantum numbers as

$$|\Phi^{\lambda}_{\mu\nu}\rangle = \hat{P}^{\lambda}_{\mu\nu}|\Phi\rangle. \tag{3.79}$$

The GCM energy for this projected wavefunctions is

$$E_{\lambda,\mu\nu} = \frac{\langle\Phi^{\lambda}_{\mu\nu}|\hat{H}|\Phi^{\lambda}_{\mu\nu}\rangle}{\langle\Phi^{\lambda}_{\mu\nu}|\Phi^{\lambda}_{\mu\nu}\rangle} = \frac{\langle\Phi|\hat{P}^{\lambda\dagger}_{\mu\nu}\hat{H}\hat{P}^{\lambda}_{\mu\nu}|\Phi\rangle}{\langle\Phi|\hat{P}^{\lambda\dagger}_{\mu\nu}\hat{P}^{\lambda}_{\mu\nu}|\Phi\rangle} = \frac{\langle\Phi|\hat{H}\hat{P}^{\lambda}_{\mu\nu}|\Phi\rangle}{\langle\Phi|\hat{P}^{\lambda}_{\mu\nu}|\Phi\rangle}, \tag{3.80}$$

where the projection operators commute with the Hamiltonian according to 3.50 and can be combined into a single projector as shown for example in [12]. Since every state follows

$$|\Phi\rangle = \sum_{\lambda\mu} f_{\lambda\mu}|\Phi^{\lambda}_{\mu\mu}\rangle = \sum_{\lambda\mu} f_{\lambda\mu}\hat{P}^{\lambda}_{\mu\nu}|\Phi\rangle, \tag{3.81}$$

the projection results in lower values of energy for each component than the original symmetry breaking state.

The case of rotational symmetry

Rotational symmetry is relevant for nuclear physics since the electromagnetic observables which are some of the most important probes to study the nucleus depend on it for their calculations (see chapter 4). Thus the restoration of rotational symmetry is a crucial step to be able to access those observables after mean-field calculations. The states associated to this symmetry are the angular momentum $|IM\rangle$ that hold the well-known relations $\hat{I}^2|IM\rangle = I(I+1)|IM\rangle$ and $\hat{I}_z|IM\rangle = M|IM\rangle$ and the parameters

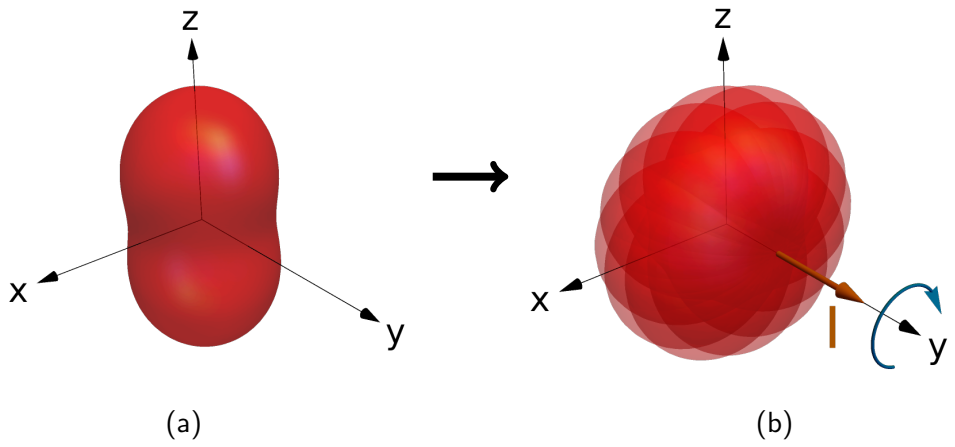

Figure 3.2: Schematic representation of the active rotational symmetry restoration of an axially deformed quantum body. (a) Symmetry breaking wavefunction. (b) Symmetry restored wavefunction in the sense of 3.53 where the mixing is performed over the Euler angle β corresponding to the rotation along the y-axis.

are the Euler angles α, β and γ.

The projection operator for rotational symmetry is given by space rotations about angles $\boldsymbol{q} = (\alpha, \beta, \gamma)$ as

$$\hat{P}^I_{MK} = \frac{2I+1}{8\pi^2} \int_0^{2\pi} d\alpha \int_0^{\pi} d\beta \sin(\beta) \int_0^{2\pi} d\gamma \, D^{I*}_{MK}(\alpha, \beta, \gamma) \hat{R}(\alpha, \beta, \gamma), \tag{3.82}$$

where the group operator can be expressed in terms of angular momentum operators $\hat{I}_i$ in a given reference frame as

$$\hat{R}(\alpha, \beta, \gamma) = e^{-i\frac{\alpha}{\hbar}\hat{I}_z} e^{-i\frac{\beta}{\hbar}\hat{I}_y} e^{-i\frac{\gamma}{\hbar}\hat{I}_z}. \tag{3.83}$$

and the projected states are

$$|\Psi_{IM}\rangle = \sum_K f^{IK} \hat{P}^I_{MK} |\Phi\rangle = \sum_K |\tilde{\Phi}_{IMK}\rangle, \tag{3.84}$$

where the f^{IK} are interpreted as probability amplitudes of measuring the wavefunction at a particular orientation.

It is common practice to retain the axial symmetry of the nucleus, that is, to conserve the quantum number M. This reduces the $3D$ integration over the three Euler angles to a $1D$ integral over the angle β of rotations around y, reducing the computational costs by several orders of magnitude [71]. The projector operator 3.82 simplifies to

$$\hat{P}^I_{MK} = \frac{2I+1}{2} \delta(\hat{I}_z - M) \int_0^{\pi} d\beta \sin(\beta) \, d^{I*}_{MK}(\beta) e^{-i\frac{\beta}{\hbar}\hat{I}_y} \, \delta(\hat{I}_z - K), \tag{3.85}$$

which when acting on the wavefunction it is interpreted in two ways: active and passive views. In the active view the operation $\delta(\hat{I}_z - K)$ projects on good quantum number

K in a predetermined axis followed by a rotation of the wavefunction along the y-axis restoring the angular momentum I by forming a superposition of rotated states. Finally it projects M in the same predetermined axis. The passive view acts on the reference frame where the first operation projects the angular momentum on the intrinsic z-axis frame, followed by a rotation of β to set the laboratory frame orientation and then projecting the angular momentum to M in this frame. The former view is schematically illustrated in Fig. 3.2.

4

Nuclear phenomenology: electromagnetic interactions and isomerism

A defining feature of composite systems is the appearance of emergent phenomena as their extensive quantities are scaled [11]. In the atomic nucleus, the increase in mass by changes in the number of nucleons in it leads to a diversity of structural properties enhanced by spontaneous symmetry breaking mechanisms and allowing the expression of a broad spectrum of observables. This richness of phenomena has as a consequence the absence of a complete or standard model of nuclear physics [72]. The discrete changes in mass by nucleon units are the primary source of emergent behaviour in nuclear interactions, as they enhance certain traits while suppressing others across the nuclear chart in a discontinuous fashion.

These emergent properties make each isotope uniquely characterized by its observables of binding energy, deformations, pairing, decay mechanism, collectivity, excitation structure, interactions with the environment, reaction channels *etc.* Among these, the electromagnetic interactions play a crucial role in the information that can be learned from the nucleus. Given that it is composed of electrically charged protons and magnetically interacting neutrons, it is susceptible to interactions with external electromagnetic fields and it constitutes one of the best sources of information to probe nuclear theories.

In this section we describe the electric moments emphasizing in the quadrupole and octupole moments, which are the quantities that describe spatial charge distributions of the nucleus or any classical or quantum extended charged body. Also, the magnetic dipole moment describes its magnetic interactions and influences strongly in the electronic configuration of the atom and the solid state structure in which these are embedded. Additionally, we explain the electromagnetic decay mechanisms and the very important emergent property of nuclear isomerism which has caught the interest of scientist across many areas for its potential applications.

4.1 Electric quadrupole and octupole moments

In classical electrodynamics, the multipole expansion of the electric potential generated by a static source is an essential tool for the study of the properties and interactions of extended charge distributions [73]. Each term in the expansion contains a characteristic aspect of the field encoded in its mathematical properties. When all charges in the distribution have the same sign (which is the case of the atomic nucleus), the terms in

the expansion can be physically interpreted as geometric deformations, with the lowest order terms providing the dominant contributions. The classical expression for the multipole moment Q, of order λ and component μ of a charge distribution in spherical coordinates is given by

$$Q_{\lambda\mu} = \int d\boldsymbol{r}\rho(\boldsymbol{r})r^{\lambda}Y_{\lambda\mu}(\Omega), \tag{4.1}$$

where the integral is performed over the charge volume and $\rho(\mathbf{r})$ is its density. The monopole term $\lambda = 0$ is scalar and contains the information about the the total charge point-like properties of the source. The first-order $\lambda = 1$ dipole moment is a vector quantity that describes the asymmetry of charge distribution with respect to a plane crossing the origin of coordinates. This quantity violates parity symmetry, which has motivated lots of research for its implications in fundamental symmetries of nature and the nuclear forces [74, 75, 76, 77]. So far, no non-zero electric dipole moment (EDM) has been measured for the nucleus or any elementary particle. Thus, the second lowest experimentally accessible observable is the the second-order $\lambda = 2$ quadrupole moment which is the traceless symmetric tensor in Cartesian form given by

$$Q^{(2)}_{ij} = \int d\boldsymbol{r}\rho(\boldsymbol{r})\big(3x_ix_j - r^2\delta_{ij}\big), \tag{4.2}$$

whose diagonal entries quantify the axially symmetric elongation or compression of the charge distribution along each axis. Similar to the dipole, the $\lambda = 3$ octupole moment breaks parity and can be expressed in Cartesian coordinates by [78]

$$Q^{(3)}_{ijk} = \int d\boldsymbol{r}\rho(\boldsymbol{r})\big(5x_ix_jx_k - r^2(x_i\delta_{jk} + x_j\delta_{ik} + x_k\delta_{ij})\big), \tag{4.3}$$

whose diagonal entries quantify the asymmetry of charge distribution along each axis. We delay comments on its experimental status in the atomic nucleus for later. Additionally, it holds the properties

$$\begin{aligned} Q^{(3)}_{ijk} &= Q^{(3)}_{\sigma(ijk)}, \\ \sum_i Q^{(3)}_{iik} &= 0 \quad \forall k, \end{aligned} \tag{4.4}$$

where $\sigma(ijk)$ is any permutation of ijk. Definitions 4.2 and 4.3 above may differ in the literature by constant pre-factors.

In quantum mechanics, the multipole expansions are equally useful albeit restricted by the rules of first quantization and the symmetries of the system. The associated operators in the multipole expansion $\hat{Q}_{\lambda\mu}$ are spherical tensors with assigned parity given by $(-1)^{\lambda}$, which imposes selection rules in the transitions between the states of the system. The associated observable is given by the expectation values of maximum projection of spherically symmetric angular momentum eigenstates like

$$\mathcal{Q}_{\lambda} = \sqrt{\frac{16\pi}{2\lambda+1}}\langle II|\hat{Q}_{\lambda 0}|II\rangle, \tag{4.5}$$

and is called the spectroscopic moment of order λ.

In order to obtain numerical values of multipole moments 4.5 (or in general of any spherical tensor) between axial deformed states $|K\rangle$ where K is the projection of angular momentum in a predetermined axis, we need to restore the rotational symmetry using the tools of section 3.3.3. The angular momentum projector operators 3.82 and any spherical tensor $\hat{Q}_{\lambda\mu}$ hold the identity [12]

$$\hat{P}^{I'}_{K'M'}\,\hat{Q}_{\lambda\mu}\,\hat{P}^{I}_{MK} = \langle I, M, \lambda, \mu | I', M'\rangle \sum_{\nu\sigma} \langle I, \nu, \lambda, \sigma | I', K'\rangle\, \hat{O}_{\lambda\sigma}\,\hat{P}^{I}_{\nu K}, \tag{4.6}$$

thus, the matrix elements between projected states $|IMK\rangle$ of the operator $\hat{Q}_{\lambda\mu}$ are

$$\begin{aligned}\langle I'M'K'|\hat{Q}_{\lambda\mu}|IMK\rangle &= \langle K'|\hat{P}^{I'}_{K'M'}\,\hat{Q}_{\lambda\mu}\,\hat{P}^{I}_{MK}|K\rangle \\ &= \langle I, M, \lambda, \mu | I', M'\rangle \sum_{\nu\sigma} \langle I, \nu, \lambda, \sigma | I', K'\rangle\, \langle K'|\hat{Q}_{\lambda\sigma}\,\hat{P}^{I}_{\nu K}|K\rangle,\end{aligned} \tag{4.7}$$

where evaluating for $IKM = I'K'M'$ and replacing projector 3.85 for axially deformed systems we get

$$\begin{aligned}\langle IMK|\hat{Q}_{\lambda\mu}|IMK\rangle &= \langle K|\hat{P}^{I}_{KM}\,\hat{Q}_{\lambda\mu}\,\hat{P}^{I}_{MK}|K\rangle \\ &= \langle I, M, \lambda, \mu | I, M\rangle \frac{2I+1}{2} \sum_{\sigma} \langle I, K-\sigma, \lambda, \sigma | I, K\rangle \\ &\qquad \times \int_0^{\pi} d\beta \sin(\beta)\, d^{*I}_{K-\sigma,K}(\beta)\, \langle K|\hat{Q}_{\lambda\sigma} e^{-i\frac{\beta \hat{I}_y}{\hbar}}|K\rangle.\end{aligned} \tag{4.8}$$

Thus, we can perform a Taylor expansion over the operator $e^{-i\frac{\beta \hat{I}_y}{\hbar}}$ [12]. Considering the large-axial-deformation approximation where the matrix element $\langle K|\hat{Q}_{\lambda\sigma} e^{-i\frac{\beta \hat{I}_y}{\hbar}}|K\rangle$ is a rapidly-varying function of β and taking the zeroth-order term we get

$$\langle IMK|\hat{Q}_{\lambda\mu}|IMK\rangle \approx \langle I, M, \lambda, \mu | I, M\rangle \langle I, K, \lambda, 0 | I, K\rangle\, \langle K|\hat{Q}_{\lambda 0}|K\rangle, \tag{4.9}$$

For $M = I$ and $\mu = 0$, we get the matrix element of the right hand side of 4.5

$$\langle IIK|\hat{Q}_{\lambda 0}|IIK\rangle \approx \langle I, I, \lambda, 0 | I, I\rangle \langle I, K, \lambda, 0 | I, K\rangle\, \langle K|\hat{Q}_{\lambda 0}|K\rangle, \tag{4.10}$$

from which we derive

$$\mathcal{Q}_{\lambda} \approx \langle I, I, \lambda, 0 | I, I\rangle \langle I, K, \lambda, 0 | I, K\rangle\, \mathcal{Q}^0_{\lambda}, \tag{4.11}$$

where $\mathcal{Q}^0_{\lambda}$ is the intrinsic moment of order λ.

The atomic nucleus can be viewed as an extended system of positively charged matter, thus the study of its geometrical shape is a legitimate area of research and a necessity to understand its structure, excitation spectra, physical size, reaction mechanisms and even connections with fundamental questions of physics [79, 80, 77, 81]. A rule of thumb to know the largest multipole that is expected to contribute to the nuclear deformation is given by the condition $\lambda < A^{1/3}$ [23]. Observations show that

$Q_{\lambda\mu}$	$K=0$	$K\neq 0$
Q_{20}	 $\hat{\mathcal{P}}$, $\hat{\mathcal{S}}_y$, $\hat{\mathcal{T}}$	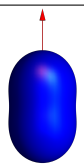 $\hat{\mathcal{P}}$, $\hat{\mathcal{S}}_y\hat{\mathcal{T}}$
Q_{30}	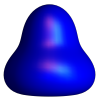 $\hat{\mathcal{P}}\hat{\mathcal{S}}_y$, $\hat{\mathcal{T}}$	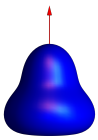 $\hat{\mathcal{P}}\hat{\mathcal{S}}_y\hat{\mathcal{T}}$

Table 4.1: Symmetries of an axially deformed quadrupole and octupole quantum body.

nuclear interaction preserves parity, so the lowest multipole orders that carry information about deformation are the monopole and quadrupole moments. By definition, the observable associated with quadrupole deformation is given by

$$\mathcal{Q} = \sqrt{\frac{16\pi}{5}}\langle II|\hat{Q}_{20}|II\rangle, \tag{4.12}$$

where the component of the multipole is taken to be the one along the predetermined z-axis and calculated between the projected states of maximum angular momentum projection. The quantity in 4.12 is called the spectroscopic quadrupole moment. To calculate the intrinsic quadrupole moment $\mathcal{Q}_0$ we evaluate 4.11 for $\lambda = 2$ from which we get

$$\mathcal{Q} = \frac{3K^2 - I(I+1)}{(2I+3)(I+1)}\mathcal{Q}_0, \tag{4.13}$$

where it can be seen that $\mathcal{Q}$ vanishes for $I = 0, 1/2$ even for non-zero $\mathcal{Q}_0$ values.

The symmetry restoration features of the octupole moment follow essentially the same rules since it is also a spherical tensor. Several reviews have compiled the properties to be expected for intrinsic octupole deformed nuclei [82, 83, 84, 85, 86]. Some suggest that certain configurations of protons and neutrons around the values 34, 56, 88 and 134 [87] seem to posses an enhanced octupole deformation which is manifested by the presence of a low energy negative parity rotational band in even-even nuclei and the presence of parity doublet bands in odd-A nuclei. These experimental observations have motivated lots of research in recent years, like for instance the experimental measurements of strong E3 transitions between 3^-_1 and 0^+_1 states in even-even nuclei that indicate intrinsic octupole moments [79]. It has also been demonstrated that octupole deformation enhances parity breaking Schiff and anapole moments, making actinides the best candidates for accessible experimental studies on fundamental symmetries [5, 88].

Deformed shapes hold certain symmetries with respect to spatial rotations an reflections useful for its description [89, 90]. Axial deformations are the ones of most interest because they setup the lowest energy deformation in most of nuclei, even though in

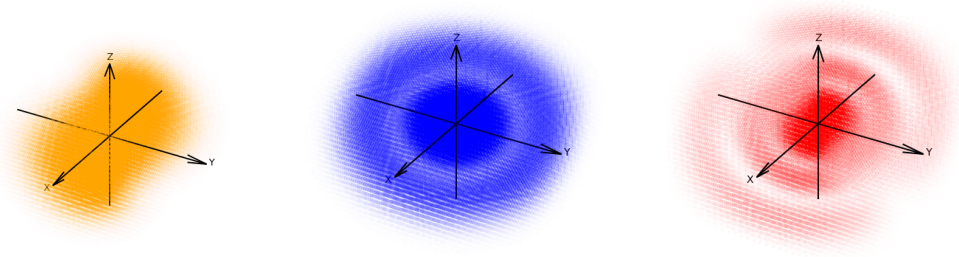

(a) $0d_{5/2}$ (b) $1p_{1/2}$ (c) $2p_{3/2}$

Figure 4.1: Probability densities of single-particle orbitals of the isotropic harmonic oscillator potential.

some regions of the nuclear chart triaxiality is relevant [91, 90]. The minimal set of symmetries to describe an axially deformed nucleus along a predefined z-axis are given by the following operators: parity $\hat{\mathcal{P}}$ which inverts the Cartesian axes as

$$\begin{aligned} x &\to -x, \\ y &\to -y, \\ z &\to -z, \end{aligned} \tag{4.14}$$

the y-signature $\hat{\mathcal{S}}_y$ which performs a rotation of π around the y-axis (by convention) given by

$$\hat{\mathcal{S}}_y = e^{-\frac{i\pi}{\hbar}\hat{I}_y}, \tag{4.15}$$

and time reversal $\hat{\mathcal{T}}$ which inverts the orientation of spins as described in section 2.1.4 by

$$t \to -t, \tag{4.16}$$

and compositions of them. Axial shapes defined in this way are invariant under rotations around z-axis given by

$$\hat{\mathcal{R}}_z = e^{-\frac{i\theta}{\hbar}\hat{I}_z}, \tag{4.17}$$

for any angle θ. Table 4.1 summarizes the symmetries for axial quadrupole and axial octupole deformations with projections of angular momentum $K = 0$ and $K \neq 0$. A relevant composition of the symmetry operators above is the simplex-y operator which performs reflections with respect to the xz-plane given by

$$\hat{\Sigma}_y = \hat{\mathcal{P}}\hat{\mathcal{S}}_y, \tag{4.18}$$

and the y-simplex^T which reflects with respect to the xz-plane and inverts the orientation of spins and momenta given by

$$\hat{\Sigma}_y = \hat{\mathcal{T}}\hat{\mathcal{P}}\hat{\mathcal{S}}_y. \tag{4.19}$$

Several nuclear models have been devised to account for deformation, some con-

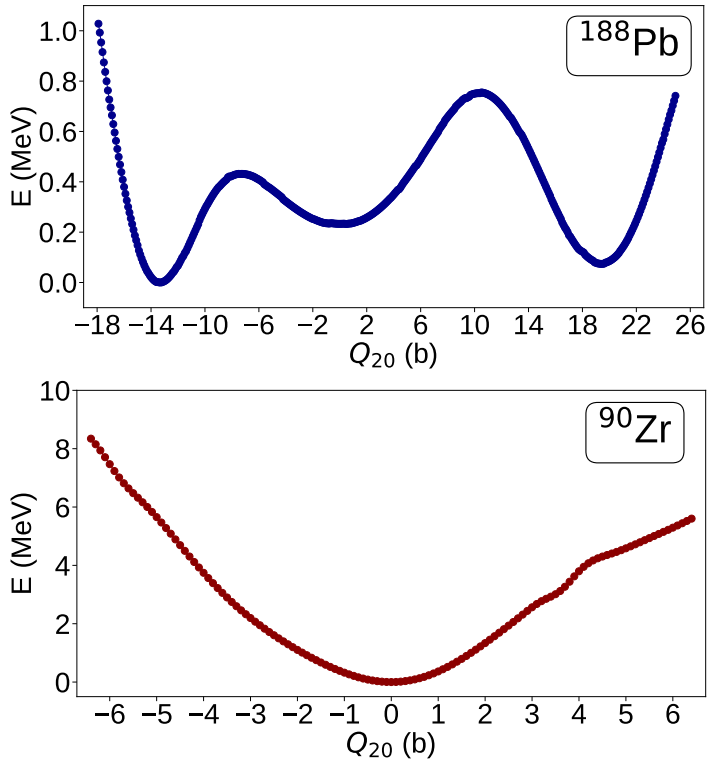

Figure 4.2: Unprojected energy surfaces with respect to quadrupole moment in Q_{20} for semi-magic nuclei ^{188}Pb and ^{90}Zr using the functional UNEDF1. The minima correspond to spherical, oblate and prolate deformations in the case of ^{188}Pb.

sider collective degrees of freedom to explain rotational phenomena, others calculate single-particle orbitals in anisotropic potentials like the Nilsson model [34]. A more advanced level of sophistication combines both single-particle and collective variables in the so called particle-rotor models, which are applied mostly to odd-mass deformed nuclei [92, 93]. In models based in group theory, deformation emerges from particular configurations of the many-body state and the associated irreducible representations favoured by the algebraic structure of the interaction [94].

The elementary single-particle estimates offer an important perspective for analysing the electromagnetic static properties of the nucleus and its transitions [95]. In the single-particle shell model the potential is approximated by a harmonic oscillator, where only the proton eigenfunctions $\psi^{\pi}_{nljm}(\boldsymbol{r})$ carry non-zero quadrupole moment for a total angular momentum $j > 1/2$ given by

$$\mathcal{Q}_{\text{s.p.}} = -e\frac{2j-1}{2(j+1)}\langle r^2\rangle, \tag{4.20}$$

where e is the elementary charge and $\langle r^2\rangle$ is the mean square radius of the isotropic harmonic oscillator wavefunctions. Fig. 4.1 represent the probability distributions of single-particle orbitals where the spherical distribution of the $j = 1/2$ orbital carrying no quadrupole deformation is evident while the other two $j = 3/2$ and $j = 5/2$ spread along the xy-plane. For n protons in a shell j coupled to total angular momentum j

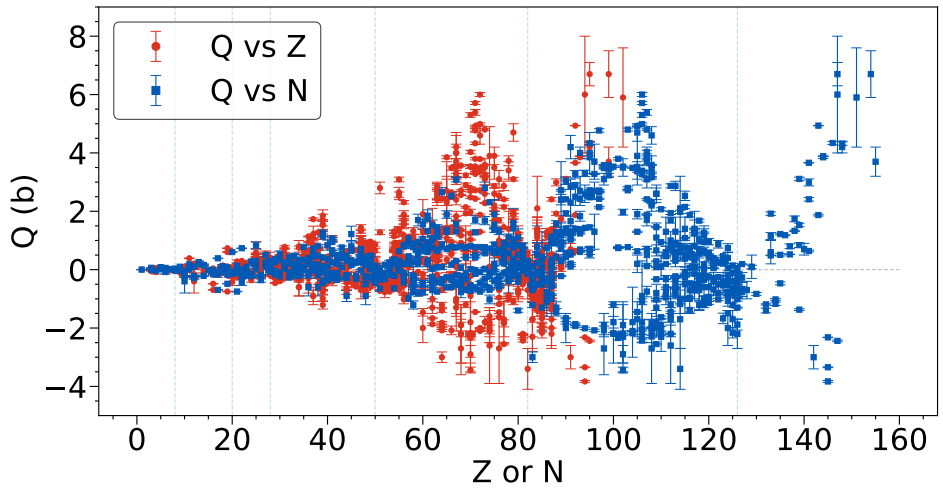

Figure 4.3: Experimental spectroscopic electric quadrupole moments of ground states plotted with respect to the number of neutrons and protons simultaneously. Vertical lines denote the magic numbers. Data retrieved from [3].

(that is seniority 1), the quadrupole moment is given by [96]

$$\mathcal{Q}^{(n)}_{\text{s.p.}} = \mathcal{Q}_{\text{s.p.}}\left[1 - 2\frac{n-1}{2j-1}\right], \tag{4.21}$$

In this elementary approach, the charge source comes solely from the protons which show clear disagreement with experiment [12], showing that the quadrupole moments must emerge from coherent contributions of many proton states. A placebo solution to this issue comes from the introduction of effective charges for protons and neutrons in order to account for the contributions of the protons outside the valence space. Usually, effective charges become adjustable free parameters not possible to determine from within the model itself, which improve the agreement with experiment but loose explanatory power to the actual processes that cause deformation and transitions. On the other hand, in the self-consistent methods, the deformation is attained by the organization of the nucleons via the nuclear interaction alone. In Fig. 4.2 are depicted energy surfaces with respect to different values of quadrupole moments where unconstrained calculations would lead to the local minima of the surface. This figure displays how several deformation properties like the shape coexistence can be reproduced self-consistently.

There is a large dataset of spectroscopic quadrupole moments [97, 98] from several techniques [99, 100, 101], which evidence that most of the nuclei are deformed. This data is displayed in Fig. 4.3. Positive values mean prolate deformation, where the charge accumulates along the intrinsic $z-$axis and negative values mean oblate deformation where the charge accumulates along the intrinsic $xy-$plane. The data displays a pattern where its values are greatly diminished around the magic numbers and display its largest values in the mid-shell regions. Also, there appears to be a prolate dominance over the oblate, which explained by few models, for example [102, 103].

4.2 The magnetic dipole moment

In classical electrodynamics, magnetism is generated by currents, that is, the motion of electric charges. In a similar way as for the potential of a static charge distribution, the magnetic vector potential $\boldsymbol{A}(\boldsymbol{r})$ can be expressed in terms proportional to the vector multipoles

$$\boldsymbol{M}_{\lambda\mu} = \int d\boldsymbol{r}\, \boldsymbol{j}(\boldsymbol{r}) r^{\lambda} Y_{\lambda\mu}(\theta, \phi), \tag{4.22}$$

where the integral is performed over the current distribution and $\boldsymbol{j}(\boldsymbol{r})$ is the current density. Since charge currents have to form closed loops, the monopole term $\lambda = 0$ vanishes. The contribution of the dipole term $\lambda = 1$ can be rewritten using the magnetic dipole moment

$$\boldsymbol{\mu} = \frac{1}{2} \int d\boldsymbol{r}\, \boldsymbol{r} \times \boldsymbol{j}(\boldsymbol{r}), \tag{4.23}$$

which quantifies the strength and direction of the magnetic field generated by the current density.

The most elementary classical experience of magnetism comes from permanent magnets. However, it has been demonstrated that all magnetic properties of solids can only be explained by quantum mechanics [104], from the bounded motion of its subatomic constituents and their intrinsic spins. Thus, the quantum expression for the operator $\hat{\boldsymbol{j}}(\boldsymbol{r})$ has contributions from convection current $\hat{\boldsymbol{j}}_c$ and magnetization current $\hat{\boldsymbol{j}}_m$. $\hat{\boldsymbol{j}}_c$ is proportional to the angular momentum $\hat{\boldsymbol{L}}$, while $\hat{\boldsymbol{j}}_m$ is proportional to the spin $\hat{\boldsymbol{S}}$ of the constituents of the system. Thus, a general expression for the magnetic multipole operator has the form

$$\hat{M}_{\lambda\mu} \propto \boldsymbol{\nabla}(r^{\lambda} Y_{\lambda\mu}(\Omega)) \cdot \left(g_s \hat{\boldsymbol{S}} + g_l \tfrac{2}{\lambda+1} \hat{\boldsymbol{L}} \right), \tag{4.24}$$

where g_s and g_l are gyromagnetic factors dependent on the specific particle of the system.

Different than in the electric case, both protons and neutrons are direct causes of the magnetic dipole moment, the former from their motion in the nucleus and spin, and the latter exclusively from its spin. From relativistic quantum mechanics [12], the one-body magnetic moment generated by the individual nucleons is given by

$$\hat{\boldsymbol{\mu}}^{\sigma} = \mu_N \left[g_S^{\sigma} \hat{\boldsymbol{S}} + g_L^{\sigma} \hat{\boldsymbol{L}} \right], \tag{4.25}$$

where $\sigma = \pi, \nu$ and in Gaussian units the nuclear magneton μ_N is given by

$$\mu_N = \frac{e\hbar}{2m_{\pi}c}, \tag{4.26}$$

and the free nucleon gyromagnetic factors have values of

$$g_L^{\pi} = 1, \qquad g_L^{\nu} = 0, \qquad g_S^{\pi} = 5.587, \qquad g_S^{\nu} = -3.826. \tag{4.27}$$

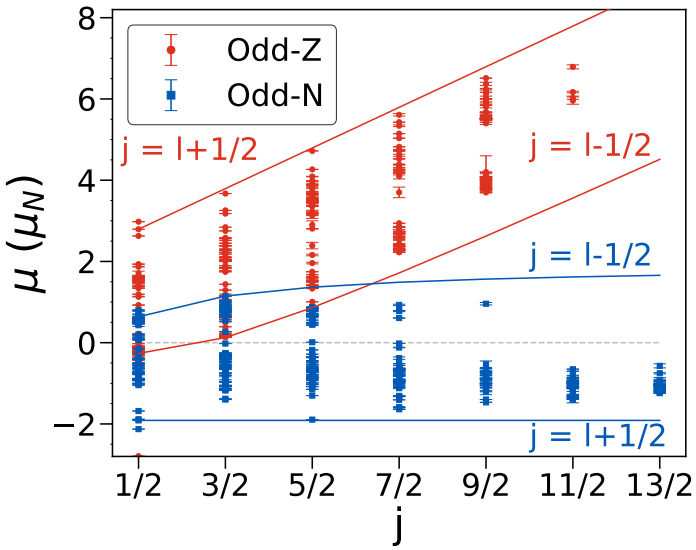

Figure 4.4: Experimental magnetic dipole moments and Schmidt lines. Data from [2].

The associated magnetic multipole operators are spherical tensors and their parity is given by $(-1)^{\lambda-1}$. Thus, the operator associated to the magnetic dipole moment is given by

$$\mu = \sqrt{\frac{4\pi}{3}}\langle II|\hat{\mu}_{10}|II\rangle, \tag{4.28}$$

where the only component measured is along the predetermined z-axis of 4.25 and the projected states are prepared with the maximum projection of angular momentum. Extensions of operator 4.25 to include two-body terms from meson exchange currents have been developed and its effect in the calculations is a current area of research [12].

In a similar manner as for the single-particle quadrupole moments of Eq. 4.20, the magnetic moment of a single nucleon in orbital $j = l \pm 1/2$ is given by

$$\mu^{\sigma}_{\text{s.p.}} = \begin{cases} \left[\left(j-\frac{1}{2}\right)g^{\sigma}_{L} + \frac{1}{2}g^{\sigma}_{S}\right]\mu_N, & j = l+1/2, \\ \frac{j}{j+1}\left[\left(j+\frac{3}{2}\right)g^{\sigma}_{L} - \frac{1}{2}g^{\sigma}_{S}\right]\mu_N, & j = l-1/2, \end{cases} \tag{4.29}$$

these expressions give the so called Schmidt lines which are limiting values for the case of independent nucleons. Few nuclei behave accordingly as can be seen from measurements in Fig. 4.4. From these experimental results, it is clear that the origin of magnetic moments is of strict single-particle character in only a few limited cases. An analogous placebo solution to this issue is the implementation of effective gyromagnetic factors to improve theoretical output. In the non-parametric approaches, the organization of nucleons and orbitals gives rise to the self-consistent polarization of the core due to the odd nucleon and from it a collective magnetic moment is obtained.

4.3 Electromagnetic transitions and spin isomers

In quantum mechanics, the eigenstates of a Hamiltonian are stationary. It means that if a nucleus is prepared in a given excited state it should remain in it indefinitely. This is contrary to experimental observations where nuclei transition to the lowest energy state. In the case where the process is due to electromagnetism, the field oscillations of vacuum and couplings to the electromagnetic field of photons cause the excited states not be eigenstates of the full interaction and thus the decay occurs. The strength of the coupling of the excited states with the vacuum oscillations make half-lives vary in a wide range from picoseconds to billions of years.

From classical electrodynamics it is known that the interaction between external electromagnetic fields $\varphi(\mathbf{r})$ and $\mathbf{A}(\mathbf{r})$ with matter is given by the Hamiltonian

$$H_{\text{int}} = \int d\boldsymbol{r} \left[\varphi(\boldsymbol{r})\rho(\boldsymbol{r}) - \frac{1}{c}\boldsymbol{j}(\boldsymbol{r}) \cdot \boldsymbol{A}(\boldsymbol{r}) \right], \tag{4.30}$$

which after expanding the field in the centre of the charge distribution we can express the interaction in terms of multipoles as [105]

$$H_{\text{int}} = Q\varphi(0) - \boldsymbol{P} \cdot \nabla\varphi(\boldsymbol{r})\Big|_{\boldsymbol{r}=\boldsymbol{0}} - \frac{1}{c}\boldsymbol{\mu} \cdot \Big(\nabla \times \boldsymbol{A}(\boldsymbol{r})\Big)\Big|_{\boldsymbol{r}=\boldsymbol{0}} - \frac{1}{12}\sum_{ij} Q_{ij}\frac{\partial E_j}{\partial x_i}\Big|_{\boldsymbol{r}=\boldsymbol{0}} + ..., \tag{4.31}$$

where the terms that emerge are

$$\begin{aligned} Q &= \int d\boldsymbol{r}\ \rho(\boldsymbol{r}), \\ \boldsymbol{P} &= \int d\boldsymbol{r}\ \boldsymbol{r}\rho(\boldsymbol{r}), \\ \boldsymbol{\mu} &= \frac{1}{2}\int d\boldsymbol{r}\ \boldsymbol{r} \times \boldsymbol{j}(\boldsymbol{r}), \\ Q_{ij} &= \int d\boldsymbol{r}\ \rho(\boldsymbol{r})(3x_i x_j - r^2\delta_{ij}), \end{aligned} \tag{4.32}$$

and can be identified with the multipoles of the previous sections.

To step into quantum mechanics, expressions in 4.32 have to turn into operators obeying first quantization. Thus, if we adopt the spherical tensor character of the operators we obtain for the electric and magnetic spherical tensors

$$\begin{aligned} \hat{Q}_{\lambda\mu} &= \int d\boldsymbol{r}\ \rho(\boldsymbol{r}) r^\lambda Y_{\lambda\mu}(\theta,\phi), \\ \hat{M}_{\lambda\mu} &= \int d\boldsymbol{r}\ \boldsymbol{\mu}(\boldsymbol{r}) \cdot \Big[\nabla\Big(r^\lambda Y_{\lambda\mu}(\theta,\phi)\Big)\Big], \end{aligned} \tag{4.33}$$

where the magnetic dipole moment has two sources, from the motion of charged particles and from spin currents.

Thus the electromagnetic transition operators have the same mathematical form

that describe charge and current distribution of the nucleus. They carry parity and impose selection rules of angular momentum for initial state $|i\rangle$ and final state $|f\rangle$ with total angular momentum j_i and j_f respectively, given by

$$\pi_i\pi_f = \begin{cases} (-1)^\lambda & \text{for E}\lambda \text{ transition,} \\ (-1)^{\lambda-1} & \text{for M}\lambda \text{ transition,} \end{cases} \tag{4.34}$$

and impose the so called triangular rule

$$|j_i - j_f| \leq \lambda \leq j_i + j_f. \tag{4.35}$$

The decay amplitude is given by Fermi golden rule as

$$T_{fi} = \frac{2\pi}{\hbar}\big|\langle f|\hat{H}_{int}|i\rangle\big|^2 \rho_f(E). \tag{4.36}$$

where $\rho_f(E)$ is the density of final states. After calculating $\rho_f(E)$ [23] considering the multipole expansion of the interaction Hamiltonian 4.31 and from the fact that transition probabilities are additive, we can isolate each multipole and get

$$T_{fi}^{\Sigma\lambda} = \frac{2}{\epsilon_0\hbar}\frac{\lambda+1}{\lambda((2\lambda+1)!!)^2}\Big(\frac{E_\gamma}{\hbar c}\Big)^{2\lambda+1} B(\Sigma\lambda; j_i \to j_f), \tag{4.37}$$

where $\Sigma = \text{E}, \text{M}$, the energy of the emitted photon is E_γ and the factor $B(\Sigma\lambda)$ is the reduced transition probability given by

$$B(\Sigma\lambda; j_i \to j_f) = \frac{1}{2j_i+1}\big|\langle j_f||\hat{\Sigma}_\lambda||j_i\rangle\big|^2, \tag{4.38}$$

notice that the factor preceding the reduced matrix element depends on the convention of the Wigner-Eckart theorem, which in this case we use the convention of [106, 25].

The electromagnetic transitions are a key observables to probe nuclear theories since we can infer several structural and dynamical properties from them. For instance, by measuring electromagnetic transitions it is possible to obtain values of intrinsic deformation as converging series of transitions [107]. In the case of octupole moment, recent measurements of large values of $B(\text{E3})$ suggests that certain actinide nuclei posses an intrinsic octupole shape [79].

As has been emphasized above for the multipole moments, the single-particle estimates are always an important guide for the understanding of the nucleus. Electromagnetic transitions are no different, so an artificial unit for the observables $B(\Sigma\lambda)$ was devised to quantify the degree of collectivity or single-particle character of transitions. This is called the Weisskopf unit denoted by W.u. and given by expressions [95]

$$1 \text{ W.u. } (\text{E}\lambda) = \frac{1.2^{2\lambda}}{4\pi}\left(\frac{3}{\lambda+3}\right)^2 A^{2\lambda/3}\, e^2\text{fm}^{2\lambda}, \tag{4.39}$$

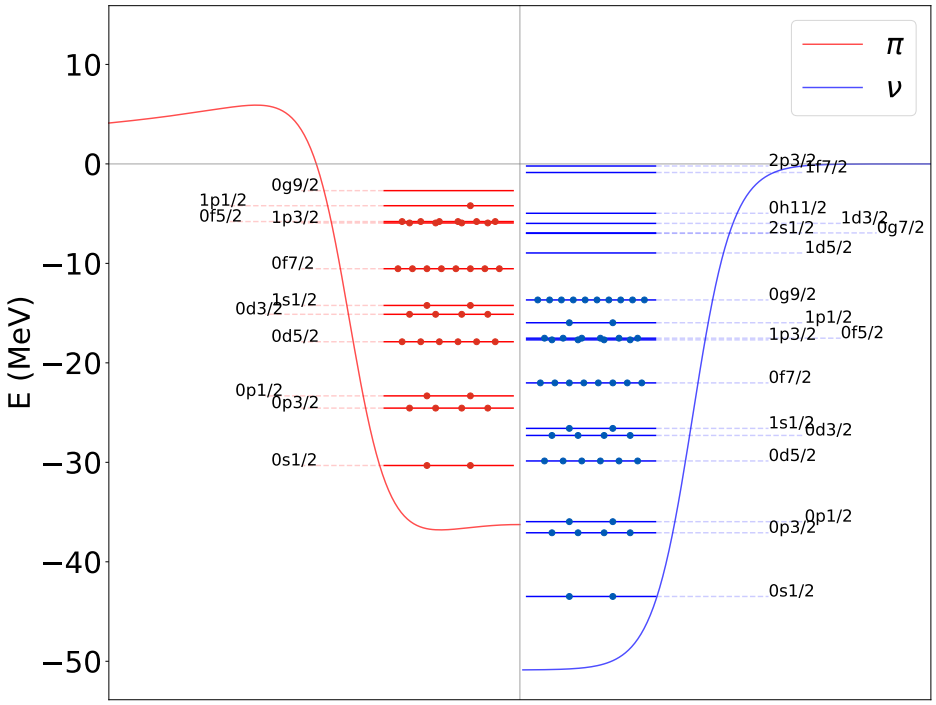

Figure 4.5: Single-particle orbitals and schematic occupations of protons and neutrons for ^{89}Y using the Woods-Saxon spherical potential. The $g_{9/2}$ orbital is an accessible excited state in the proton space which explains the presence of several $9/2^+$ isomers in odd-A yttrium isotopes.

$$1\ \text{W.u.}\ (\text{M}\lambda) = \frac{10}{\pi} 1.2^{2\lambda-2} \left(\frac{3}{\lambda+3}\right)^2 A^{(2\lambda-2)/3} \mu_N^2\ \text{fm}^{2\lambda-2}, \tag{4.40}$$

which are used extensively in experimental databases and theoretical studies. The values of these transition strengths help in the grouping of excitation spectra into collective or single-particle states.

From expression 4.37, it is evidenced the dependence of transition lifetimes on energy, multipolarity and internal structure which allows for the emergence of a wide domain of values, from picoseconds to nanoseconds, minutes or several billions of years. In general the intensity of the transition will be dominated by the lowest multipoles that preserve the selection rules and be strongly influenced by the difference in energy between the initial and final states. This set of variables fortuitously configure so that the decay is delayed from the domain of picoseconds to much longer time spans [108, 109], constituting the mechanisms of spin-isomerism. We adopt the convention of [108] and consider as isomers only the states with a half-life larger than 10 ns. Although there are other mechanisms of isomerism like the shape, seniority and K-isomerism explored extensively in the literature, we will focus only in the spin and extremely low-energy in this thesis.

The spin isomerism emerges mainly because of the strong spin-orbit interaction in the nucleus. In the shell model picture, it causes levels of large angular momentum from certain shells to migrate to contiguous shells, placing themselves among states of opposite parity and lower angular momentum values. These are called intruder

(or deserter) states. For a given shell η, the values of orbital angular momentum are $l = \eta, \eta-2, \eta-4, ...,$ 0 or 1 and the total angular momentum values are $j = l \pm 1/2$. The spin orbit interaction removes the j degeneracy of single-particle orbitals by introducing a term in the Hamiltonian proportional to $\propto j(j+1) - l(l+1) - 3/4$. Thus, the values of larger total angular momentum are pushed to the immediate lower shell of opposite parity $\eta - 1$. Because the spin orbit gets stronger the heavier the nucleus, this happens only in shells above the *sd* ($\eta = 2$), having as consequence the breaking of the simple harmonic oscillator symmetries [110, 111, 112, 113] and the appearance of isomers. The main generating orbitals are $1f^{-}_{7/2}$, $1g^{+}_{9/2}$, $1h^{-}_{11/2}$ and $1i^{+}_{13/2}$, for which systematic studies of their occurrence exist in the literature [108] causing the transition to lower energy states via high multi-polarities (E4, M4, E5, *etc.*) and thus hindering the transition.

As an example, in the odd-A isotopes of yttrium, seven isomeric states of angular momentum and parity $9/2^{+}$ have been identified experimentally [108]. In Fig. 4.5 are shown the single-particle levels and occupations of the Woods-Saxon potential with spin-orbit interaction for ^{89}Y from which the intruder orbital $1g^{+}_{9/2}$ can be observed in the proton spectrum as the lowest excited configuration for the odd proton. The isotopic chains of yttrium and zirconium will be reviewed in chapter 5.

Another electromagnetic isomer mechanism that emerges across the nuclear chart is due to the appearance of extremely low-energy excited states that hinder the half-life due to the proportionality in expression 4.37 on E_γ. Even though, the typical energy ranges of nuclear interaction are keV and MeV, in few cases across the nuclear chart these excited states go down to eV. Currently, the mechanism for this phenomenon is not fully known and is challenging to study from both theory and experiment. The most exceptional examples are the isomers of ^{229}Th and ^{235}U with energies of 8.4 eV and 76.7 eV and half-lifes in vacuum of 29 and 26 minutes, respectively [114, 115]. The former is subject of study for chapter 5 where we calculate its B(M1) transition strengths.

5 Nuclear structure calculations

Every theoretical model is judged by its inner consistency and agreement with experimental data. While no theory can be proven to describe nature with absolute certainty, any attempt must reproduce experimental observations and additionally be consistent, that is, it has to be free of contradictions and disagreements with previously established principles [116]. In particular, the observables of the atomic nucleus serve this purpose for nuclear physics by reflecting our understanding of the interaction, the equations of motion and their associated mathematical structures.

We present applications of the theoretical results of previous chapters with actual calculations and comparisons with experimental data. We detail methodologies and procedures followed in the implementation of the code HFODD [15] which serves as our tool to study the nuclear properties of pairing, electromagnetic moments and transitions. Although the emphasis is on comparisons with experimental data, predictions are also a useful possibility and constitute a distinctive characteristic of a good theoretical approach.

In particular, we dedicate this chapter to showing calculations of pairing and symmetry breaking properties in certain regions of the nuclear chart. We apply these methods to calculate wavefunctions and electromagnetic moments of the odd-A isotopic chains of yttrium and zirconium. We also calculate the transition strength and electromagnetic moments of the ^{229}Th isomer and ground states using advanced DFT techniques developed in the preceding chapters. We analyse and contrast the results with the existing experimental data.

5.1 General remarks

Several computational implementations of the pairing and DFT approaches of chapters 2 and 3 have been developed over the years [15, 117, 118]. One of the key advantages of the code HFODD is its formulation in the 3D harmonic oscillator Cartesian basis, which is a natural framework to describe symmetry-breaking for systems whose deformation is not previously known [44]. It allows for the self-consistent solution to smoothly acquire axial parity breaking (dipole, octupole, *etc.*) and parity conserving (quadrupole, hexadecapole, *etc.*) deformations. Non-axial moments can also be described naturally in a more unrestricted but considerable more computationally expensive approach. See section 4.1 for a review of these concepts.

It is well established that deformation is one of the mechanisms by which the energy

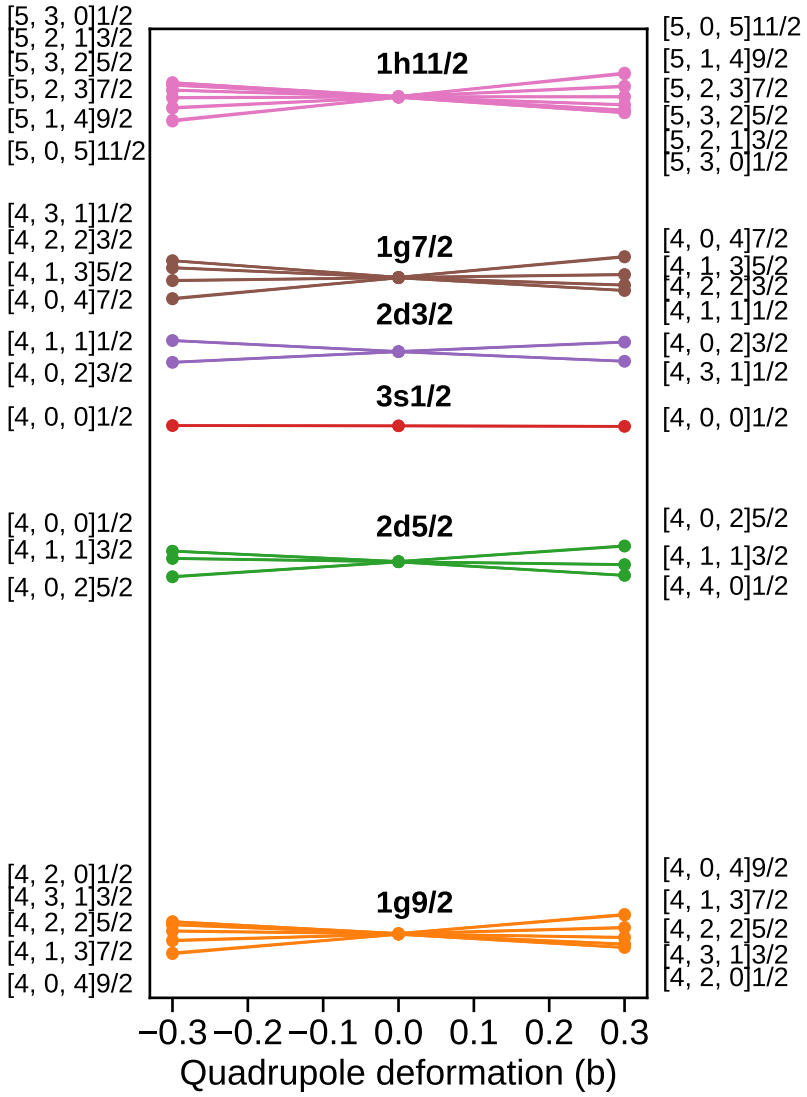

Figure 5.1: Splitting of spherical orbitals by the deformation and associated Nilsson labels.

of the nucleus is lowered. In odd-A systems, the unpaired nucleon enhances deformation further by polarizing the shape of the core and thus accessing lower single-particle energies. This mechanism occurs via couplings of the unpaired nucleon wavefunction to the states 2^+, 4^+, 6^+, ... of the core [33, 119]. Thus, it is a basic requirement to be able to describe how spherical single-particle orbitals split according to the different projections of angular momentum once spherical symmetry is broken. Fig. 5.1 illustrates the effect of a small deformation in the spherical orbitals between shells 50 and 82, which split according to the projections of angular momentum. This effect is well known from the Nilsson model [34] and represents an essential aspect for the identification of states to be blocked in the HFB and BCS calculations.

The inclusion of time-odd terms in the nuclear functionals is crucial for a reliable description of nuclei across the entire nuclear chart. In even–even systems, the occupation of time-reversed single-particle states in the ground state leads to the cancellation of time-odd densities. However, odd-A and odd–odd nuclei break time-reversal symmetry, giving rise to non-zero contributions from time-odd densities and breaking signature

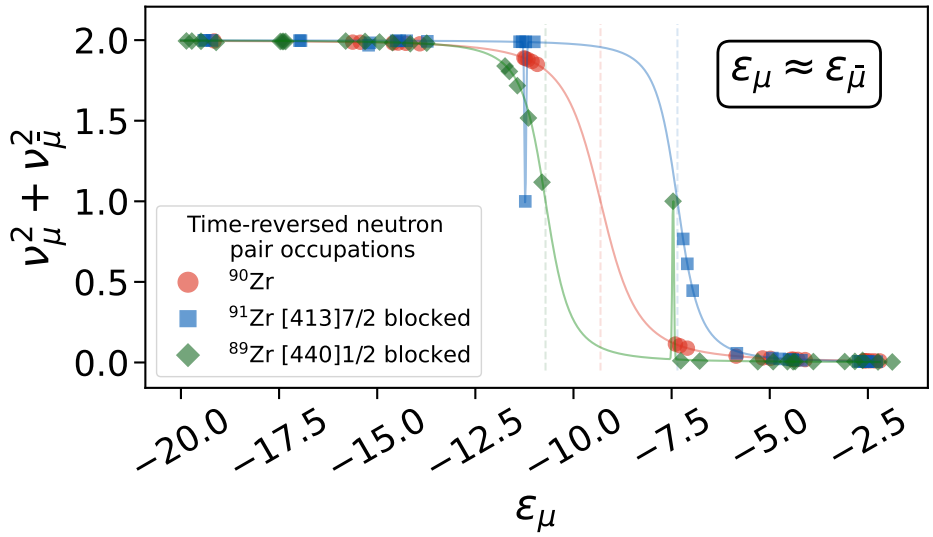

Figure 5.2: Effects of pairing interaction and blocking in nuclear time reversed pair occupations of neutrons. The blocking is set in two cases, above and below the Fermi energy. Time reversed states are not exactly degenerate due to the time-odd terms which break time-reversal symmetry.

symmetry. The odd particle interacts asymmetrically with the nucleons of the core depending on their alignment of angular momentum breaking the time-reversal of the core and polarizing it so that it acquires a small net spin. This contributes to the magnetic properties of the nucleus and drives magnetic moments away from the limiting values of the Schmidt lines. This mechanism happens via couplings of the unpaired nucleon wavefunction to the states 1^+, 3^+, 5^+, ... of the core [33]. The presence of an unpaired particle or more generally any broken pair leads to the appearance of non-zero magnetic observables and corrections to the associated time-even observables, introducing simultaneously several technical complications.

The other pillar for the description of nuclei is the pairing interaction. In chapter 2 we introduced the three main theoretical frameworks that deal with pairing in the nucleus, namely the seniority, BCS and HFB models. One of the main consequences of pairing in any fermion system is the breaking of particle number conservation which is reflected in a smoother non-integer occupations of single-particle orbitals around the Fermi energy. In systems with an odd number of particles, one must block a specific orbital and force the vacancy of its time-reversed partner. These features are illustrated in Fig. 5.2, where we show the neutron occupations for time reversed pairs in an even-even ^{90}Zr and in the odd-A contiguous ^{91}Zr and ^{89}Zr where blocking is applied.

Additionally, two central parameters of these models are the pairing gap and Fermi energy, which quantify the strength of the pairing and the dependence of the total energy with particle number, respectively. At the magic numbers, the pairing gap goes to zero since shell effects are not overcome and the pair condensation does not occur, however, pairing still contributes to the total energy. The Fermi energy increases monotonically with the neutron number indicating that the nucleons become less bound as mass increases due to the short-range nature of the nuclear force. This features are

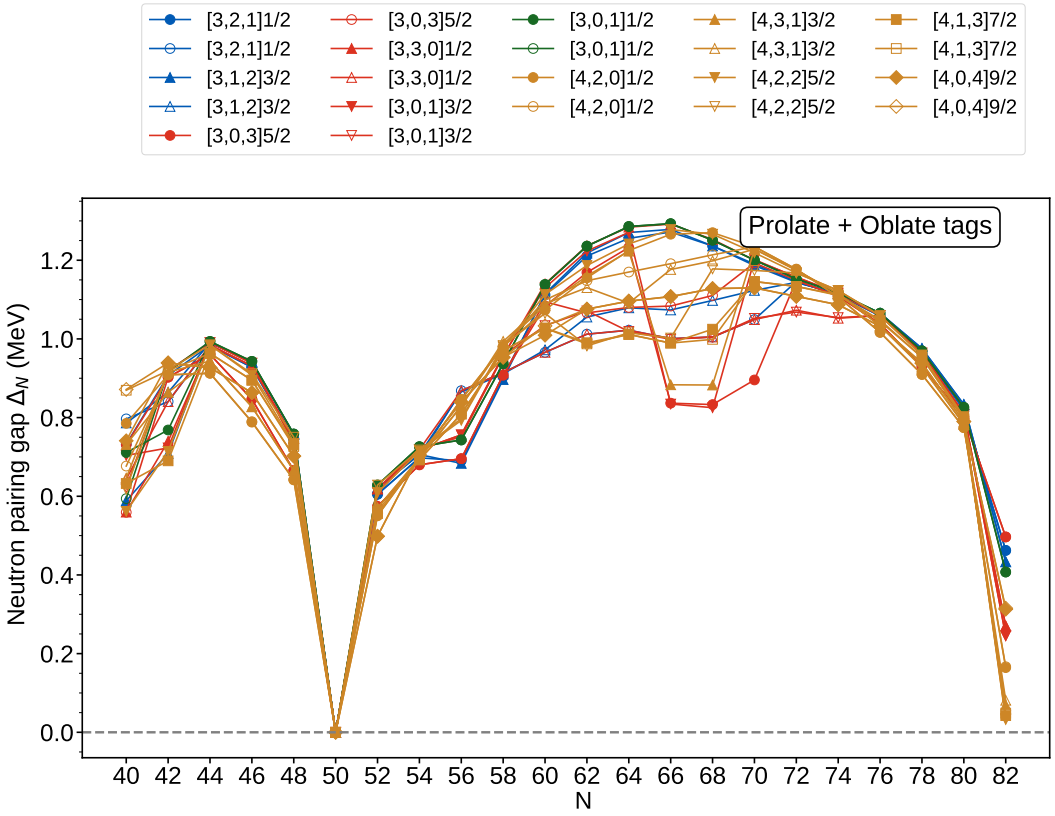

(a) Neutron pairing gaps Δ_N.

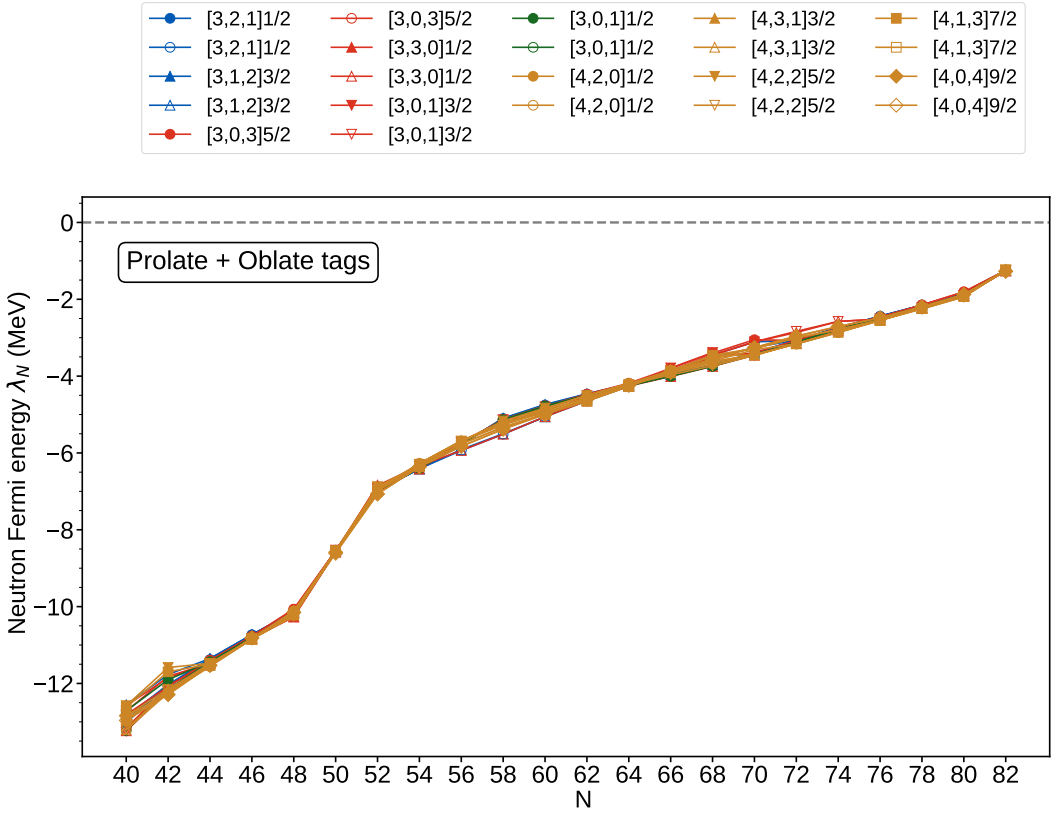

(b) Neutron Fermi energies λ_N.

Figure 5.3: Neutron pairing gaps and Fermi energies for the odd-A isotopic chain $^{83-101}$Y. Open (full) markers indicate oblate (prolate) tags.

shown in Fig. 5.3 for the odd-A isotopic chain $^{83-101}$Y for a set of blocked quasiparticle configurations.

The code HFODD has been developed for almost three decades now with special emphasis in aiming to describe (among many other aspects) the properties and wave-functions of heavy deformed open shell nuclei. As mentioned above, this requires an adequate treatment of symmetry breaking, pairing and polarization effects via time-odd terms and projection theory, all done self-consistently and parameter free. HFODD has been published in nine articles over the years announcing new implementations and improvements. We give now a short account of the main developments. Publications I-III [44, 120, 121] implemented the HF solver with Skyrme interactions. Publication IV [122] included the pairing interaction within the HFB framework. Publications V-VI [123, 30] implemented the angular-momentum projection and quasiparticle blocking. Publication VII [124] implemented the augmented Lagrangian method (ALM) for stronger constraints in multipole moments. Version VIII [125] implemented the Gogny force. The most recent publication IX [15] implemented improvements in the nuclear potentials, particle number and parity symmetry restorations. Current unpublished version is capable of multi configuration mixing and transitions between these and also fine two-body corrections to magnetic moments. Additionally, a guide for keyword input files is available [126].These complexity makes HFODD a valuable tool for progress in theoretical nuclear physics.

5.2 Isotopic chains of yttrium and zirconium

We present the methods and results for calculations of electromagnetic moments of the odd-A isotopic chain of yttrium and zirconium. These particular nuclei are of special interest because they exhibit interesting phenomenology that serve as good tests of nuclear DFT regarding deformation, blocking effects and core polarization. These isotopes present a sudden shape transition in $A \approx 100$ [127, 128, 129] and systematically exhibit $9/2^+$ and $1/2^-$ spin isomeric states from dominant single-particle configurations [109]. Fig. 5.4 summarizes the isotopes studied in this section and the available experimental electric quadrupole and magnetic dipole moments.

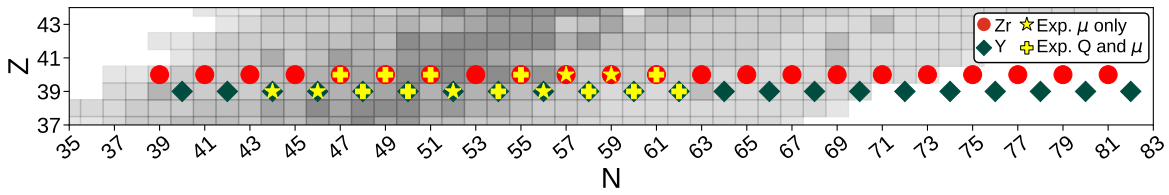

Figure 5.4: Isotopic chains of Y and Zr studied. Green diamonds and red circles represent the odd mass isotopes studied. Yellow cross signs represent isotopes where measurements of multipole moments Q and μ are available for the ground or any of its excited states while the yellow stars represent measurements of μ only.

5.2.1 Methodology

We adopt an iterative strategy in which the nuclear mean-field and corresponding wave function are calculated through a sequence of ordered steps. Physical constraints are applied progressively leading to a self-consistent solution with restored symmetries as the final outcome. Starting from a spherical even–even solution the calculation is guided towards a deformed odd-A solution where we can calculate the spectroscopic electric quadrupole and magnetic dipole moments given by

$$Q = \sqrt{\frac{16\pi}{5}}\langle II|\hat{Q}_{20}|II\rangle, \tag{5.1}$$

$$\mu = \sqrt{\frac{4\pi}{3}}\langle II|\hat{\mu}_{10}|II\rangle, \tag{5.2}$$

after the restoration of rotational symmetry. Results for expressions 5.1 and 5.2 can be compared directly with experimental data. Refer to chapters 3 and 4 for discussions on the interplay between intrinsic and spectroscopic moments.

These stages have been developed and applied previously in [32, 33, 31] for which we give a summary now for our particular applications. The first stage of calculations begin with the HFB spherical calculations of a semi-magic or doubly-magic nuclei near the isotopic chain of interest using the parametrization UNEDF1. Then a small axial deformation constraint of $\approx \pm 0.1$ b and a cranking frequency of $\omega_z = 0.001$ MeV/$\hbar$ are imposed so that the angular momentum of the now weakly deformed nucleus is aligned along the z-axis. We continue the calculations from the small deformed solutions but now constrain the quadrupole moments to relatively large values of $\approx \pm 10$ b and fix the pairing gaps to $\Delta_N = \Delta_P$ =1 MeV to get prolate and oblate starting points. This means that all calculations for a given configuration are two-folded, one for the prolate and another for oblate starting points. This is done so that the energy surface is scanned in case minima are found simultaneously at prolate and oblate deformation. In case there is a single minimum, both calculations will simply converge to the same state (see Fig. 4.2).

In the second stage we select a set of quasiparticle configurations from the solutions in stage one. We block these by using the tagging technology which allows us to track a given orbital across the self-consistent iterations regardless of their changing energies and deformations [31]. The physical properties of these tags are obtained from the largest overlap with Nilsson wavefunctions which might change over the self consistent iterations due to the breaking of symmetries. We denote the tags by parenthesis $(N, n_z, \Lambda)\Omega$ and the self consistent labels by the standard brackets $[N, n_z, \Lambda]\Omega$. This blocking is done for each of the odd-A isotopes where we break simplex-y, signature-y and time reversal symmetries while keeping a large deformation constraint and fixed pairing gap. Due to the breaking of spherical symmetry, the total nuclear angular momentum I is no longer conserved and thus it is not a good quantum number to label the nuclear state. Then, we identify the states by the axial Nilsson labels $[N, n_z, \Lambda]\Omega$ which conserve both parity and projection Ω.

The third stage releases the constraints of deformation and pairing set previously

so that calculations reach energy minima in a self-consistent way. Due to the breaking of time-reversal symmetry and particle-number conservation, a strong core polarization of the mean field is induced which makes the self-consistent iterations sensitive to level crossings of single-particle states [130, 131] resulting sometimes in oscillatory or non-convergent behaviour. This technicalities regarding the iterative algorithm need to be dealt with to achieve the desired convergence by manipulating degree of mixing of potentials between iterations [126, 132]. The output of this stage is the symmetry breaking self consistent solutions which must be treated with symmetry restoration methods to recover good quantum numbers and be able to access experimentally relevant observables.

In the last stage we restore the spherical symmetry via the angular momentum projection (AMP) technique detailed in section 3.3.3. Due to the axial symmetry, the actual application is for the case of equation 3.85 which reduces computations by about two orders of magnitude. This allowed us to get an expansion of the symmetry breaking state of each calculation in terms of states $|I\Omega\rangle$ where $\Omega \leq I$ for which the component $|\Omega\Omega\rangle$ is used to calculate spectroscopic moments 5.1 and 5.2. The values we compare with experiment are the lowest energy $|\Omega\Omega\rangle$ among the several blocked configuration. This also allows us to form a spectrum of each isotope which we show in appendix C and determine if the oblate and prolate calculations reached the same minimum or found two different minima in the axial energy surface.

This methodology allows for systematic large-scale calculations of electromagnetic moments across the entire nuclear chart reaching open-shell odd and odd-odd deformed nuclei. This technique is free of effective charges or g-factors, proposing a consistent treatment of deformations and core polarizations exclusively from the nuclear interaction so that our understanding of the nucleus can be systematically tested.

5.2.2 Results

For stage one we calculated the spherical, small deformed and large deformed lowest energy states of ^{89}Y and ^{90}Zr from which we obtained the single-particle spectra to block in the calculations of the 22 odd-A isotopes in the chains $^{79-101}$Y and $^{79-101}$Zr, respectively. For the Y chain we blocked the 11 proton orbitals between magic numbers 28 and 50, while for the Zr chain we blocked the 27 neutron orbitals between magic numbers 28 and 82. These are shown in tables 5.1 and 5.2, and accounted for a total of 484 and 1188 calculations for the Y and Zr chains, respectively. We performed these calculations in HFODD version 3.28k and used the Cartesian harmonic oscillator basis of up to shell $n_x + n_y + n_z = N_0 \leq 16$.

These calculations were performed throughout the four stages described in the previous section from which we obtained excitation spectra, electric quadrupole and magnetic dipole moments for each of the configurations. We obtained 435 and 1119 converged calculations in the Y and Zr isotopic chains, representing around 90% and 94% useful results of the total, respectively. The full results are shown in appendix C and comparisons with available experimental magnetic moments and quadrupole moments are shown in figures 5.5 and 5.6. Numerical values are compiled in appendix

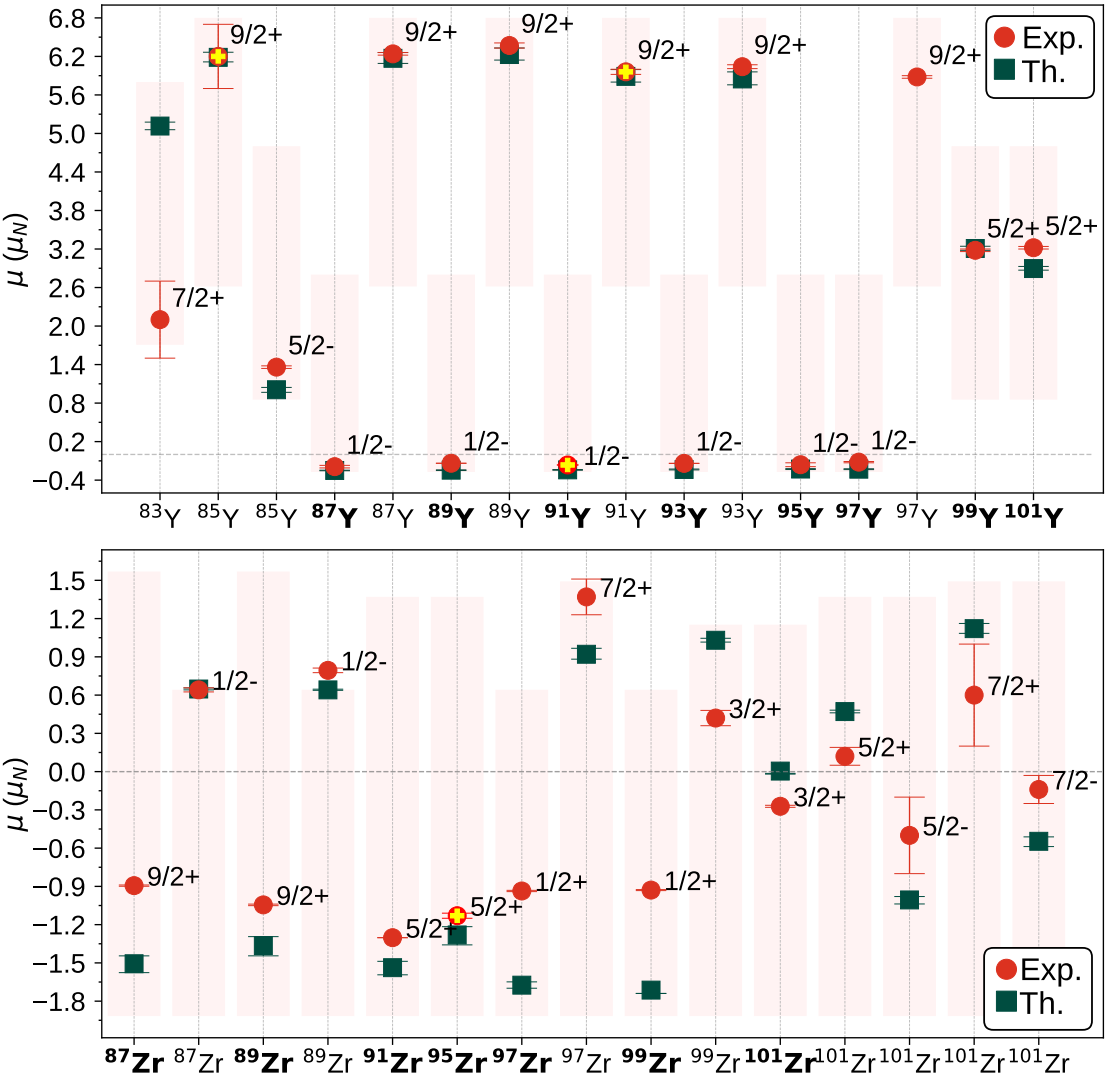

Figure 5.5: Spectroscopic magnetic dipole moments of $^{83-101}$Y and $^{87-101}$Zr compared to experimental data. Background bars are the area between Schmidt lines. Bold font in isotope names correspond to ground sates. Yellow crosses denote experimentally undetermined signs suggested by theory. The theoretical value for ^{97}Y did not converge. Theoretical error bars were calculated by evaluating the Landau parameter g_0' at 1.3 and 2.1.

Shell	Spherical orbital	Nilsson orbitals
3	$2p_{3/2}$	$(3\,2\,1)\frac{1}{2}$, $(3\,1\,2)\frac{3}{2}$
	$1f_{5/2}$	$(3\,0\,3)\frac{5}{2}$, $(3\,3\,0)\frac{1}{2}$, $(3\,0\,1)\frac{3}{2}$
	$2p_{1/2}$	$(3\,0\,1)\frac{1}{2}$
4	$1g_{9/2}$	$(4\,2\,0)\frac{1}{2}$, $(4\,3\,1)\frac{3}{2}$, $(4\,2\,2)\frac{5}{2}$, $(4\,1\,3)\frac{7}{2}$, $(4\,0\,4)\frac{9}{2}$

Table 5.1: Nilsson orbitals tags blocked in the Y isotopic chain.

C. The optimum value of the isovector Landau parameter (see section 3.2.1) for the functional UNEDF1 was determined to be $g_0' = 1.7$ which was fit to electromagnetic

Shell	Spherical orbital	Nilsson orbitals
3	$2p_{3/2}$	$(3\,3\,0)\frac{1}{2}$, $(3\,0\,1)\frac{3}{2}$
	$1f_{5/2}$	$(3\,2\,1)\frac{1}{2}$, $(3\,1\,2)\frac{3}{2}$, $(3\,0\,3)\frac{5}{2}$
	$2p_{1/2}$	$(3\,0\,1)\frac{1}{2}$
4	$1g_{9/2}$	$(4\,2\,0)\frac{1}{2}$, $(4\,3\,1)\frac{3}{2}$, $(4\,2\,2)\frac{5}{2}$, $(4\,1\,3)\frac{7}{2}$, $(4\,0\,4)\frac{9}{2}$
	$2d_{5/2}$	$(4\,4\,0)\frac{1}{2}$, $(4\,1\,1)\frac{3}{2}$, $(4\,0\,2)\frac{5}{2}$
	$3s_{1/2}$	$(4\,0\,0)\frac{1}{2}$
	$2d_{3/2}$	$(4\,3\,1)\frac{1}{2}$, $(4\,0\,2)\frac{3}{2}$
	$1g_{7/2}$	$(4\,1\,1)\frac{1}{2}$, $(4\,2\,2)\frac{3}{2}$, $(4\,1\,3)\frac{5}{2}$, $(4\,0\,4)\frac{7}{2}$
5	$1h_{11/2}$	$(5\,3\,0)\frac{1}{2}$, $(5\,2\,1)\frac{3}{2}$, $(5\,3\,2)\frac{5}{2}$, $(5\,2\,3)\frac{7}{2}$, $(5\,1\,4)\frac{9}{2}$, $(5\,0\,5)\frac{11}{2}$

Table 5.2: Nilsson orbitals tags blocked in the Zr isotopic chain.

moments of doubly magic neighbours [133]. Due to the sensibility of magnetic operators with respect to the parameter g_0', we estimate theoretical error bars for the magnetic dipole by performing all calculations within an interval of 0.4 around the optimum, *i. e.*, $g_{0-}' = 1.3$ and $g_{0+}' = 2.1$. These give the theoretical error bars shown in Fig. 5.5.

We observe from quadrupole moments in Figs.C.3 and C.7 that the strong shape transition documented around $A \approx 100$ builds up quickly but begins late in the Y isotopes. This has already been reported in [134] for odd-odd yttrium isotopes. It indicates that potential energy surfaces have a tendency to be flat where spherical minima competes with weakly deformed states. This underestimation in deformation indicates that this region is transitional rather than well-deformed as mentioned in the literature [127, 128]. Figs.C.6 and C.2 evidence the appearance of a secondary minima in the axial energy surface observed to happen mostly for mid shell isotopes with lower prolate minima for Zr and lower oblate minima for Y. Around the magic numbers, nearly all configurations collapse to a single minimum as expected. Few experimental values have been measured in this region which are shown in Fig. 5.6. In the available data for the Y chain we find both remarkable agreement and deviations. At mass number $A = 99$, a sudden change in the nuclear mean square radius has been reported [129], which might be correlated to the remarkable deviation from calculations in masses $A = 99$ and $A = 101$ as this sudden shape transition is not properly reproduced. Similar situation happens for the Zr isotopic chain where the value at mass $A = 101$ indicates an analogous situation, although no further experimental data is available. We obtain root mean square (RMS)deviations of 1.06 and 0.397 for the Y and Zr chains, respectively.

The magic dipole moments calculated for the Y isotopic chain display a predominantly single-particle character given their overall closeness to the Schmidt values.

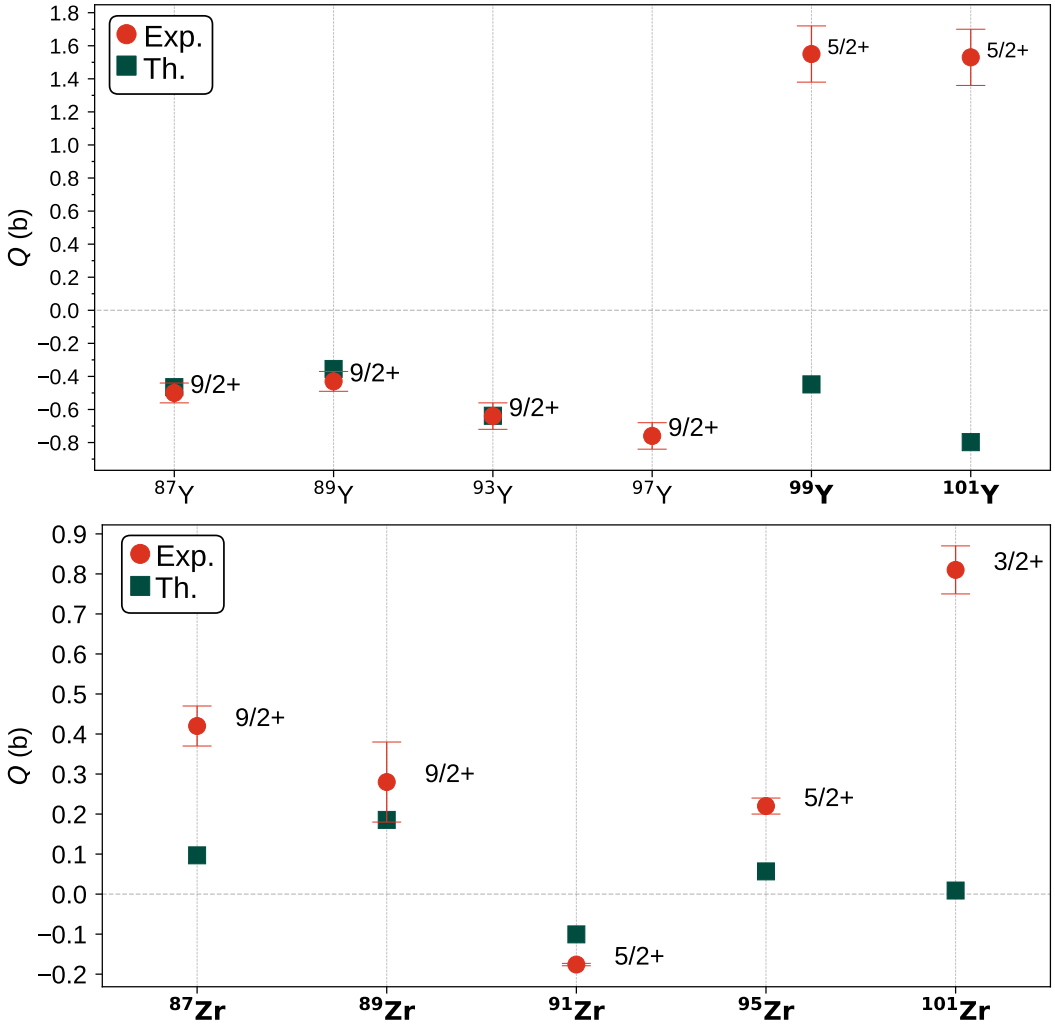

Figure 5.6: Spectroscopic electric quadrupole moments of $^{83-101}$Y and $^{87-101}$Zr compared to experimental data. The theoretical value for ^{97}Y could not be converged. Bold font in isotope names correspond to ground sates.

The most deviated cases from the limiting single-particle origin is seen in ^{99}Y and ^{101}Y where their values are reproduced closely. A smaller degree of core polarization is observed for the 9/2− states. Clear deviation from experiment is seen in ^{83}Y where a behaviour opposite to the single-particle regime is predicted. In the neutron rich chain, a more pronounced deviation from the Schmidt lines is seen but the results struggle to reproduce consistently. However, they follow the trends of experimental data. We obtain RMS deviations of 0.800 and 0.8634 for the Y and Zr chains, respectively. It has long been recognized that one-body magnetic dipole operators do not fully account for the magnetic contributions in nuclei [135]. Additional two-body meson exchange currents can play a non-negligible role in the description of magnetic observables [136]. The real impact of these two-body contributions is still to be tested in systematic dedicated calculations.

Another interesting feature of these results comes from the spectra displayed in Figs. C.1 and C.5. In the Zr chain, several configurations take over as ground states as the mass increases while for the Y chain the angular momentum and parity 1/2−

state results as ground state in all 22 isotopes analyzed. Ground states spins and parities have been measured for chains $^{79-103}$Y and $^{81-103}$Zr. These quantum numbers are correctly reproduced for $^{85-97}$Y. Also for the isotopes ^{89}Zr, ^{89}Zr, ^{89}Zr, ^{89}Zr and ^{89}Zr with values $9/2^+$, $5/2^+$, $1/2^+$, $1/2^+$ and $3/2^+$ respectively.

Overall, these results demonstrate that the mean-field approach captures the dominant trends in these isotopic chains but with limitations in developing the onset of deformations around $A \approx 100$. Experimental efforts in this region of measurements of electromagnetic observables are required to test our models further and figure out the nature of the rapid shape transition observed in these nuclei.

5.3 The thorium isomer

The nearly degenerate isomeric and ground states of ^{229}Th were discovered almost half a century ago. Since then, substantial work from both experimental and theoretical communities has been dedicated on elucidating and characterizing this remarkable emergent feature. At present, the state ^{229m}Th remains the lowest-lying excited state known across the entire nuclear chart, standing out as a uniquely interesting isomer for experiments, theoretical investigations and prospective technological applications [137, 138, 139, 140, 141, 142]. This unusual isomer poses significant challenges, pushing current experimental and theoretical techniques to their limits.

The isomer was first detected from the γ spectrum of the α decay of ^{233}U, in which an excited state with an energy below 100 eV was postulated in order to account for the observed decay scheme [143]. A series of subsequent spectroscopic investigations refined the level scheme and narrowed down the energy of this state [144, 145, 146, 147]. Later, the direct observations of internal conversion electrons enabled a more accurate determination of the properties of the isomeric state [148]. Recently, alternative production mechanisms and experimental techniques have been developed to precisely establish its decay parameters and multipole moments [149, 150, 151, 152] as well as to investigate internal conversion processes originating from excited electronic configurations [153].

Because this radiative transition occurs at very low energy, its characteristics are strongly affected by the surrounding electronic environment having huge internal conversion coefficients. Consequently, measured lifetimes depend on the particular experimental conditions and must be corrected to extract the corresponding transition rates in vacuum. Recent measurements report a transition energy of $E_\gamma = 8.35574(3)$ eV, a vacuum half-life of $t_{1/2} = 1740(50)$ s and a transition strength of $B(\mathrm{M1}) = 0.0217(6)$ W.u. $= 0.0388(12)\,\mu_N^2$ [115]. Notice that $1\,\mathrm{W.u.}_{\mathrm{M1}} = 1.7905\,\mu_N^2$ obtained from equation 4.40. In Fig. 5.7, we show the low energy spectrum including the ground and isomeric bands along with Nilsson labels assigned. Additionally, the electromagnetic moments have been measured for both the isomeric and ground states [154, 155, 156, 157]. The latest results of spectroscopic electric quadrupole moments are $Q(^{229m}\mathrm{Th}) = 1.77(1)$ b and $Q(^{229}\mathrm{Th}) = 3.11(2)$ b [158]. For the magnetic dipole moments, the latest reports are $\mu(^{229m}\mathrm{Th}) = -0.378(8)\,\mu_N$ and $\mu(^{229}\mathrm{Th}) = 0.366(6)\,\mu_N$ [159]. The deviation from the Schmidt limits $\mu_{\mathrm{Sch.}}(5/2)$ =[1.366, -1.913] μ_N and

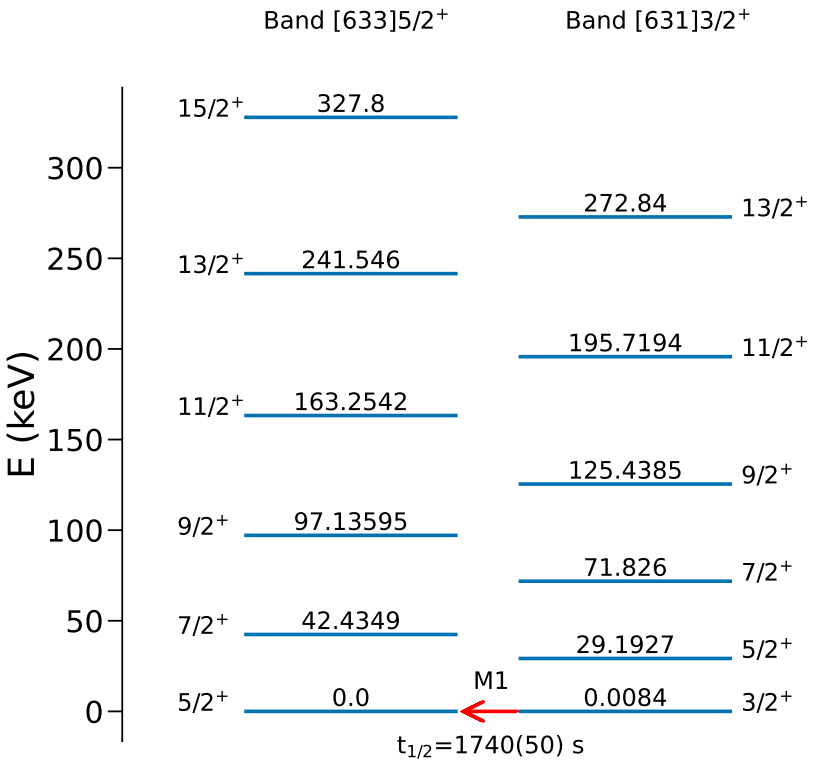

Figure 5.7: Spectrum of ^{229}Th with the isomeric transition latest measurements and dominant multipolarity [4].

$\mu_{\text{Sch.}}(3/2)$ =[1.148, -1.913] μ_N indicate a strong core polarization effect in this isotope.

Progress in the experimental front have driven prospective technological applications in areas like precision chronometry [160, 161, 162, 163], γ-ray laser technology [164, 165], satellite-based navigational and chronological geodesy systems [138]. These advances could enable a new generation of ultra-high-precision methods that ultimately deepen our understanding of fundamental physics [140, 137, 141]. Realizing these technologies requires sophisticated manipulation of excitation and de-excitation processes between the isomeric $3/2_1^+$ state and the $5/2_1^+$ ground state, where the M1 multipolarity overwhelmingly dominates over the competing E2 channel by roughly 10^{13} orders of magnitude due to the exceptionally low transition energy [166]. Recent work in controlled laser excitations of the isomeric state show that these applications are within reach [167, 115, 168, 169].

Theoretical attempts to describe and predict the observables of this highly elusive isomeric transition have employed a variety of frameworks, including phenomenological models [166], core-plus-particle approaches [146, 170, 171], projected shell-model calculations [172] and mean-field methods [137, 173, 174]. In these treatments, the use of adjustable parameters and effective charges has been essential for achieving agreement with experimental observables.

We present the first analysis based on nuclear DFT aiming to calculate multipole moments Q, μ and reduced transition probabilities B(M1) implemented within the methodology of [133] predating the measurement reported in [115]. We perform calculations with pairing and octupole deformation for three single-particle configurations of

each projection $\Omega = 3/2$ and $\Omega = 5/2$ and for seven parametrizations of Skyrme forces. We then apply the multi-reference DFT (MR-DFT) (se section 3.3) to eventually mix these configurations and estimate the values of Q, μ and B(M1). The only parameters fit were the pairing strengths, $V_{0,N}$ and $V_{0,P}$ (see equations 3.44 and 3.45), adjusted to the mass staggering near ^{229}Th and ^{227}Ac [175], respectively. Also the Landau parameter g_0' was fit in [133] to constrain the isovector spin-spin coupling constants (see section 3.2.1) with magnetic dipole moments of doubly magic nuclei neighbors.

5.3.1 Methodology

Similarly as for the isotopic chains of yttrium and zirconium, we performed a multi-stage calculation of the ground and isomeric nuclear wave functions of ^{229}Th to determine the magnetic dipole transition strength $B(\mathrm{M1}; 3/2_1^+ \rightarrow 5/2_1^+)$ and multipole moments of the states $3/2_1^+$ and $5/2_1^+$. We implemented these calculations for seven parametrizations of the Skyrme force, namely, SIII [54], SkO′ [176], SkM* [56], SLy4 [55], SkX$_\mathrm{c}$ [177], UNEDF1 [49] and UNEDF0 [48]. Because none of these parametrizations were adjusted to octupole degrees of freedom, systematic differences among the various calculations were expected. Following [5, 175], we investigate the correlations between the predicted Q, μ and B(M1) with calculated intrinsic octupole moments Q_0^3, using the experimentally determined values of Q_0^3 as reference benchmarks. For this purpose, we calculated the ground-state octupole moments of symmetry-broken, self-consistent wave functions for ^{226}Ra and ^{230}Th. The experimental values for these nuclei are $Q_0^3(^{226}\mathrm{Ra}) = 1080(30)$ efm^3 [178, 179] and $Q_0^3(^{230}\mathrm{Th}) = 800(40)$ efm^3 [180].

Our computational strategy consists in blocking selected odd-neutron axial quasiparticle configurations in ^{229}Th and releasing the constraints on parity and odd-multipole moments so that octupole deformation can be obtained. This procedure produced deformed, symmetry-breaking solutions characterized by non-zero intrinsic octupole moments Q_0^3. These intrinsic states were subsequently projected onto good parity and angular momentum, then mixed and used to calculate the electromagnetic observables. As detailed in reference [12] and the literature cited therein, magnetic moments obtained within DFT are strongly influenced by the so-called time-odd (TO) components of the mean-field [181, 182, 10] which are an essential feature of these kind of calculations in addition to the time-even components (TE).

The multi-step calculation follows a similar path as the yttrium and zirconium calculations. First, for each Skyrme functional, we calculated the axially deformed, parity-breaking paired ground-state wave functions of the neighbouring even–even nucleus ^{228}Th, from which the corresponding single-particle (s.p.) states were extracted. Next, for each angular-momentum projection onto the symmetry axis, $\Omega = 5/2$ and $\Omega = 3/2$, we chose three states in the vicinity of the Fermi level to be blocked [7, 30, 183] in the odd-N nucleus ^{229}Th.

In the second step, the ^{228}Th single-particle wave functions are used as reference states to self-consistently identify the quasiparticle configurations in ^{229}Th, as described in reference [184]. As mentioned in the previous section and following [59], we denote the tags by Nilsson labels in parentheses rather than square brackets. For $\Omega = 3/2$,

these are (642)3/2, (741)3/2 and (631)3/2, while for $\Omega = 5/2$ they are (633)5/2, (752)5/2 and (622)5/2. We also considered parity-broken configurations with Nilsson quantum number $N_0 = 7$, since such states may acquire positive-parity components after parity restoration. Using this procedure, we obtained self-consistent, symmetry-breaking wave functions for ^{229}Th and ^{229m}Th, which we denote as $|\Phi_{n\Omega}\rangle$ for the three lowest configurations, $n = 1, 2, 3$, for both $\Omega = 5/2$ and $\Omega = 3/2$. In certain cases, the Nilsson labels of the blocked, self-consistent quasiparticle orbitals differ from those of the corresponding states. This can occur when the contribution of a specific Nilsson component $[N_0 n_z \Lambda]\Omega$ is not strongly dominant, as discussed in reference [12].

In the third step, we restore the broken spherical and parity symmetries [1] by projecting the wave functions $|\Phi_{n\Omega}\rangle$ onto states of good angular momentum I and positive parity $\pi = +$. The resulting band-head states with $I = |\Omega|$ are denoted as $|\Phi_{nI^+\Omega}\rangle$, that is, by $|\Phi_{n5/2^+5/2}\rangle$ and $|\Phi_{n3/2^+3/2}\rangle$. Previous benchmark studies have shown [12] that restoring particle number has no significant effect on the magnetic moments so we do not project into good particle number states also because it would increase the computational cost by roughly two orders of magnitude. As mentioned in section 3.3.3, when restoring symmetries in the GCM formalism, the restored wavefunctions might attain near orthogonality causing discontinuities or divergences in the energy kernels of 3.80. This added to the instabilities arising of level crossing and pairing reduce the calculations useful for analysis, giving an argument in favour of implementing several parametrizations of the Skyrme forces for a comprehensive analysis of the relevant observables for this isotope.

The yttrium and zirconium calculations finish in this stage, but now we go one step further and proceed to mix these solutions using the GCM techniques (see section 3.3). We calculate two sets of 3×3 matrix elements of the energy and overlap kernels $H^I_{nn'} = \langle \Phi_{nI^+\Omega} | \hat{H} | \Phi_{n'I^+\Omega} \rangle$ and $N^I_{nn'} = \langle \Phi_{nI^+\Omega} | \Phi_{n'I^+\Omega} \rangle$, respectively for $I = 5/2$ and $I = 3/2$ along with the set of 6×6 M1 and Q2 transition matrix elements of the magnetic dipole operator, $M^{II'}_{nn'} = \langle \Phi_{nI^+I} | \hat{M}1 | \Phi_{n'I'^+I'} \rangle$ and $Q^{II'}_{nn'} = \langle \Phi_{nI^+I} | \hat{Q}2 | \Phi_{n'I'^+I'} \rangle$.. Then for each $I = 5/2$ and $I = 3/2$ solutions, we solve independently two sets of configuration–interaction Hill–Wheeler equations (see section 3.3)

$$\sum_{n'} H^{I^+\Omega}_{nn'} a_{n'I^+\Omega} = E \sum_{n'} N^{I^+\Omega}_{nn'} a_{n'I^+\Omega}, \tag{5.3}$$

where we take only the solutions with the lowest energies E to calculate the M1 transition strength. This results in the mixing coefficients (weight functions) $a_{n'I^+\Omega}$ and the normalized mixed wave functions $|\Phi_{I^+\Omega}\rangle = \sum_{n'} a_{n'I^+\Omega} |\Phi_{n'I^+\Omega}\rangle$. With these results we can determine the MR-DFT matrix element of the M1 transition given by

$$\langle \Phi_{5/2^+5/2} | \hat{M}1 | \Phi_{3/2^+3/2} \rangle = \sum_{nn'} a^*_{n5/2^+5/2} M_{nn'} a_{n'3/2^+3/2}, \tag{5.4}$$

and the corresponding reduced transition strength,

$$B(\mathrm{M1}; 3/2^+_1 \to 5/2^+_1) = \frac{1}{4} |\langle \Phi_{5/2^+5/2} | \hat{M}1 | \Phi_{3/2^+3/2} \rangle|^2. \tag{5.5}$$

Similarly, for the multipole moments we determine

$$\langle \Phi_{I^+I} | \hat{M}1 | \Phi_{I^+I} \rangle = \sum_{nn'} a^*_{nI^+I} M_{nn'} a_{n'I^+I}, \tag{5.6}$$

$$\langle \Phi_{I^+I} | \hat{Q}2 | \Phi_{I^+I} \rangle = \sum_{nn'} a^*_{nI^+I} Q_{nn'} a_{n'I^+I}, \tag{5.7}$$

from which we obtain the multipole moments from equations 5.1 and 5.2.

5.3.2 Results

We implement the independent block-states mixing in HFODD version 3.33k where we performed these calculations using a spherical 3D harmonic oscillator basis of $N_0 \leq 16$ shells with TE and TO terms in the functionals. The parameters g'_0, $V_{0,N}$ and $V_{0,P}$ used are summarized in table 5.3. Additionally, the blocked neutron Nilsson tags are shown in table 5.4.

Skyrme	g'_0	$V_{0,N}$	$V_{0,P}$
$\mathrm{SkX_c}$	1.2	139.02	173.63
SkM*	1.2	181.47	216.25
UNEDF1	1.7	145.35	169.79
SIII	1.2	181.14	220.19
SkO′	1.0	163.82	184.34
SLy4	1.3	207.76	231.89
UNEDF0	1.2	130.61	158.39

Table 5.3: The Landau parameters g'_0 and the strengths of the volume proton and neutron pairing interactions, V_P and V_N, used in this study.

Shell	Spherical orbital	Nilsson orbitals
6	$1i_{11/2}$	$(642)\frac{3}{2}$, $(633)\frac{5}{2}$
	$2g_{9/2}$	$(622)\frac{5}{2}$, $(631)\frac{3}{2}$
7	$2h_{11/2}$	$(741)\frac{3}{2}$
	$1j_{13/2}$	$(752)\frac{5}{2}$

Table 5.4: Nilsson orbitals tags blocked in the ^{229}Th calculations.

Figs. 5.8, 5.9, 5.10 and table 5.5 summarize the principal results. We present the TE+TO, parity breaking and pairing calculations after angular momentum, parity projection and mixing gauged using the measured intrinsic octupole moments in ^{226}Ra (left panels) and ^{230}Th (panels). In each case, the results were analysed using a linear regression method which served to perform statistical predictions of the models and

estimate error bars of theoretical values [5]. It is remarkable that these parameter-free calculations orbit around the experimental values for all three observables but do not show a strong systematic relation with octupole moments. We obtain theoretical values that agree with experiment within error bars for the B(M1) observables and magnetic dipole moments of $5/2^+$ ground states for both extrapolations. In the other data points, the agreement is closer for individual functionals but deviates in the collective prediction.

The main challenge in obtaining the results is to retain the stability in the calculation of the Hamiltonian mixing matrix elements $H_{nn'}^{I^+\Omega}$ which are often singular due to non-zero self-interaction and self-pairing energies that characterize Skyrme functionals [1]. Because of this, several data points have to be severed from the calculations so the initial blocks of 3×3 matrices have to be reduced to smaller configuration spaces for the mixing. These results represent sophisticated MR-DFT machinery implemented to the calculation of these electromagnetic observables. However, in reference [185] we present this analysis for cases where we conserve parity and perform single configuration calculations demonstrating a small influence of mixing and the need of octupole deformation to properly model this isotope.

This work is the first consistent application of nuclear DFT with no parameter adjustment to describe the electromagnetic properties of the ^{229m}Th, namely, its transition strength and electromagnetic moments. One of the crucial aspects for this results was accounting properly for the octupole degrees of freedom in the Skyrme forces. Thus, to advance both DFT and MR-DFT methodologies it is necessary to refine the description of the octupole polarizability already at the stage of global fitting of the functionals to experimental data. In addition, a fundamental limitation of current functionals lies in their persistent issues with self-interaction and self-pairing, which leads to unreliable and often unsatisfactory results in many applications. A substantial, focused effort in addressing these two aspects is urgently needed.

Skyrme	B(M1)	$\mu(5/2+)$	$Q(5/2+)$	$\mu(3/2+)$	$Q(3/2+)$
SkX_c	—	0.4103	2.8080335	—	—
SkM*	0.07176	0.55101	2.9567549	-0.0199	1.6953374
UNEDF1	0.04833	0.25525	3.0641712	-0.26823	1.6418052
SIII	0.06880	0.96563	2.8825213	-0.15283	1.5379411
SkO′	—	—	—	—	—
SLy4	0.00456	0.3141	2.9925722	-0.32877	1.6755628
UNEDF0	0.00588	-0.13349	3.0328231	-0.23921	1.6789627
^{226}Ra regression:	0.04(3)	0.4(3)	3.01(7)	-0.1(1)	1.69(6)
^{230}Th regression:	0.03(2)	0.2(2)	2.96(6)	-0.2(1)	1.73(1)
Experiment:	0.0388(12)	0.366(6)	3.11(2)	-0.378(8)	1.77(1)

Table 5.5: Unrounded numerical values of the B(M1;$3/2_1^+ \to 5/2_1^+$) transition probabilities (in μ_N^2) and spectroscopic magnetic dipole μ moments (in μ_N) and electric quadrupole Q moments (in e·barn) calculated for the mixed $5/2^+$ and $3/2^+$ states. Values obtained from the regression analysis relative to the ^{226}Ra and ^{230}Th data, along with the experimental values, are also shown. Instabilities caused missing data in potentials SkO′ and SkX_c.

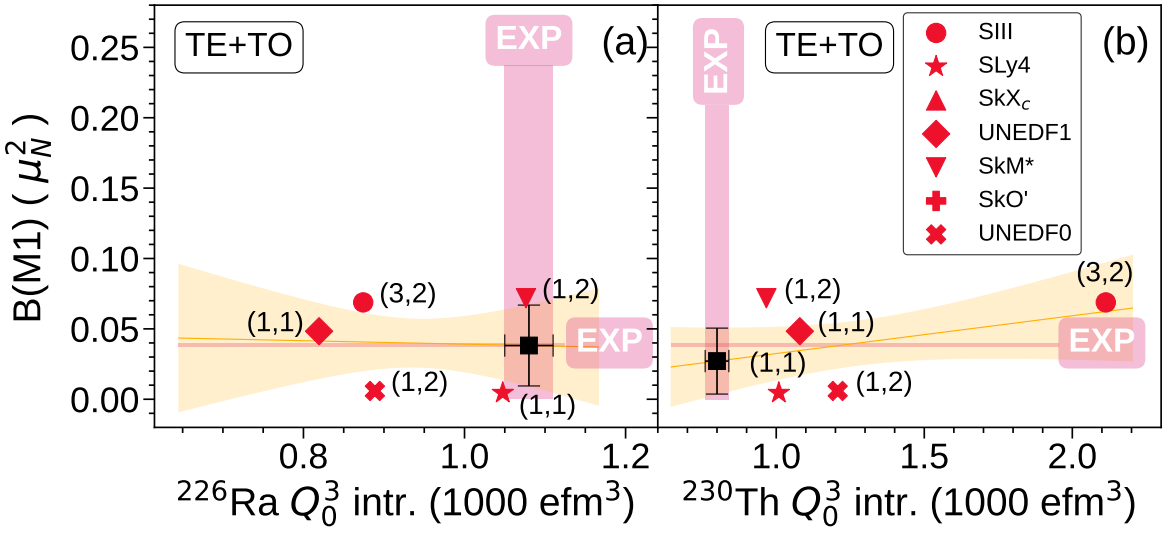

Figure 5.8: B(M1) values with respect to the intrinsic octupole moments Q_{30} of ^{226}Ra (a) and ^{230}Th (b), determined for functionals with time-even and time-odd mean-fields (TE+TO). The numbers in parentheses represent the number of successfully mixed wave functions for the two configurations, namely $(5/2^+, 3/2^+)$. The vertical and horizontal stripes labeled EXP are the experimental values of Q_{30} and B(M1), respectively. Thick lines and shaded bands denote the regression results and their uncertainties, respectively [5].

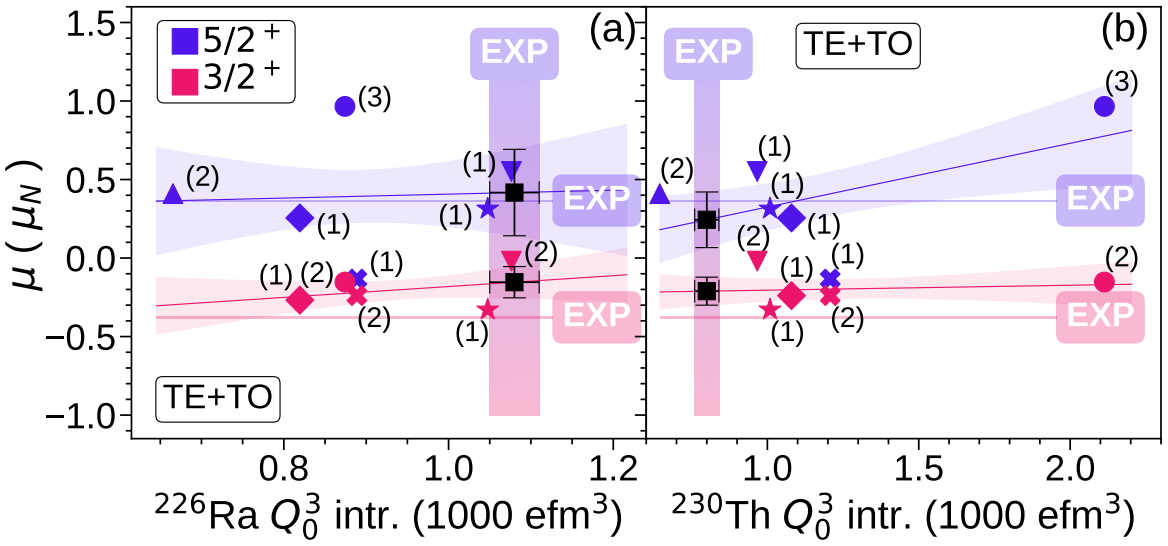

Figure 5.9: Same as Fig. 5.8 but for magnetic dipole moments. Numbers in parenthesis denote the number of configurations mixed to calculate the observable. Markers are the same as Fig. 5.8.

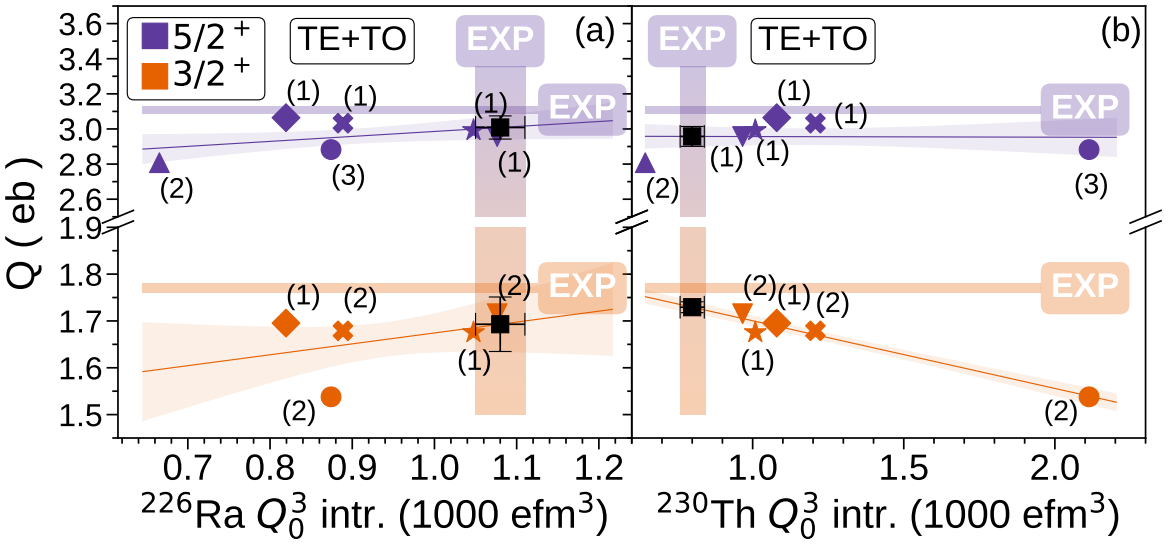

Figure 5.10: Same as figure 5.8 but for spectroscopic quadrupole moments. Numbers in parenthesis denote the number of configurations mixed to calculate the observable. Markers are the same as Fig. 5.8.

6 Conclusions

In this thesis we explored the structure of atomic nuclei through the study of its electromagnetic moments and transitions within the framework of nuclear DFT. We combined mean-field approaches with pairing interaction and advanced symmetry restoration techniques to perform a robust and consistent theoretical description of nuclear electromagnetic observables. We reviewed the theoretical developments from the role of pairing and its mean-field formulations of BCS and HFB theories. The role of symmetry breaking by shape deformations and intrinsic structure of the nucleus along with its subsequent symmetry restoration played a central role in the applied methodologies in order to access electromagnetic observables that test our understanding of the nuclear interaction. These tools allow for systematic and realistic studies of even-even, odd and odd-odd open shell deformed nuclei across the nuclear chart via proper treatment of blocking and the implementation of time-odd mean-fields.

We performed calculations of spectroscopic electric quadrupole and magnetic dipole moments for the odd-mass isotopic chains of yttrium and zirconium implementing a rigorous and parameter-free methodology. We obtained overall good agreement with available experimental data and managed to reproduce the main trends. These results demonstrate how pairing and deformation play an essential role in nuclear structure and we posses tools to systematically compute them without loosing explanatory arguments by using parameters like effective charges or gyromagnetic factors.

The study of the isomeric transition of the ^{229}Th poses a big challenge for both theory and experiment. Thus, we implemented advanced beyond mean-field DFT techniques to describe its transition strength. Despite the ambition of this task, we achieved close agreement with experimental data which reaffirms DFT as a well-established and strong theoretical framework to study the atomic nucleus, even in its extreme emergent features. At the same time, it highlights the shortcomings of the current models for which certain degrees of freedom are demonstrated to gain relevance in certain regions of the nuclear chart requiring dedicated efforts to improve our picture of the nucleus. This thesis contributes to the ongoing work of building consistent predictive nuclear models and motivates future studies of exotic nuclei, particularly in regions of the nuclear chart where experimental data remains scarce.

Appendices

A

Wick's theorem

Calculations of observables in quantum mechanics follow a general procedure given by the next sequential steps: *i*) the mathematical formulation of the associated operator that holds the rules of first quantization and describes as complete as possible a given physical quantity, *ii*) the computation of the wavefunctions of the system and *iii*) the calculation of the matrix elements of the operator in *i*) between the states of *ii*). Wick's theorem is a useful tool to perform step *iii*) in an efficient way with a limited knowledge of the expectation values of individual operators and commutation rules between them. Here we present Wick's theorem without a rigorous proof following the formulation of professor Jacek Dobaczewski, several other different approaches can be found in the literature.

Wick's theorem states that the expectation value of an ordered string of operators $A_1A_2...A_n$ with respect to a state $|\Psi\rangle$ can be reduced to a summation of products of scalar factors called contractions. Actually, these contractions are only scalars in the case where $|\Psi\rangle$ is of a particular form called product state, as will be described in appendix B. Suspending that assumption for a while, we have that for any state $|\Psi\rangle$ and any operator A, we can decompose it as

$$A = A_0 + A_- + A_+, \tag{A.1}$$

where

$$\begin{aligned} A_0 &= \langle\Psi|A|\Psi\rangle, \\ A_- &= (A - \langle\Psi|A|\Psi\rangle)(1 - |\Psi\rangle\langle\Psi|), \\ A_+ &= (1 - |\Psi\rangle\langle\Psi|)A|\Psi\rangle\langle\Psi|, \end{aligned} \tag{A.2}$$

so that

$$\begin{aligned} A_-|\Psi\rangle &= 0, \\ \langle\Psi|A_+ &= 0. \end{aligned} \tag{A.3}$$

Now consider the quantity $\langle\Psi|A_1A_2...A_n|\Psi\rangle$. In this formalism, n is allowed to be even or odd. We can decompose A_1 in the form A.1 to get

$$\langle\Psi|A_1A_2...A_n|\Psi\rangle = A_{1,0}\langle\Psi|A_2...A_n|\Psi\rangle + \langle\Psi|A_{1,-}A_2...A_n|\Psi\rangle, \tag{A.4}$$

by commuting $A_{1,-}$ with $A_{i>1}$ using

$$A_{1,-}A_i = \{A_{1,-}, A_i\} - A_iA_{1,-} = \overbrace{A_1A_i} - A_iA_{1,-}, \tag{A.5}$$

and adopting the definitions of auto-contraction

$$A_{1,0} = \overset{\sqcap}{A_1}, \tag{A.6}$$

and two-operator contraction

$$\overbrace{A_1 A_i} = \{A_{1,-}, A_i\}, \tag{A.7}$$

we get by assuming $|\Psi\rangle$ is a product state

$$\langle\Psi|A_1 A_2 ... A_n|\Psi\rangle = \overset{\sqcap}{A_1}\langle\Psi|A_2 ... A_n|\Psi\rangle + \sum_i (-1)^i \overbrace{A_1 A_i}\langle\Psi|A_2 ... A_{i-1} A_{i+1} ... A_n|\Psi\rangle, \tag{A.8}$$

where the phase $(-1)^i$ arises from the number of times that a commutation must happen so that A_1 and A_i are contiguous in the operator string. Applying iteratively A.8 for the remaining matrix elements, it can be shown that

$$\langle\Psi|A_1 A_2 ... A_n|\Psi\rangle = \sum_{\substack{i=0 \text{ or } 1 \\ \text{step } 2}}^{n} \left(\prod_{j=0 \text{ or } 1}^{i} \overset{\sqcap}{A_j} \right) \left(\sum_{k,l,...,y,z \neq j} \sigma(kl...yz) \overbrace{A_k A_l} ... \overbrace{A_y A_z} \right), \tag{A.9}$$

where i and j start at 0 or 1 depending if n is even or odd, respectively. The phase $\sigma(kl...yz)$ is the signature of the permutation $kl...yz$ that sets all operators contiguous as shown explicitly in A.9. The values of $j = 0$ means no auto-contractions at all, so in the case of n even, it accounts for the terms where all operators are pair-contracted. Thus, the matrix element of a string of operators has been expressed as products of the matrix elements of the individual operators and the anti-commutators between them. The total number of terms in expression A.9 is given by

$$\mathcal{N} = \sum_{\substack{m=0 \text{ or } 1 \\ \text{step } 2}}^{n} \binom{n}{m} \frac{(n-m)!}{2^{\frac{n-m}{2}} (\frac{n-m}{2})!}, \tag{A.10}$$

where m starts at 0 if n is even or at 1 if n is odd. In A.10, the first factor accounts for m possible auto-contractions and the second one for two-operator contractions. Applications of the theorem to up to four operators result explicitly in

$$\begin{aligned}
\langle\Psi|A|\Psi\rangle &= \overset{\sqcap}{A}, \\
\langle\Psi|AB|\Psi\rangle &= \overset{\sqcap}{A}\overset{\sqcap}{B} + \overbrace{AB}, \\
\langle\Psi|ABC|\Psi\rangle &= \overset{\sqcap}{A}\overset{\sqcap}{B}\overset{\sqcap}{C} + \overset{\sqcap}{A}\overbrace{BC} + \overbrace{A\overset{\sqcap}{B}C} + \overbrace{AB}\overset{\sqcap}{C}, \\
\langle\Psi|ABCD|\Psi\rangle &= \overset{\sqcap}{A}\overset{\sqcap}{B}\overset{\sqcap}{C}\overset{\sqcap}{D} + \overset{\sqcap}{A}\overset{\sqcap}{B}\overbrace{CD} + \overset{\sqcap}{A}\overbrace{B\overset{\sqcap}{C}D} + \overset{\sqcap}{A}\overbrace{BC}\overset{\sqcap}{D} + \overbrace{A\overset{\sqcap}{B}}\overset{\sqcap}{C}\overset{\sqcap}{D} + \overbrace{A\overset{\sqcap}{B}C}\overset{\sqcap}{D} + \overbrace{AB}\overset{\sqcap}{C}\overset{\sqcap}{D} \\
&\quad + \overbrace{A\overset{\sqcap}{B}\overset{\sqcap}{C}D} + \overbrace{A\overset{\sqcap}{B}CD} + \overbrace{AB\overset{\sqcap}{C}D} + \overbrace{ABC}\overset{\sqcap}{D} + \overbrace{AB}\overbrace{CD} \\
&\quad + \overbrace{A\overbrace{BC}D} + \overbrace{A\overbrace{B}\overbrace{CD}}
\end{aligned} \tag{A.11}$$

B

Product states

Wick's theorem introduced in the previous appendix is an essential operational tool for calculations in quantum mechanics, however, its usefulness is constrained by the requirement that all contractions need to be scalars. This is only realized when the state between which the expectation values are calculated has a specific mathematical structure called product state. In this section we describe them along with some useful formulas and properties without rigorous proofs. The approach presented here is based in professor Jacek Dobaczewski formulation.

B.0.1 Operational definition

The fermion space is described in second quantization by a set of N single-particle states with the associated set of operators $\{a_1^\dagger, ..., a_N^\dagger, a_1, ..., a_N\}$ and a vacuum $|0\rangle$. Consider the decomposition A.1 for operators $a_i^\dagger$ and a_i with respect to a state $|\Psi\rangle$ to be determined. We require the quantities

$$\begin{aligned}
\overbrace{a_i^\dagger a_j^\dagger} &= \{a_{i-}^\dagger, a_j^\dagger\}, \\
\overbrace{a_i^\dagger a_j} &= \{a_{i-}^\dagger, a_j\}, \\
\overbrace{a_i a_j^\dagger} &= \{a_{i-}, a_j^\dagger\}, \\
\overbrace{a_i a_j} &= \{a_{i-}, a_j\},
\end{aligned} \tag{B.1}$$

to be scalars. Since the $-$ components are operators in the fermion space, they can be expressed as a linear superposition of products of m creation and n destruction operators as

$$a_{i-}^\dagger = \sum_{m,n=0}^{N} \hat{S}(m,n), \tag{B.2}$$

$$a_{i-} = \sum_{m,n=0}^{N} \hat{T}(m,n). \tag{B.3}$$

It can be seen that the only terms of expansions B.2 and B.3 that result in scalars after replacement in B.1 are $\hat{S}(1,0)$, $\hat{S}(0,1)$ and $\hat{T}(1,0)$, $\hat{T}(0,1)$. Thus

$$a_{i-}^\dagger = \sum_j \left(A_{ij} a_j + B_{ij} a_j^\dagger \right), \tag{B.4}$$

$$a_{i-} = \sum_j \Big(C_{ij} a_j + D_{ij} a_j^\dagger \Big), \tag{B.5}$$

are a set of $2N$ linearly independent operators that span the whole fermion space. We can postulate a unitary transformation between these $-$ components to operators

$$\begin{aligned} \alpha_i &= \sum_j U_{ij}^{-1} a_{j-}, \\ \alpha_i^\dagger &= \sum_j U_{ji}^{-1*} (a_{j-})^\dagger, \end{aligned} \tag{B.6}$$

which fulfill anti-commutation relations

$$\begin{aligned} \{\alpha_i^\dagger, \alpha_j^\dagger\} = \{\alpha_i, \alpha_j\} &= 0, \\ \{\alpha_i, \alpha_j^\dagger\} &= \delta_{ij}, \end{aligned} \tag{B.7}$$

as long as U is non-singular. Since the operators $\alpha^\dagger$ and α emerge from invertible (non-singular) linear relations, B.5 is equivalent to

$$\alpha_i = \sum_j \Big(C'_{ij} a_j + D'_{ij} a_j^\dagger \Big), \tag{B.8}$$

$$\alpha_i^\dagger = \sum_j \Big(D'^*_{ij} a_j + C'^*_{ij} a_j^\dagger \Big), \tag{B.9}$$

which from B.6 also holds

$$\alpha_i |\Psi\rangle = 0, \tag{B.10}$$

thus we arrived at the central theorem of this appendix which states that the product states for which Wick's theorem holds true are the vacuum of generalized Bogoliubov transformations between fermion operators $a^\dagger$, a and $\alpha^\dagger$, α. The Pauli exclusion principle constrains the possible transformations greatly since all quadratic combinations annihilate thus simplifying the space where Wick's theorem operates to well-known linear transformations.

B.0.2 Thouless theorem

For the fermion space described by the set of operators $\{a_1^\dagger, ..., a_N^\dagger, a_1, ..., a_N\}$ and a vacuum $|0\rangle$, we can perform a unitary transformation $\mathcal{U}$ to get a different set $\{\alpha_1^\dagger, ..., \alpha_N^\dagger, \alpha_1, ..., \alpha_N\}$ and vacuum $|\Phi\rangle$ such that

$$\begin{aligned} \alpha_i^\dagger &= \mathcal{U} a_i^\dagger \mathcal{U}^\dagger, \\ \alpha_i &= \mathcal{U} a_i \mathcal{U}^\dagger, \\ |\Phi\rangle &= \mathcal{U} |0\rangle. \end{aligned} \tag{B.11}$$

Thouless theorem connects all vacua of fermion operators by a simple equation dependent on the Bogoliubov transformations between them. If $|\Phi\rangle$ and $|\Psi\rangle$ are the

quasiparticle vacua of fermion operators α_i and β_i, respectively, and $\langle\Phi|\Psi\rangle \neq 0$, then

$$|\Phi\rangle = \langle\Psi|\Phi\rangle \exp\left(\frac{1}{2}\sum_{i,j} Z_{ij}\beta_i^\dagger\beta_j^\dagger\right)|\Psi\rangle, \tag{B.12}$$

where Z is skew-symmetric and is called the Thouless matrix. It is given by

$$Z = V^* U^{-1*}, \tag{B.13}$$

with U and V given by

$$\begin{aligned} U &= U_\Psi^\dagger U_\Phi + V_\Psi^\dagger V_\Phi, \\ V &= V_\Psi^T U_\Phi + U_\Psi^T V_\Phi, \end{aligned} \tag{B.14}$$

where U_Φ, V_Φ and U_Ψ, V_Ψ are the generalized Bogoliubov transformation matrices of 2.95 for states Φ and Ψ, respectively.

B.0.3 Onishi and Bertsch-Robledo theorems

In equation B.12 the overlap $\langle\Psi|\Phi\rangle$ needs to be calculated. It is also a recurring task in the multi-reference methods of 3.3. A useful formula to calculate overlaps between vacua is given by the Onishi theorem [7, 10] which states

$$\langle\Psi|\Phi\rangle = \sqrt{\det(U_\Phi^\dagger U_\Psi + V_\Phi^\dagger V_\Psi)}, \tag{B.15}$$

and leaves the overlap undefined by a phase. This was corrected by Bertsch and Robledo [186] via the formula

$$\langle\Psi|\Phi\rangle = (-1)^{N/2}\frac{\det(C_\Phi)^*\det(C_\Psi)}{\prod_i v_{\Phi,i}\prod_j v_{\Psi,j}}\mathrm{pf}\begin{pmatrix} V_\Phi^T U_\Phi & V_\Phi^T V_\Psi^* \\ -V_\Psi^\dagger V_\Phi & U_\Psi^\dagger V_\Psi^* \end{pmatrix}, \tag{B.16}$$

where C_Ψ and C_Φ are the quasiparticle transformation matrices of the Bloch-Messiah-Zumino theorem 2.98.

B.0.4 Canonical basis

Thouless theorem relates all product states via the simple relation B.12. However, this relation can be simplified further by performing a unitary transformation over the space $\{\beta\dagger, \beta\}$ so that the Thouless matrix Z_{ij} has a simpler form. This transformed outputs the canonical basis. This result relies in a theorem from matrix algebra that states that for any skew-symmetric matrix Z, there exist an unitary matrix U such that

$$U^T Z U = \bar{Z}, \tag{B.17}$$

where

$$\bar{Z}_{ij} = s_{\bar{i}}^* z_i \delta_{\bar{i}j}, \tag{B.18}$$

$$z_{\bar{i}} = z_i \geq 0, \qquad s_{\bar{i}} = -s_i, \qquad s_i^* s_i = 1, \tag{B.19}$$

where the transformation imposes a grouping of the indices in pairs associated by the bar above the index. These are called canonical pairs and are usually chosen to be time-reversed pairs. If we consider the density matrix 2.25 and pairing tensor calculated 2.34 calculated between product states B.12 we get

$$\begin{aligned} \rho &= Z^\dagger (1 + ZZ^\dagger)^{-1} Z, \\ \kappa &= -Z^\dagger (1 + ZZ^\dagger)^{-1}, \end{aligned} \tag{B.20}$$

in the canonical basis we get a diagonal and skew-symmetric forms

$$\begin{aligned} \bar{\rho}_{ij} &= (U^\dagger \rho U)_{ij} = \frac{z_i^2}{1 + z_i^2} \delta_{ij} = -v_i^2 \delta_{ij} \\ \bar{\kappa}_{ij} &= (U^\dagger \kappa U^*)_{ij} = \frac{s_{\bar{i}} z_i}{1 + z_i^2} \delta_{\bar{i}j} = s_{\bar{i}} u_i v_i \delta_{\bar{i}j} \end{aligned} \tag{B.21}$$

presented also in 2.104 via the Bloch-Messiah-Zumino theorem.

The transformation rule over the creation operators is then

$$\begin{aligned} \bar{\beta}_i^\dagger &= \sum_j U_{ji} \beta_j^\dagger, \\ \bar{\beta}_i &= \sum_j U_{ji}^\dagger \beta_j, \end{aligned} \tag{B.22}$$

when replaced in B.12 results in

$$|\Phi\rangle = \langle \Psi | \Phi \rangle \exp\left(\sum_{i>0} s_i^* z_i \bar{\beta}_{\bar{i}}^\dagger \bar{\beta}_i^\dagger \right) |\Psi\rangle, \tag{B.23}$$

where the summation $i > 0$ denotes summation over a single representative of the canonical pair. After mathematical manipulations we get to the form

$$|\Phi\rangle = \langle \Psi | \Phi \rangle \prod_{i>0} (1 + s_i^* z_i \bar{\beta}_{\bar{i}}^\dagger \bar{\beta}_i^\dagger) |\Psi\rangle, \tag{B.24}$$

which is the ground state ansatz of BCS theory.

C Complete dataset of calculations

We present in graphs the complete set of calculated spectra and electromagnetic moments for the odd-mass isotopic chains of yttrium and zirconium. We restrict the plots to calculations that converged, any missing points correspond to cases with numerical instabilities. We separate the dataset by oblate and prolate tags analogously as in [59].

C.1 Odd-A zirconium calculations plots

We performed 1188 calculations by blocking 27 states specified in table 5.2 in the odd-A isotopic chain of $^{79-101}$Zr. Fig. C.1 displays excitation energy of the 27 configurations. Fig. C.2 displays the energy difference between oblate and prolate minima. Figs. C.3 and C.4 show electric quadrupole and magnetic dipole moments, respectively.

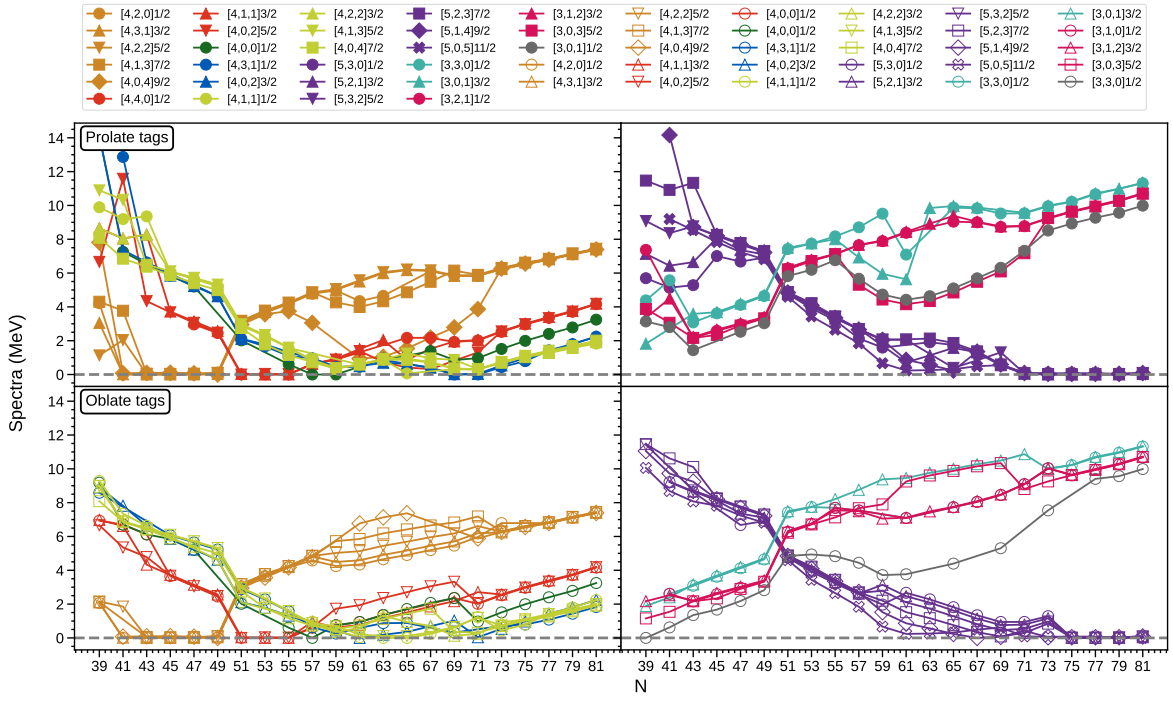

Figure C.1: Calculated spectra of $^{79-101}$Zr.

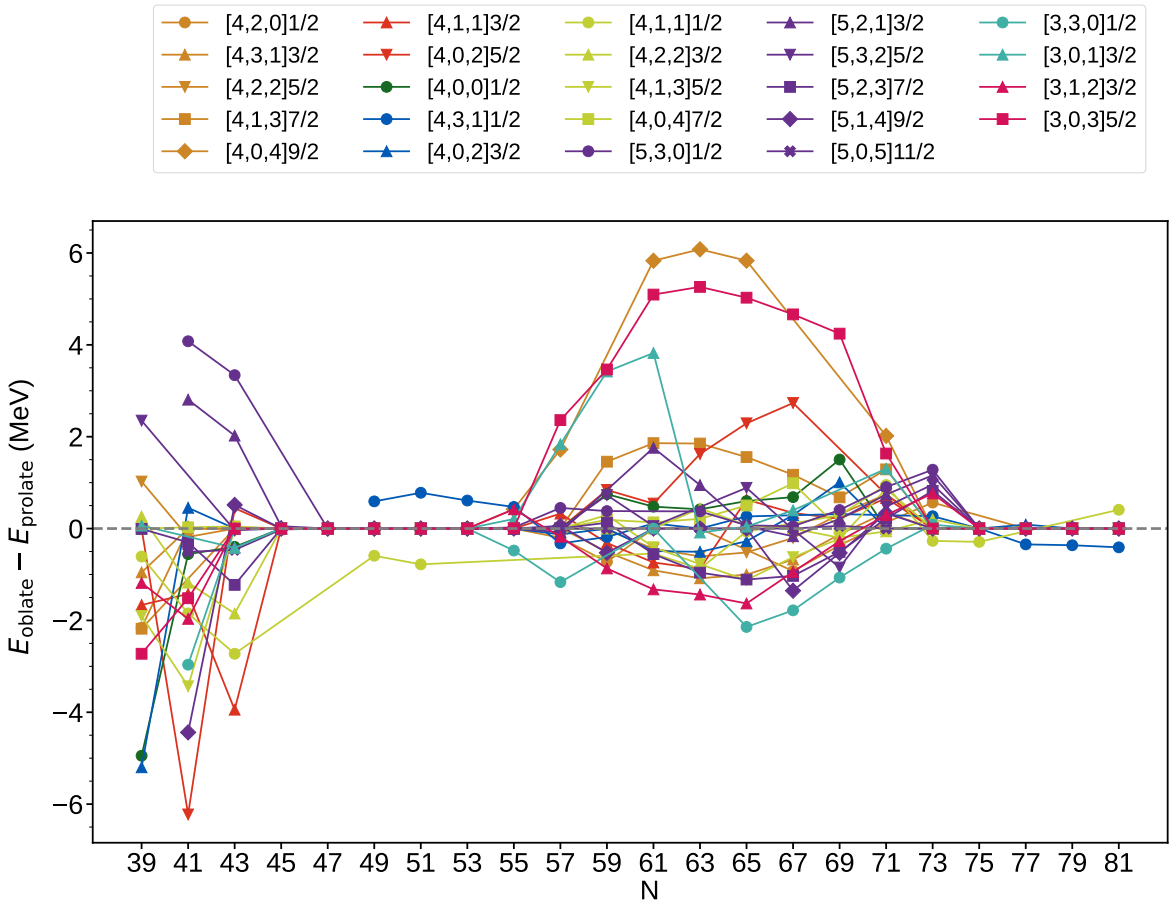

Figure C.2: Energy differences in prolate and oblate tags for the spectra of $^{79-101}$Zr.

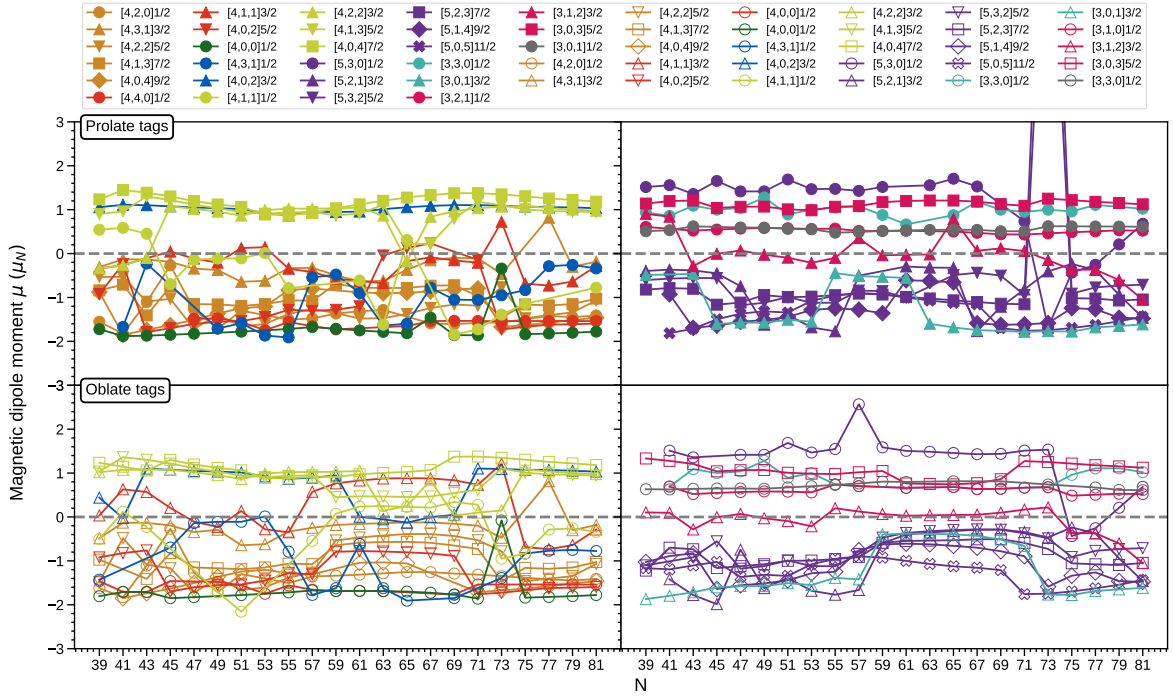

Figure C.4: Calculated magnetic dipole moments of $^{79-101}$Zr.

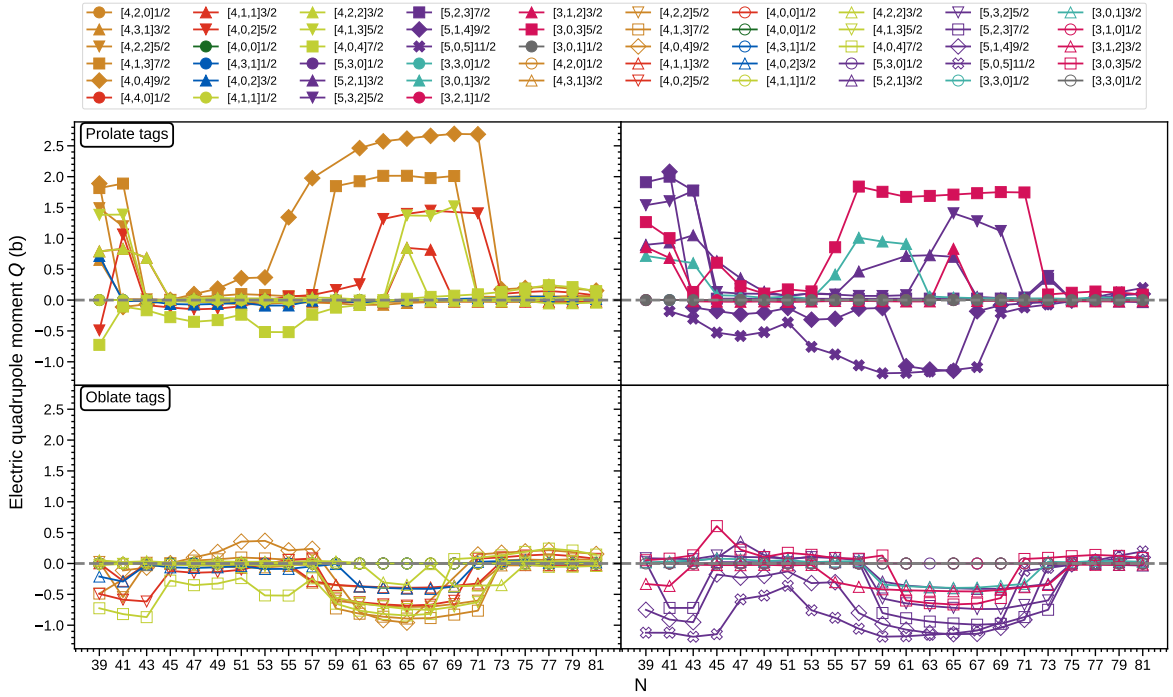

Figure C.3: Calculated spectroscopic electric quadrupole moments of $^{79-101}$Zr.

C.2 Odd-A yttrium calculations plots

We performed 448 calculations by blocking 11 states specified in table 5.1 in the odd-A isotopic chain of $^{79-101}$Y. Fig. C.5 displays excitation energy of the 11 configurations. Fig. C.6 displays the energy difference between oblate and prolate minima. Figs. C.7 and C.8 show electric quadrupole and magnetic dipole moments, respectively.

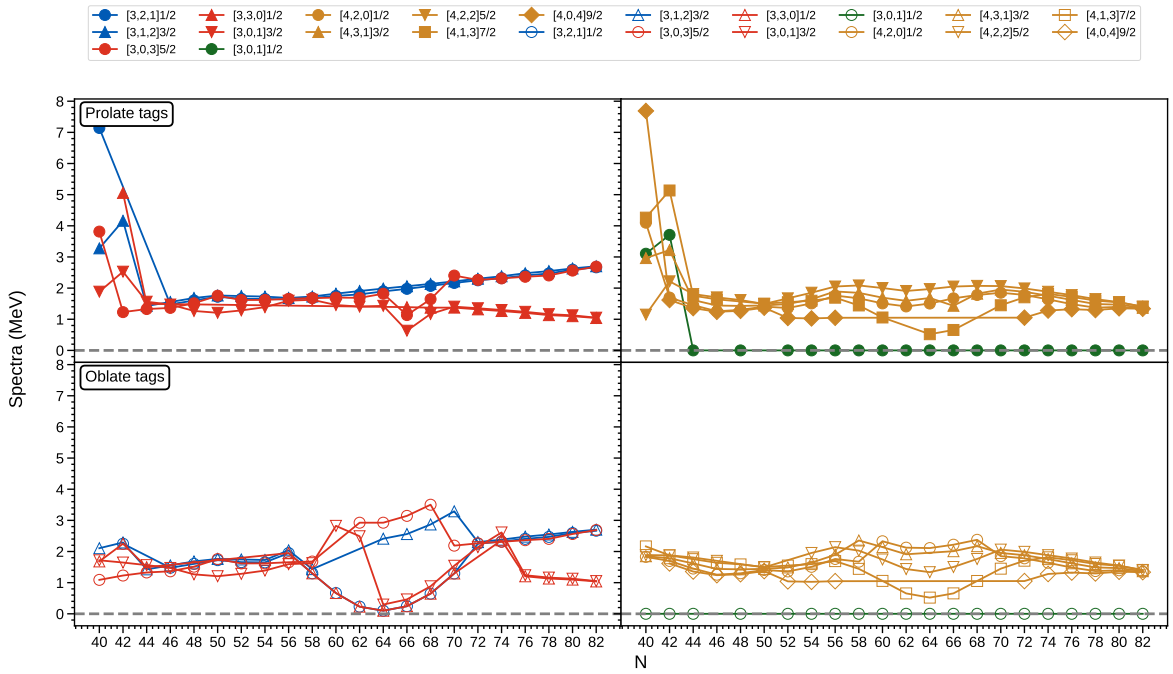

Figure C.5: Calculated spectra of $^{79-101}$Y.

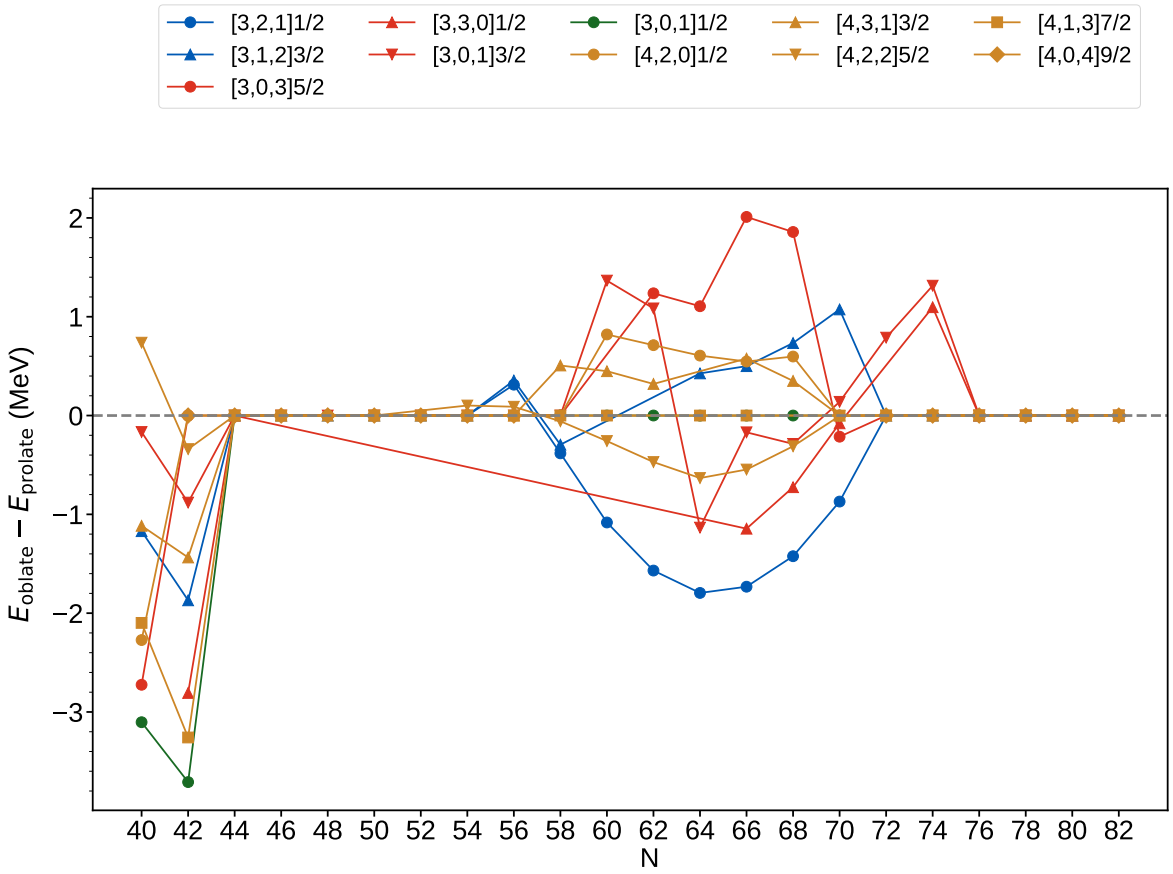

Figure C.6: Energy differences in prolate and oblate tags for the spectra of $^{79-101}$Y.

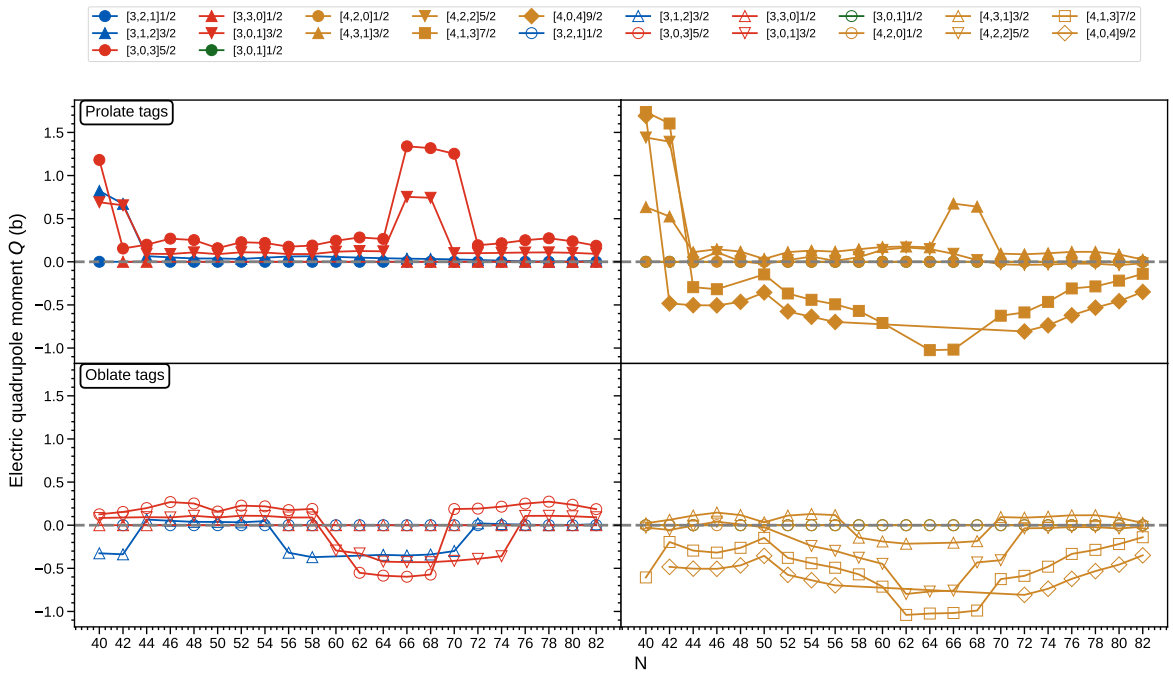

Figure C.7: Calculated spectroscopic electric quadrupole moments of $^{79-101}$Y.

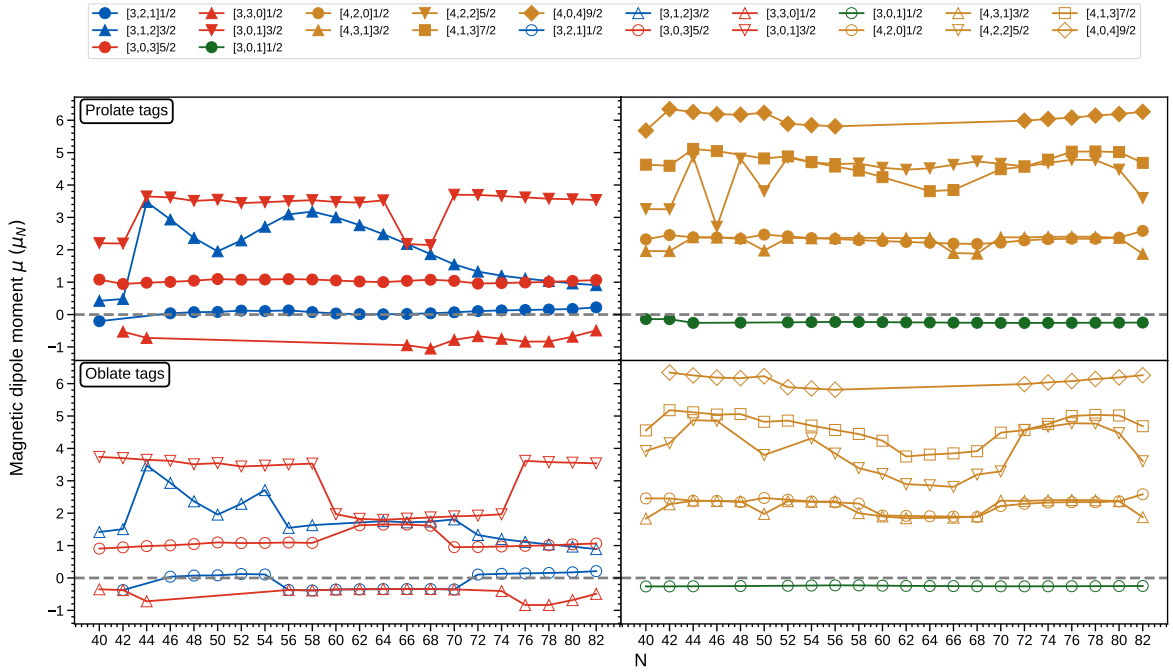

Figure C.8: Calculated magnetic dipole moments of $^{79-101}$Y.

C.3 Numerical values of available experimental data

Isotope	I^π	μ_{exp} (μ_N)	μ_{th} (μ_N)
^{87}Zr	$9/2^+$	$-0.894(5)$	$-1.5065^{+0.0618}_{-0.0698}$
^{87}Zr	$1/2^-$	$+0.641(16)$	$+0.6492^{+0.0067}_{-0.0083}$
^{89}Zr	$9/2^+$	$-1.045(6)$	$-1.3637^{+0.0697}_{-0.0809}$
^{89}Zr	$1/2^-$	$+0.794(18)$	$+0.6422^{+0.0043}_{-0.0048}$
^{91}Zr	$5/2^+$	$-1.3022(4)$	$-1.5374^{+0.0498}_{-0.0560}$
^{95}Zr	$5/2^+$	$+1.13(2)$	$-1.2806^{+0.0648}_{-0.0780}$
^{97}Zr	$1/2^+$	$-0.936(5)$	$-1.6745^{+0.0258}_{-0.0241}$
^{97}Zr	$7/2^+$	$+1.37(14)$	$+0.9202^{+0.0386}_{-0.0470}$
^{99}Zr	$1/2^+$	$-0.929(4)$	$-1.7132^{+0.0000}_{-0.0262}$
^{99}Zr	$3/2^+$	$+0.42(6)$	$+1.0301^{+0.0145}_{-0.0155}$
^{101}Zr	$(3/2^+)$	$-0.272(8)$	$+0.0042^{+0.0237}_{-0.0180}$
^{101}Zr	$(5/2^+)$	$+0.12(7)$	$+0.4708^{+0.0098}_{-0.0098}$
^{101}Zr	$(5/2^-)$	$-0.5(3)$	$-1.0062^{+0.0266}_{-0.0316}$
^{101}Zr	$(7/2^+)$	$+0.6(4)$	$+1.1211^{+0.0368}_{-0.0398}$
^{101}Zr	$(7/2^-)$	$-0.14(11)$	$-0.5465^{+0.0348}_{-0.0414}$
			RMS: 0.8634

Table C.1: Experimental and theoretical magnetic dipole moments for Zr isotopes. Experimental values from [2]. Coloured signs are assigned by theory.

Isotope	I^π	Q_{exp} (b)	Q_{th} (b)
^{87}Zr	$9/2^+$	$+0.42(5)$	$+0.09689$
^{89}Zr	$9/2^+$	$+0.28(10)$	$+0.18542$
^{91}Zr	$5/2^+$	$-0.176(3)$	-0.10061
^{95}Zr	$5/2^+$	$+0.22(2)$	$+0.05676$
^{101}Zr	$3/2^+$	$+0.81(6)$	$+0.00896$
			RMS: 0.397

Table C.2: Experimental and theoretical electric quadrupole moments for Zr isotopes. Experimental values from [3].

Isotope	I^π	μ_{exp} (μ_N)	μ_{th} (μ_N)
^{83}Y	$7/2^+$	$+2.1(6)$	$+5.1153^{+0.000}_{-0.0613}$
^{85}Y	$(9/2)^+$	$+6.2(5)$	$+6.1856^{+0.000}_{-0.0794}$
^{85}Y	$(5/2)^-$	$+1.36(2)$	$+1.0079^{+0.0362}_{-0.0403}$
^{87}Y	$1/2^-$	$-0.19(2)$	$-0.2494^{+0.0041}_{-0.0044}$
^{87}Y	$9/2^+$	$+6.24(2)$	$+6.1705^{+0.000}_{-0.0907}$
^{89}Y	$1/2^-$	$-0.137298(5)$	$-0.2449^{+0.0051}_{-0.0056}$
^{89}Y	$9/2^+$	$+6.37(4)$	$+6.2293^{+0.000}_{-0.1020}$
^{91}Y	$1/2^-$	$+0.1639(8)$	$-0.2401^{+0.0055}_{-0.0061}$
^{91}Y	$9/2^+$	$+5.96(4)$	$+5.8889^{+0.000}_{-0.1062}$
^{93}Y	$1/2^-$	$-0.139(1)$	$-0.2340^{+0.0069}_{-0.0067}$
^{93}Y	$9/2^+$	$+6.04(3)$	$+5.8490^{+0.000}_{-0.1101}$
^{95}Y	$1/2^-$	$-0.16(3)$	$-0.2274^{+0.0067}_{-0.0077}$
^{97}Y	$1/2^-$	$-0.12(1)$	$-0.2294^{+0.0064}_{-0.0066}$
^{97}Y	$9/2^+$	$+5.88(2)$	Not converged
^{99}Y	$9/2^+$	$+3.18(2)$	$+3.2081^{+0.000}_{-0.0349}$
^{101}Y	$5/2^+$	$+3.22(2)$	$+2.8956^{+0.000}_{-0.0329}$
			RMS: 0.800

Table C.3: Experimental and theoretical magnetic dipole moments of Y isotopes. Experimental values from [2]. Coloured signs are assigned by theory.

Isotope	I^π	Q_{exp} (b)	Q_{th} (b)
^{87}Y	$9/2^+$	$-0.50(6)$	-0.4650
^{89}Y	$9/2^+$	$-0.43(6)$	-0.3552
^{93}Y	$9/2^+$	$-0.64(8)$	-0.6380
^{97}Y	$9/2^+$	$-0.76(8)$	Not converged
^{99}Y	$5/2^+$	$+1.55(17)$	-0.4483
^{101}Y	$5/2^+$	$+1.53(17)$	-0.7975
			RMS: 1.06

Table C.4: Experimental and theoretical electric quadrupole moments for Y isotopes. Experimental values from [3].

References

[1] J A Sheikh, J Dobaczewski, P Ring, L M Robledo, and C Yannouleas. Symmetry restoration in mean-field approaches. *Journal of Physics G: Nuclear and Particle Physics*, 48(12):123001, nov 2021.

[2] N. J. Stone. Table of recommended nuclear magnetic dipole moments: Long-lived states. *Atom. Data Nucl. Data Tabl.*, 2019.

[3] N. J. Stone. Table of nuclear electric quadrupole moments. *Atom. Data Nucl. Data Tabl.*, 2021.

[4] Peter Thirolf. Shedding light on the Thorium-229 nuclear clock isomer. *Physics*, 17:71, 2024.

[5] Jacek Dobaczewski, Jonathan Engel, Markus Kortelainen, and Pierre Becker. Correlating Schiff moments in the light actinides with octupole moments. *Phys. Rev. Lett.*, 121:232501, Dec 2018.

[6] Ricardo A. Broglia and Vladimir Zelevinsky, editors. *Fifty Years of Nuclear BCS: Pairing in Finite Systems*. World Scientific, Singapore, 2013.

[7] P. Ring and P. Schuck. *The Nuclear Many-Body Problem*. Physics and astronomy online library. Springer, 2004.

[8] P. Hohenberg and W. Kohn. Inhomogeneous electron gas. *Phys. Rev.*, 136:B864–B871, Nov 1964.

[9] W. Kohn and L. J. Sham. Self-consistent equations including exchange and correlation effects. *Phys. Rev.*, 140:A1133–A1138, Nov 1965.

[10] Nicolas Schunck, editor. *Energy Density Functional Methods for Atomic Nuclei*. 2053-2563. IOP Publishing, 2019.

[11] P. W. Anderson. More is different. *Science*, 177(4047):393–396, 1972.

[12] J. Dobaczewski, B. C. Backes, R. P. de Groote, A. Restrepo-Giraldo, X. Sun, and H. Wibowo. Electromagnetic and exotic moments in nuclear DFT. `https://arxiv.org/abs/2511.04632`, 2025.

[13] J. Bardeen, L. N. Cooper, and J. R. Schrieffer. Theory of superconductivity. *Phys. Rev.*, 108:1175–1204, Dec 1957.

[14] A. Bohr, B. R. Mottelson, and D. Pines. Possible analogy between the excitation spectra of nuclei and those of the superconducting metallic state. *Phys. Rev.*, 110:936–938, May 1958.

[15] J. Dobaczewski, P. Baczyk, P. Becker, M. Bender, K. Bennaceur, J. Bonnard, Y. Gao, A. Idini, M. Konieczka, M. Kortelainen, L. Prochniak, A. M. Romero, W. Satuła, Y. Shi, L. F. Yu, and T. R. Werner. Solution of universal nonrelativistic nuclear DFT equations in the cartesian deformed harmonic-oscillator basis. (IX) HFODD (v3.06h): a new version of the program. *Journal of Physics G: Nuclear and Particle Physics*, 48(10):102001, 2021.

[16] W.H. Dickhoff and D. Van Neck. *Many-body Theory Exposed!: Propagator Description of Quantum Mechanics in Many-body Systems*. G - Reference,Information and Interdisciplinary Subjects Series. World Scientific, 2008.

[17] D. J. Dean and M. Hjorth-Jensen. Pairing in nuclear systems: from neutron stars to finite nuclei. *Rev. Mod. Phys.*, 75:607–656, Apr 2003.

[18] J. Suhonen. *From Nucleons to Nucleus: Concepts of Microscopic Nuclear Theory*. Theoretical and Mathematical Physics. Springer Berlin Heidelberg, 2007.

[19] J S C McKee. The three-body problem in nuclear physics. *Reports on Progress in Physics*, 33(2):691, may 1970.

[20] M. Sambataro and N. Sandulescu. Four-body correlations in nuclei. *Phys. Rev. Lett.*, 115:112501, Sep 2015.

[21] A. Staszczak, M. Stoitsov, A. Baran, and W. Nazarewicz. Augmented lagrangian method for constrained nuclear density functional theory. *The European Physical Journal A*, 46(1):85–90, Oct 2010.

[22] I.Z. Petkov and M.V. Stoitsov. *Nuclear Density Functional Theory*. Oxford science publications. Clarendon Press, 1991.

[23] W. Greiner, D.A. Bromley, and J.A. Maruhn. *Nuclear Models*. Springer Berlin Heidelberg, 2012.

[24] A. Messiah. *Quantum Mechanics*. Dover books on physics. Dover Publications, 1999.

[25] D.A. Varshalovich, D.A. Varshalovich, A.N. Moskalev, V.K. Khersonski, and World Scientific (Singapur). *Quantum Theory of Angular Momentum: Irreducible Tensors, Spherical Harmonics, Vector Coupling Coefficients, 3nj Symbols*. World Scientific Pub., 1988.

[26] M.E. Rose. *Elementary Theory of Angular Momentum*. Dover Books on Physics Series. Dover Publications, Incorporated, 2013.

[27] Rok Žitko. Sneg – mathematica package for symbolic calculations with second-quantization-operator expressions. *Computer Physics Communications*, 182(10):2259–2264, 2011.

[28] Jan Kvasil. Nuclear structure and nuclear processes (ns + nr). Lecture notes, Institute of Particle and Nuclear Physics (IPNP), Czech Technical University, Prague, 2023. Online: `https://ipnp.cz/~kvasil/valya/NS+NR.pdf`.

[29] W. Greiner, L. Neise, and H. Stöcker. *Thermodynamics and Statistical Mechanics*. Classical theoretical physics. Springer-Verlag, 1997.

[30] J. Dobaczewski, W. Satuła, B.G. Carlsson, J. Engel, P. Olbratowski, P. Powałowski, M. Sadziak, J. Sarich, N. Schunck, A. Staszczak, M. Stoitsov, M. Zalewski, and H. Zduńczuk. Solution of the Skyrme-Hartree-Fock-Bogolyubov equations in the cartesian deformed harmonic-oscillator basis. (VI) HFODD (v2.40h): a new version of the program. *Computer Physics Communications*, 180(12):2361–2391, 2009.

[31] H Wibowo, B C Backes, J Dobaczewski, R P de Groote, A Nagpal, A Sánchez-Fernández, X Sun, and J L Wood. Electromagnetic moments in the Sn-Gd region determined within nuclear DFT. *Journal of Physics G: Nuclear and Particle Physics*, 52(6):065104, jul 2025.

[32] P L Sassarini, J Dobaczewski, J Bonnard, and R F Garcia Ruiz. Nuclear DFT analysis of electromagnetic moments in odd near doubly magic nuclei. *Journal of Physics G: Nuclear and Particle Physics*, 49(11):11LT01, sep 2022.

[33] J. Bonnard, J. Dobaczewski, G. Danneaux, and M. Kortelainen. Nuclear DFT electromagnetic moments in heavy deformed open-shell odd nuclei. *Physics Letters B*, 843:138014, 2023.

[34] S. G. Nilsson. Binding states of individual nucleons in strongly deformed nuclei. *Kgl. Danske Videnskab. Selskab., Mat.-Fys. Medd.*, 29(16):1–69, 1955.

[35] I. Ragnarsson and S.G. Nilsson. *Shapes and Shells in Nuclear Structure*. Cambridge University Press, 1995.

[36] Claude Bloch and Albert Messiah. The canonical form of an antisymmetric tensor and its application to the theory of superconductivity. *Nuclear Physics*, 39:95–106, 1962.

[37] Frieder Selisko. The Bloch-Messiah theorem and its application to overlaps. `https://lup.lub.lu.se/student-papers/search/publication/9109501`, 2023. Student Paper.

[38] E. Engel and R.M. Dreizler. *Density Functional Theory: An Advanced Course*. Theoretical and Mathematical Physics. Springer Berlin Heidelberg, 2011.

[39] I.Z. Petkov and M.V. Stoitsov. *Nuclear Density Functional Theory*. Oxford science publications. Clarendon Press, 1991.

[40] Thiago Carvalho Corso. A rigorous formulation of density functional theory for spinless electrons in one dimension. `https://arxiv.org/abs/2504.05501`, 2025.

[41] Nicolas Hadjisavvas and Andreas Theophilou. Rigorous formulation of the kohn and sham theory. *Phys. Rev. A*, 30:2183–2186, Nov 1984.

[42] John E. Harriman. Orthonormal orbitals for the representation of an arbitrary density. *Phys. Rev. A*, 24:680–682, Aug 1981.

[43] Michael Bender, Paul-Henri Heenen, and Paul-Gerhard Reinhard. Self-consistent mean-field models for nuclear structure. *Rev. Mod. Phys.*, 75:121–180, Jan 2003.

[44] J. Dobaczewski and J. Dudek. Solution of the Skyrme-Hartree-Fock equations in the cartesian deformed harmonic oscillator basis. (I) The method. *Computer Physics Communications*, 102(2–3):183–196, 1997.

[45] T.H.R. Skyrme. The effective nuclear potential. *Nuclear Physics*, 9(4):615–634, 1958.

[46] J. Dobaczewski and J. Dudek. Time-odd components in the mean field of rotating superdeformed nuclei. *Phys. Rev. C*, 52:1827–1839, Oct 1995.

[47] B. K. Agrawal, S. Shlomo, and V. Kim Au. Determination of the parameters of a skyrme type effective interaction using the simulated annealing approach. *Phys. Rev. C*, 72:014310, Jul 2005.

[48] M. Kortelainen, J. McDonnell, W. Nazarewicz, P.-G. Reinhard, J. Sarich, N. Schunck, M. V. Stoitsov, and S. M. Wild. Nuclear energy density optimization: Large deformations. *Phys. Rev. C*, 85:024304, Feb 2012.

[49] M. Kortelainen, T. Lesinski, J. Moré, W. Nazarewicz, J. Sarich, N. Schunck, M. V. Stoitsov, and S. Wild. Nuclear energy density optimization. *Phys. Rev. C*, 82:024313, Aug 2010.

[50] M. Bender, J. Dobaczewski, J. Engel, and W. Nazarewicz. Gamow-Teller strength and the spin-isospin coupling constants of the Skyrme energy functional. *Phys. Rev. C*, 65:054322, May 2002.

[51] J. Dobaczewski and J. Dudek. Time-odd components in the mean field of rotating superdeformed nuclei. *Phys. Rev. C*, 52:1827–1839, Oct 1995.

[52] M. Dutra, O. Lourenço, J. S. Sá Martins, A. Delfino, J. R. Stone, and P. D. Stevenson. Skyrme interaction and nuclear matter constraints. *Phys. Rev. C*, 85:035201, Mar 2012.

[53] N. Kaiser. Spin-orbit coupling in nuclei and realistic nucleon-nucleon potentials. *Phys. Rev. C*, 70:034307, Sep 2004.

[54] M. Beiner, H. Flocard, Nguyen Van Giai, and P. Quentin. Nuclear ground-state properties and self-consistent calculations with the Skyrme interaction: (I). spherical description. *Nuclear Physics A*, 238(1):29–69, 1975.

[55] E. Chabanat, P. Bonche, P. Haensel, J. Meyer, and R. Schaeffer. A Skyrme parametrization from subnuclear to neutron star densities Part II. Nuclei far from stabilities. *Nuclear Physics A*, 635(1):231–256, 1998.

[56] J. Bartel, P. Quentin, M. Brack, C. Guet, and H.-B. Håkansson. Towards a better parametrisation of Skyrme-like effective forces: A critical study of the SkM force. *Nuclear Physics A*, 386(1):79 – 100, 1982.

[57] P.-G. Reinhard, D. J. Dean, W. Nazarewicz, J. Dobaczewski, J. A. Maruhn, and M. R. Strayer. Shape coexistence and the effective nucleon-nucleon interaction. *Phys. Rev. C*, 60:014316, Jun 1999.

[58] B. Alex Brown. New Skyrme interaction for normal and exotic nuclei. *Phys. Rev. C*, 58:220–231, Jul 1998.

[59] J. Dobaczewski, A. E. Stuchbery, G. Danneaux, A. Nagpal, P. L. Sassarini, and H. Wibowo. Electromagnetic moments of ground and excited states calculated in heavy odd-N open-shell nuclei. `https://arxiv.org/abs/2509.26549`, 2025.

[60] J. Dechargé and D. Gogny. Hartree-Fock-Bogolyubov calculations with the $D1$ effective interaction on spherical nuclei. *Phys. Rev. C*, 21:1568–1593, Apr 1980.

[61] J.F. Berger, M. Girod, and D. Gogny. Time-dependent quantum collective dynamics applied to nuclear fission. *Computer Physics Communications*, 63(1):365–374, 1991.

[62] T Duguet and J Sadoudi. Breaking and restoring symmetries within the nuclear energy density functional method. *Journal of Physics G: Nuclear and Particle Physics*, 37(6):064009, apr 2010.

[63] T. Otsuka, Y. Tsunoda, N. Shimizu, Y. Utsuno, T. Abe, and H. Ueno. Prevailing triaxial shapes in atomic nuclei and a quantum theory of rotation of composite objects. *The European Physical Journal A*, 61(5):126, Jun 2025.

[64] Alejandro Frank, Jan Jolie, and Pieter van Isacker. *Symmetries in Atomic Nuclei: From Isospin to Supersymmetry*, volume 776 of *Lecture Notes in Physics*. Springer, 1st edition, 2009.

[65] R. Gilmore. *Lie Groups, Lie Algebras, and Some of Their Applications*. Dover Books on Mathematics. Dover Publications, 2012.

[66] M. Hamermesh. *Group Theory and Its Application to Physical Problems*. Addison Wesley Series in Physics. Dover Publications, 1989.

[67] Alejandro Restrepo-Giraldo. Structure of heavy nuclei based on nucleon quartets. `https://arxiv.org/abs/2306.11996`, 2024. Bachelors thesis.

[68] David Lawrence Hill and John Archibald Wheeler. Nuclear constitution and the interpretation of fission phenomena. *Phys. Rev.*, 89:1102–1145, Mar 1953.

[69] James J. Griffin and John A. Wheeler. Collective motions in nuclei by the method of generator coordinates. *Phys. Rev.*, 108:311–327, Oct 1957.

[70] R E Peierls and J Yoccoz. The collective model of nuclear motion. *Proceedings of the Physical Society. Section A*, 70(5):381, may 1957.

[71] Tomás R. Rodríguez and J. Luis Egido. Triaxial angular momentum projection and configuration mixing calculations with the Gogny force. *Phys. Rev. C*, 81:064323, Jun 2010.

[72] G. Colò. Density functional theory (DFT) for atomic nuclei: a simple introduction. `https://arxiv.org/abs/1807.02643`, 2018.

[73] John David Jackson. *Classical electrodynamics*. Wiley, New York, NY, 3rd ed. edition, 1999.

[74] Jonathan Engel. Nuclear schiff moments and CP violation. *Annual Review of Nuclear and Particle Science*, 75:129–151, Jan 2025.

[75] E. M. Purcell and N. F. Ramsey. On the possibility of electric dipole moments for elementary particles and nuclei. *Phys. Rev.*, 78:807–807, Jun 1950.

[76] Naftali Auerbach and Vladimir Zelevinsky. Nuclear structure and the search for collective enhancement of PT-violating schiff moments. *Journal of Physics G: Nuclear and Particle Physics*, 35(9):093101, aug 2008.

[77] V. Spevak, N. Auerbach, and V. V. Flambaum. Enhanced T-odd, P-odd electromagnetic moments in reflection asymmetric nuclei. *Phys. Rev. C*, 56:1357–1369, Sep 1997.

[78] Vadim Kaplunovsky. Multipole expansion (class notes). `https://web2.ph.utexas.edu/~vadim/Classes/2024s-u/multipole.pdf`, 2024. Lecture notes, University of Texas at Austin.

[79] L. P. Gaffney, P. A. Butler, M. Scheck, A. B. Hayes, F. Wenander, M. Albers, B. Bastin, C. Bauer, A. Blazhev, S. Bönig, N. Bree, J. Cederkäll, T. Chupp, D. Cline, T. E. Cocolios, T. Davinson, H. De Witte, J. Diriken, T. Grahn, A. Herzan, M. Huyse, D. G. Jenkins, D. T. Joss, N. Kesteloot, J. Konki, M. Kowalczyk, Th. Kröll, E. Kwan, R. Lutter, K. Moschner, P. Napiorkowski, J. Pakarinen, M. Pfeiffer, D. Radeck, P. Reiter, K. Reynders, S. V. Rigby, L. M. Robledo, M. Rudigier, S. Sambi, M. Seidlitz, B. Siebeck, T. Stora, P. Thoele, P. Van Duppen, M. J. Vermeulen, M. von Schmid, D. Voulot, N. Warr, K. Wimmer, K. Wrzosek-Lipska, C. Y. Wu, and M. Zielinska. Studies of pear-shaped nuclei using accelerated radioactive beams. *Nature*, 497(7448):199–204, May 2013.

[80] Jonathan Engel, Michael J. Ramsey-Musolf, and U. van Kolck. Electric dipole moments of nucleons, nuclei, and atoms: The standard model and beyond. *Progress in Particle and Nuclear Physics*, 71:21–74, 2013. Fundamental Symmetries in the Era of the LHC.

[81] Kris Heyde and John L. Wood. Shape coexistence in atomic nuclei. *Rev. Mod. Phys.*, 83:1467–1521, Nov 2011.

[82] P. A. Butler and W. Nazarewicz. Intrinsic reflection asymmetry in atomic nuclei. *Rev. Mod. Phys.*, 68:349–421, Apr 1996.

[83] A. Restrepo and J. P. Valencia. Quadrupole-octupole residual interaction in the Proxy-SU(3) scheme. *Phys. Rev. C*, 110:054312, Nov 2024.

[84] I. Ahmad and P. A. Butler. Octupole shapes in nuclei. *Annual Review of Nuclear and Particle Science*, 43:71–116, 1993.

[85] P. A. Butler. Pear-shaped atomic nuclei. *Proceedings of the Royal Society A: Mathematical, Physical and Engineering Sciences*, 476(2239):20200202, 2020.

[86] S. Pancholi. *Pear-Shaped Nuclei*. World Scientific Publishing Company, Singapore, 2020.

[87] P A Butler. Octupole collectivity in nuclei. *Journal of Physics G: Nuclear and Particle Physics*, 43(7):073002, jun 2016.

[88] J. Engel, M. Bender, J. Dobaczewski, J. H. de Jesus, and P. Olbratowski. Time-reversal violating Schiff moment of ^{225}Ra. *Phys. Rev. C*, 68:025501, Aug 2003.

[89] J. Dobaczewski, J. Dudek, S. G. Rohoziński, and T. R. Werner. Point symmetries in the Hartree-Fock approach. I. Densities, shapes, and currents. *Phys. Rev. C*, 62:014310, Jun 2000.

[90] Dennis Bonatsos, Andriana Martinou, S. K. Peroulis, D. Petrellis, P. Vasileiou, T. J. Mertzimekis, and N. Minkov. Triaxial shapes in even-even nuclei: A theoretical overview. `https://arxiv.org/abs/2505.19753`, 2025.

[91] Dennis Bonatsos, Andriana Martinou, S K Peroulis, D Petrellis, P Vasileiou, T J Mertzimekis, and N Minkov. Preponderance of triaxial shapes in atomic nuclei predicted by the proxy-SU(3) symmetry. *Journal of Physics G: Nuclear and Particle Physics*, 52(1):015102, dec 2024.

[92] A. Bohr and B.R. Mottelson. *Nuclear structure; Volume I.* World Scientific, 1998.

[93] Aage Bohr and Ben R. Mottelson. *Nuclear structure; Volume II Nuclear deformations*. World scientific, 1988.

[94] V. K. B. Kota. *SU(3) Symmetry in Atomic Nuclei*. Springer Singapore, 2020.

[95] V. F. Weisskopf. Radiative transition probabilities in nuclei. *Phys. Rev.*, 83:1073–1073, Sep 1951.

[96] R.D. Lawson. *Theory of the Nuclear Shell Model*. Oxford studies in nuclear physics. Clarendon Press, 1980.

[97] Nuclear data sheets. Journal, 1966–present. Published by the National Nuclear Data Center.

[98] N. J. Stone. Table of nuclear electric quadrupole moments, 2021. INDC International Nuclear Data Committee, report INDC(NDS)-0833.

[99] Gerda Neyens. Nuclear magnetic and quadrupole moments for nuclear structure research on exotic nuclei. *Reports on Progress in Physics*, 66(4):633, mar 2003.

[100] Klaus Blaum, Jens Dilling, and Wilfried Nörtershäuser. Precision atomic physics techniques for nuclear physics with radioactive beams. *Physica Scripta*, 2013(T152):014017, jan 2013.

[101] X.F. Yang, S.J. Wang, S.G. Wilkins, and R.F. Garcia Ruiz. Laser spectroscopy for the study of exotic nuclei. *Progress in Particle and Nuclear Physics*, 129:104005, 2023.

[102] Dennis Bonatsos, I. E. Assimakis, N. Minkov, Andriana Martinou, S. Sarantopoulou, R. B. Cakirli, R. F. Casten, and K. Blaum. Prolate dominance and prolate-oblate shape transition in the proxy-SU(3) model. `https://arxiv.org/abs/1706.05844`, 2017.

[103] Naoki Tajima and Norifumi Suzuki. Prolate dominance of nuclear shape caused by a strong interference between the effects of spin-orbit and l^2 terms of the nilsson potential. *Phys. Rev. C*, 64:037301, Aug 2001.

[104] Baptiste Savoie. A rigorous proof of the Bohr–van Leeuwen theorem in the semiclassical limit. *Reviews in Mathematical Physics*, 27(08):1550019, 2015.

[105] Noboru Takigawa and Kouhei Washiyama. *Fundamentals of Nuclear Physics*. Springer, 2020.

[106] A.R. Edmonds. *Angular Momentum in Quantum Mechanics*. Investigations in Physics Series. Princeton University Press, 1996.

[107] Krishna Kumar. Intrinsic quadrupole moments and shapes of nuclear ground states and excited states. *Phys. Rev. Lett.*, 28:249–253, Jan 1972.

[108] Swati Garg, Bhoomika Maheshwari, Balraj Singh, Yang Sun, Alpana Goel, and Ashok Kumar Jain. Atlas of nuclear isomers—second edition. *Atomic Data and Nuclear Data Tables*, 150:101546, 2023.

[109] Ashok Kumar Jain, Bhoomika Maheshwari, and Alpana Goel. *Nuclear Isomers: A Primer*. Springer Nature Switzerland AG, Cham, Switzerland, 1 edition, 2021.

[110] J. P. Elliott. Collective motion in the nuclear shell model. I. Classification schemes for states of mixed configurations. *Proceedings of the Royal Society of London. Series A*, 245:128–145, 1958.

[111] J. P. Elliott. Collective motion in the nuclear shell model. II. The introduction of intrinsic wave-functions. *Proceedings of the Royal Society of London. Series A*, 245:562–581, 1958.

[112] Dennis Bonatsos, I. E. Assimakis, N. Minkov, Andriana Martinou, R. B. Cakirli, R. F. Casten, and K. Blaum. Proxy-SU(3) symmetry in heavy deformed nuclei. *Phys. Rev. C*, 95:064325, Jun 2017.

[113] A. Arima, M. Harvey, and K. Shimizu. Pseudo-LS coupling and pseudo-SU(3) scheme. *Physics Letters B*, 30(8):517–522, 1972.

[114] F. Ponce, E. Swanberg, J. Burke, R. Henderson, and S. Friedrich. Accurate measurement of the first excited nuclear state in ^{235}U. *Phys. Rev. C*, 97:054310, May 2018.

[115] J. Tiedau, M. V. Okhapkin, K. Zhang, J. Thielking, G. Zitzer, E. Peik, F. Schaden, T. Pronebner, I. Morawetz, L. Toscani De Col, F. Schneider, A. Leitner, M. Pressler, G. A. Kazakov, K. Beeks, T. Sikorsky, and T. Schumm. Laser excitation of the Th-229 nucleus. *Phys. Rev. Lett.*, 132:182501, Apr 2024.

[116] Peter O. Hess. The power of symmetries in nuclear structure and some of its problems. *Symmetry*, 15(6), 2023.

[117] P. Marević, N. Schunck, E.M. Ney, R. Navarro Pérez, M. Verriere, and J. O'Neal. Axially-deformed solution of the Skyrme-Hartree-Fock-Bogoliubov equations using the transformed harmonic oscillator basis (IV) HFBTHO (v4.0): A new version of the program. *Computer Physics Communications*, 276:108367, 2022.

[118] K. Bennaceur and J. Dobaczewski. Coordinate-space solution of the Skyrme–Hartree–Fock–Bogolyubov equations within spherical symmetry. the program HFBRAD (v1.00). *Computer Physics Communications*, 168(2):96–122, 2005.

[119] A. R. Vernon, R. F. Garcia Ruiz, T. Miyagi, C. L. Binnersley, J. Billowes, M. L. Bissell, J. Bonnard, T. E. Cocolios, J. Dobaczewski, G. J. Farooq-Smith, K. T. Flanagan, G. Georgiev, W. Gins, R. P. de Groote, R. Heinke, J. D. Holt, J. Hustings, Á Koszorús, D. Leimbach, K. M. Lynch, G. Neyens, S. R. Stroberg, S. G. Wilkins, X. F. Yang, and D. T. Yordanov. Nuclear moments of indium isotopes reveal abrupt change at magic number 82. *Nature*, 607(7918):260–265, Jul 2022.

[120] J. Dobaczewski and J. Dudek. Solution of the Skyrme-Hartree-Fock equations in the cartesian deformed harmonic oscillator basis. (II) The program HFODD (v1.60r). *Computer Physics Communications*, 131(2):164–180, 2000.

[121] J. Dobaczewski and J. Dudek. Solution of the Skyrme-Hartree-Fock equations in the cartesian deformed harmonic-oscillator basis. (III) HFODD (v1.75r): a new version of the program. *Computer Physics Communications*, 131(2):181–194, 2000.

[122] J. Dobaczewski and P. Olbratowski. Solution of the Skyrme-Hartree-Fock-Bogolyubov equations in the Cartesian deformed harmonic-oscillator basis. (IV) HFODD (v2.08i): a new version of the program. *Computer Physics Communications*, 158(1):158–177, 2004.

[123] J. Dobaczewski and P. Olbratowski. Solution of the Skyrme-Hartree-Fock-Bogolyubov equations in the cartesian deformed harmonic-oscillator basis. (V) HFODD (v2.08k): a new version of the program. *Computer Physics Communications*, 167:214–224, 2005.

[124] N. Schunck, J. Dobaczewski, J. McDonnell, W. Satuła, J. A. Sheikh, A. Staszczak, M. Stoitsov, and P. Toivanen. Solution of the Skyrme-Hartree-Fock-Bogolyubov equations in the cartesian deformed harmonic-oscillator basis. (VII) HFODD (v2.49t): a new version of the program. *Computer Physics Communications*, 183(1):166–192, 2012.

[125] N. Schunck, J. Dobaczewski, W. Satuła, P. Baczyk, J. Dudek, Y. Gao, M. Konieczka, K. Sato, Y. Shi, X. B. Wang, and T. R. Werner. Solution of the Skyrme-Hartree-Fock-Bogolyubov equations in the cartesian deformed harmonic-oscillator basis. (VIII) HFODD (v2.73y): a new version of the program. *Computer Physics Communications*, 216:145–174, 2017.

[126] J. Dobaczewski, B. G. Carlsson, J. Dudek, J. Engel, P. Olbratowski, P. Powałowski, M. Sadziak, J. Sarich, W. Satuła, N. Schunck, A. Staszczak, M. Stoitsov, M. Zalewski, and H. Zduńczuk. HFODD (v2.40h): User's guide. arXiv preprint, 2009.

[127] W. Horiuchi, T. Inakura, S. Michimasa, and M. Tanaka. Enlarged deformation region in neutron-rich Zr isotopes promoted by the second intruder orbit. *Phys. Rev. C*, 107:L041304, Apr 2023.

[128] H. Mei, J. Xiang, J. M. Yao, Z. P. Li, and J. Meng. Rapid structural change in low-lying states of neutron-rich Sr and Zr isotopes. *Phys. Rev. C*, 85:034321, Mar 2012.

[129] I. Angeli and K.P. Marinova. Table of experimental nuclear ground state charge radii: An update. *Atomic Data and Nuclear Data Tables*, 99(1):69–95, 2013.

[130] Lawrence Wilets. Surface coupling mechanism for approaching statistical equilibrium in compound nucleus formation, with application to fission. *Phys. Rev.*, 116:372–382, Oct 1959.

[131] Jhilam Sadhukhan, J. Dobaczewski, W. Nazarewicz, J. A. Sheikh, and A. Baran. Pairing-induced speedup of nuclear spontaneous fission. *Phys. Rev. C*, 90:061304, Dec 2014.

[132] A. Restrepo-Giraldo and et. al. How to calculate your own nucleus in nuclear DFT: A primer in using the code HFODD. In preparation, 2025.

[133] P L Sassarini, J Dobaczewski, J Bonnard, and R F Garcia Ruiz. Nuclear DFT analysis of electromagnetic moments in odd near doubly magic nuclei. *Journal of Physics G: Nuclear and Particle Physics*, 49(11):11LT01, sep 2022.

[134] B. C. Backes, J. Dobaczewski, D. Muir, W. Nazarewicz, P.-G. Reinhard, M. A. Bentley, and R. Wadsworth. Quadrupole strength in isobaric triplets. *Phys. Rev. C*, 112:064311, Dec 2025.

[135] Marc Chemtob. Two-body interaction currents and nuclear magnetic moments. *Nuclear Physics A*, 123(2):449–470, 1969.

[136] T. Miyagi, X. Cao, R. Seutin, S. Bacca, R. F. Garcia Ruiz, K. Hebeler, J. D. Holt, and A. Schwenk. Impact of two-body currents on magnetic dipole moments of nuclei. *Phys. Rev. Lett.*, 132:232503, Jun 2024.

[137] Elena Litvinova, Hans Feldmeier, Jacek Dobaczewski, and Victor Flambaum. Nuclear structure of lowest ^{229}Th states and time-dependent fundamental constants. *Phys. Rev. C*, 79:064303, Jun 2009.

[138] P G Thirolf, B Seiferle, and L von der Wense. The 229-thorium isomer: doorway to the road from the atomic clock to the nuclear clock. *Journal of Physics B: Atomic, Molecular and Optical Physics*, 52(20):203001, sep 2019.

[139] Andrea Caputo, Doron Gazit, Hans-Werner Hammer, Joachim Kopp, Gil Paz, Gilad Perez, and Konstantin Springmann. Sensitivity of nuclear clocks to new physics. *Phys. Rev. C*, 112:L031302, Sep 2025.

[140] Elina Fuchs, Fiona Kirk, Eric Madge, Chaitanya Paranjape, Ekkehard Peik, Gilad Perez, Wolfram Ratzinger, and Johannes Tiedau. Searching for dark matter with the ^{229}Th nuclear lineshape from laser spectroscopy. *Phys. Rev. X*, 15:021055, May 2025.

[141] Kjeld Beeks, Georgy A. Kazakov, Fabian Schaden, Ira Morawetz, Luca Toscani de Col, Thomas Riebner, Michael Bartokos, Tomas Sikorsky, Thorsten Schumm, Chuankun Zhang, Tian Ooi, Jacob S. Higgins, Jack F. Doyle, Jun Ye, and Marianna S. Safronova. Fine-structure constant sensitivity of the Th-229 nuclear clock transition. `https://arxiv.org/abs/2407.17300`, 2024.

[142] Xiao-tao He and Zhong-zhou Ren. Enhanced sensitivity to variation of fundamental constants in the transitions of ^{229}Th and ^{249}Bk. *Journal of Physics G: Nuclear and Particle Physics*, 34(7):1611, may 2007.

[143] L.A. Kroger and C.W. Reich. Features of the low-energy level scheme of ^{229}Th as observed in the α-decay of ^{233}U. *Nuclear Physics A*, 259(1):29–60, 1976.

[144] R. G. Helmer and C. W. Reich. An excited state of ^{229}Th at 3.5 eV. *Phys. Rev. C*, 49:1845–1858, Apr 1994.

[145] E. Peik and Chr. Tamm. Nuclear laser spectroscopy of the 3.5 eV transition in Th-229. *Europhysics Letters*, 61(2):181, jan 2003.

[146] E. Ruchowska, W. A. Płóciennik, J. Żylicz, H. Mach, J. Kvasil, A. Algora, N. Amzal, T. Bäck, M. G. Borge, R. Boutami, P. A. Butler, J. Cederkäll, B. Cederwall, B. Fogelberg, L. M. Fraile, H. O. U. Fynbo, E. Hagebø, P. Hoff, H. Gausemel, A. Jungclaus, R. Kaczarowski, A. Kerek, W. Kurcewicz, K. Lagergren, E. Nacher, B. Rubio, A. Syntfeld, O. Tengblad, A. A. Wasilewski, and L. Weissman. Nuclear structure of ^{229}Th. *Phys. Rev. C*, 73:044326, Apr 2006.

[147] Sergei Matinyan. Lasers as a bridge between atomic and nuclear physics. *Physics Reports*, 298(4):199–249, 1998.

[148] Lars von der Wense, Benedict Seiferle, Mustapha Laatiaoui, Jürgen B. Neumayr, Hans-Jörg Maier, Hans-Friedrich Wirth, Christoph Mokry, Jörg Runke, Klaus Eberhardt, Christoph E. Düllmann, Norbert G. Trautmann, and Peter G. Thirolf. Direct detection of the ^{229}Th nuclear clock transition. *Nature*, 533(7601):47–51, May 2016.

[149] M. Verlinde, S. Kraemer, J. Moens, K. Chrysalidis, J. G. Correia, S. Cottenier, H. De Witte, D. V. Fedorov, V. N. Fedosseev, R. Ferrer, L. M. Fraile, S. Geldhof, C. A. Granados, M. Laatiaoui, T. A. L. Lima, P.-C. Lin, V. Manea, B. A. Marsh, I. Moore, L. M. C. Pereira, S. Raeder, P. Van den Bergh, P. Van Duppen, A. Vantomme, E. Verstraelen, U. Wahl, and S. G. Wilkins. Alternative approach to populate and study the ^{229}Th nuclear clock isomer. *Phys. Rev. C*, 100:024315, Aug 2019.

[150] Sandro Kraemer, Janni Moens, Michail Athanasakis-Kaklamanakis, Silvia Bara, Kjeld Beeks, Premaditya Chhetri, Katerina Chrysalidis, Arno Claessens, Thomas E. Cocolios, João G. M. Correia, Hilde De Witte, Rafael Ferrer, Sarina Geldhof, Reinhard Heinke, Niyusha Hosseini, Mark Huyse, Ulli Köster,

Yuri Kudryavtsev, Mustapha Laatiaoui, Razvan Lica, Goele Magchiels, Vladimir Manea, Clement Merckling, Lino M. C. Pereira, Sebastian Raeder, Thorsten Schumm, Simon Sels, Peter G. Thirolf, Shandirai Malven Tunhuma, Paul Van Den Bergh, Piet Van Duppen, André Vantomme, Matthias Verlinde, Renan Villarreal, and Ulrich Wahl. Observation of the radiative decay of the ^{229}Th nuclear clock isomer. *Nature*, 617(7962):706–710, May 2023.

[151] G. Zitzer, J. Tiedau, Ch. E. Düllmann, M. V. Okhapkin, and E. Peik. Laser spectroscopy on the hyperfine structure and isotope shift of sympathetically cooled $^{229}Th^{3+}$ ions. *Phys. Rev. A*, 111:L050802, May 2025.

[152] Yang-Yang Xu, Qiong Xiao, Jun-Hao Cheng, Wen-Yu Zhang, and Tong-Pu Yu. Charge state regulation of nuclear excitation by electron capture in ^{229}Th ions. `https://arxiv.org/abs/2510.08212`, 2025.

[153] Pavlo V. Bilous, Georgy A. Kazakov, Iain D. Moore, Thorsten Schumm, and Adriana Pálffy. Internal conversion from excited electronic states of ^{229}Th ions. *Phys. Rev. A*, 95:032503, Mar 2017.

[154] S. Gerstenkorn, P. Luc, J. Verges, D. W. Englekemeir, J. E. Gindler, and F. S. Tomkins. Structures hyperfines du spectre d'étincelle, moment magnétique et quadrupolaire de l'isotope ^{229}Th. *J. Phys. (Paris)*, 35(6):483–495, 1974.

[155] C. J. Campbell, A. G. Radnaev, and A. Kuzmich. Wigner crystals of ^{229}Th for optical excitation of the nuclear isomer. *Phys. Rev. Lett.*, 106:223001, Jun 2011.

[156] M. S. Safronova, U. I. Safronova, A. G. Radnaev, C. J. Campbell, and A. Kuzmich. Magnetic dipole and electric quadrupole moments of the ^{229}Th nucleus. *Phys. Rev. A*, 88:060501, Dec 2013.

[157] S. G. Porsev, M. S. Safronova, and M. G. Kozlov. Precision calculation of hyperfine constants for extracting nuclear moments of ^{229}Th. *Phys. Rev. Lett.*, 127:253001, Dec 2021.

[158] Kjeld Beeks, Georgy A. Kazakov, Fabian Schaden, Ira Morawetz, Luca Toscani De Col, Thomas Riebner, Michael Bartokos, Tomas Sikorsky, Thorsten Schumm, Chuankun Zhang, Tian Ooi, Jacob S. Higgins, Jack F. Doyle, Jun Ye, and Marianna S. Safronova. Fine-structure constant sensitivity of the Th-229 nuclear clock transition. *Nature Communications*, 16(1):9147, Oct 2025.

[159] Atsushi Yamaguchi, Yudai Shigekawa, Hiromitsu Haba, Hidetoshi Kikunaga, Kenji Shirasaki, Michiharu Wada, and Hidetoshi Katori. Laser spectroscopy of triply charged 229Th isomer for a nuclear clock. *Nature*, 629(8010):62–66, May 2024.

[160] C. J. Campbell, A. G. Radnaev, A. Kuzmich, V. A. Dzuba, V. V. Flambaum, and A. Derevianko. Single-ion nuclear clock for metrology at the 19th decimal place. *Phys. Rev. Lett.*, 108:120802, Mar 2012.

[161] H. W. T. Morgan, R. Elwell, J. E. S. Terhune, H. B. Tran Tan, U. C. Perera, A. Derevianko, A. N. Alexandrova, and E. R. Hudson. Proposal and theoretical investigation of ^{229}Th-doped nonlinear optical crystals for compact solid-state clocks. *Applied Physics Letters*, 126(11):111101, 03 2025.

[162] Steven M. Girvin and Leo Radzihovsky. Prospects for a solid-state nuclear clock. `https://arxiv.org/abs/2511.13017`, 2025.

[163] Takahiko Masuda, Akihiro Yoshimi, Akira Fujieda, Hiroyuki Fujimoto, Hiromitsu Haba, Hideaki Hara, Takahiro Hiraki, Hiroyuki Kaino, Yoshitaka Kasamatsu, Shinji Kitao, Kenji Konashi, Yuki Miyamoto, Koichi Okai, Sho Okubo, Noboru Sasao, Makoto Seto, Thorsten Schumm, Yudai Shigekawa, Kenta Suzuki, Simon Stellmer, Kenji Tamasaku, Satoshi Uetake, Makoto Watanabe, Tsukasa Watanabe, Yuki Yasuda, Atsushi Yamaguchi, Yoshitaka Yoda, Takuya Yokokita, Motohiko Yoshimura, and Koji Yoshimura. X-ray pumping of the 229th nuclear clock isomer. *Nature*, 573(7773):238–242, Sep 2019.

[164] V. L. Ginzburg. On superconductivity and superfluidity. *Physics–Uspekhi*, 47(11):1155–1170, 2004. Nobel Lecture, 8 December 2003.

[165] E. V. Tkalya. Proposal for a nuclear gamma-ray laser of optical range. *Phys. Rev. Lett.*, 106:162501, Apr 2011.

[166] E. V. Tkalya, Christian Schneider, Justin Jeet, and Eric R. Hudson. Radiative lifetime and energy of the low-energy isomeric level in ^{229}Th. *Phys. Rev. C*, 92:054324, Nov 2015.

[167] F. Schaden, T. Riebner, I. Morawetz, L. Toscani De Col, G. A. Kazakov, K. Beeks, T. Sikorsky, T. Schumm, K. Zhang, V. Lal, G. Zitzer, J. Tiedau, M. V. Okhapkin, and E. Peik. Laser-induced quenching of the Th-229 nuclear clock isomer in calcium fluoride. *Phys. Rev. Res.*, 7:L022036, May 2025.

[168] Chuankun Zhang, Tian Ooi, Jacob S. Higgins, Jack F. Doyle, Lars von der Wense, Kjeld Beeks, Adrian Leitner, Georgy A. Kazakov, Peng Li, Peter G. Thirolf, Thorsten Schumm, and Jun Ye. Frequency ratio of the ^{229m}Th nuclear isomeric transition and the ^{87}Sr atomic clock. *Nature*, 633(8028):63–70, Sep 2024.

[169] R. Elwell, Christian Schneider, Justin Jeet, J. E. S. Terhune, H. W. T. Morgan, A. N. Alexandrova, H. B. Tran Tan, Andrei Derevianko, and Eric R. Hudson. Laser excitation of the ^{229}Th nuclear isomeric transition in a solid-state host. *Phys. Rev. Lett.*, 133:013201, Jul 2024.

[170] Nikolay Minkov and Adriana Pálffy. Reduced transition probabilities for the gamma decay of the 7.8 eV isomer in ^{229}Th. *Phys. Rev. Lett.*, 118:212501, May 2017.

[171] A. M. Dykhne and E. V. Tkalya. Matrix element of the anomalously low-energy (3.5±0.5 eV) transition in 229Th and the isomer lifetime. *Journal of Experimental and Theoretical Physics Letters*, 67(4):251–256, Feb 1998.

[172] Zi-Rui Chen, Long-Jun Wang, and Yuanbin Wu. Microscopic nuclear structure study of ^{229}Th by projected shell model. `https://arxiv.org/abs/2508.19686`, 2025.

[173] Nikolay Minkov, Adriana Pálffy, Philippe Quentin, and Ludovic Bonneau. Skyrme-Hartree-Fock-BCS approach to ^{229m}Th and neighboring nuclei. *Phys. Rev. C*, 110:034327, Sep 2024.

[174] E. F. Zhou and J. M. Yao. Microscopic study of low-lying states in odd-mass nuclei for atomic electric dipole moment searches. `https://arxiv.org/abs/2511.05984`, 2025.

[175] M. Athanasakis-Kaklamanakis, M. Au, A. Kyuberis, C. Zülch, K. Gaul, H. Wibowo, L. Skripnikov, L. Lalanne, J. R. Reilly, A. Koszorús, S. Bara, J. Ballof, R. Berger, C. Bernerd, A. Borschevsky, A. A. Breier, K. Chrysalidis, T. E. Cocolios, R. P. de Groote, A. Dorne, J. Dobaczewski, C. M. Fajardo Zambrano, K. T. Flanagan, S. Franchoo, J. D. Johnson, R. F. Garcia Ruiz, D. Hanstorp, S. Kujanpää, Y. C. Liu, K. M. Lynch, A. McGlone, N. S. Mosyagin, G. Neyens, M. Nichols, L. Nies, F. Pastrana, S. Rothe, W. Ryssens, B. van den Borne, J. Wessolek, S. G. Wilkins, and X. F. Yang. Laser spectroscopy and CP-violation sensitivity of actinium monofluoride. `https://arxiv.org/abs/2507.05224`, 2025.

[176] P.-G. Reinhard. Skyrme forces and giant resonances in exotic nuclei. *Nucl. Phys. A*, 649:305c, 1999.

[177] B. A. Brown. New Skyrme interaction for normal and exotic nuclei. *Phys. Rev. C*, 58(1):220–231, 1998.

[178] L. P. Gaffney, P. A. Butler, M. Scheck, A. B. Hayes, F. Wenander, M. Albers, B. Bastin, C. Bauer, A. Blazhev, S. Bönig, N. Bree, J. Cederkäll, T. Chupp, D. Cline, T. E. Cocolios, T. Davinson, H. De Witte, J. Diriken, T. Grahn, A. Herzan, M. Huyse, D. G. Jenkins, D. T. Joss, N. Kesteloot, J. Konki, M. Kowalczyk, Th. Kröll, E. Kwan, R. Lutter, K. Moschner, P. Napiorkowski, J. Pakarinen, M. Pfeiffer, D. Radeck, P. Reiter, K. Reynders, S. V. Rigby, L. M. Robledo, M. Rudigier, S. Sambi, M. Seidlitz, B. Siebeck, T. Stora, P. Thoele, P. Van Duppen, M. J. Vermeulen, M. von Schmid, D. Voulot, N. Warr, K. Wimmer, K. Wrzosek-Lipska, C. Y. Wu, and M. Zielinska. Studies of pear-shaped nuclei using accelerated radioactive beams. *Nature*, 497:199, 2013.

[179] H.J. Wollersheim, H. Emling, H. Grein, R. Kulessa, R.S. Simon, C. Fleischmann, J. de Boer, E. Hauber, C. Lauterbach, C. Schandera, P.A. Butler, and T. Czosnyka. Coulomb excitation of ^{226}Ra. *Nuclear Physics A*, 556(2):261–280, 1993.

[180] F. K. McGowan, C. E. Bemis, W. T. Milner, J. L. C. Ford, R. L. Robinson, and P. H. Stelson. Coulomb excitation of vibrational-like states in the even-A actinide nuclei. *Phys. Rev. C*, 10:1146–1155, Sep 1974.

[181] Y. M. Engel, D. M. Brink, K. Goeke, S. J. Krieger, and D. Vautherin. Time-dependent Hartree-Fock theory with Skyrme's interaction. *Nucl. Phys. A*, 249(2):215, 1975.

[182] E. Perlińska, S. G. Rohoziński, J. Dobaczewski, and W. Nazarewicz. Local density approximation for proton-neutron pairing correlations: Formalism. *Phys. Rev. C*, 69:014316, Jan 2004.

[183] George Bertsch, Jacek Dobaczewski, Witold Nazarewicz, and Junchen Pei. Hartree-Fock-Bogoliubov theory of polarized fermi systems. *Phys. Rev. A*, 79:043602, Apr 2009.

[184] H Wibowo, B C Backes, J Dobaczewski, R P de Groote, A Nagpal, A Sánchez-Fernández, X Sun, and J L Wood. Electromagnetic moments in the Sn-Gd region determined within nuclear DFT. *Journal of Physics G: Nuclear and Particle Physics*, 52(6):065104, jul 2025.

[185] A. Restrepo-Giraldo, J. Dobaczewski, J. Bonnard, and X. Sun. Radiative decay and electromagnetic moments in ^{229}Th determined within nuclear DFT. `https://arxiv.org/abs/2602.02429`, 2026.

[186] G. F. Bertsch and L. M. Robledo. Symmetry restoration in Hartree-Fock-Bogoliubov based theories. *Phys. Rev. Lett.*, 108:042505, Jan 2012.